Aerotherm FR-75-135

NASA CR-
147845

DEVELOPMENT OF TPS FLIGHT TEST AND OPERATIONAL INSTRUMENTATION

by

K. R. Carnahan, G. J. Hartman, and G. J. Neuner

Aerotherm Division/Acurex Corporation
485 Clyde Avenue
Mountain View, California 94042

prepared for

NATIONAL AERONAUTICS AND SPACE ADMINISTRATION

Johnson Spacecraft Center
Houston, Texas

Contract NAS9-13543

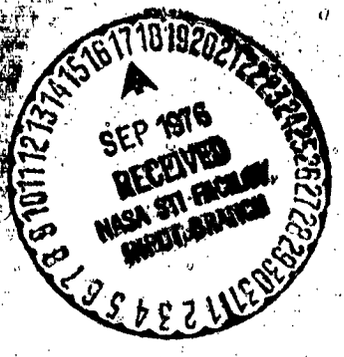

Aerotherm FR-75-135

Final Report

DEVELOPMENT OF TPS FLIGHT TEST AND OPERATIONAL INSTRUMENTATION

by

K. R. Carnahan, G. J. Hartman, and G. J. Neuner

Aerotherm Division/Acurex Corporation
485 Clyd Avenue
Mountain View, California 94042

prepared for

NATIONAL AERONAUTICS AND SPACE ADMINISTRATION

January 1975

Contract NAS9-13543

Johnson Spacecraft Center
Houston, Texas

FOREWORD

This final report was prepared by the Acurex Corporation, Aerotherm Division, for NASA/JSC Contract No. NAS9-13543, Development of TPS Flight Test and Operational Instrumentation. This work was performed under the direction of the Thermal Technology Branch of the Structures and Mechanics Division with Mr. James E. Pavlosky as the Program Director.

The following individuals were directly responsible for performing the program tasks and in the preparation of this final report: Joe Hartman, Project Engineer, Design and Testing, and Gary Neuner, Data Reduction, Design Analysis.

This report is arranged in accordance with the three major tasks performed under this contract during the period 25 June 1973 through 25 May 1974.

ABSTRACT

Thermal and flow sensor instrumentation was developed for use as an integral part of the Space Shuttle orbitor reusable thermal protection system. The effort was performed in three tasks: Task 1 to perform a study to determine the optimum instruments and instrument installations for the Space Shuttle orbitor RSI and RCC TPS, Task 2 to perform tests and/or analysis to determine the instrument installations to minimize measurement errors, and Task 3 to conduct analysis using data from the test program for comparison to analytical methods. In Task 1, a detailed review of existing state of the art instrumentation in industry was performed to determine the baseline for the departure of the research effort. From this information, detailed criteria for thermal protection system instrumentation were developed. A preliminary design study conducted on heat flux, temperature, and pressure measurements revealed a number of optimum approaches to the instrumentation both for the RCC and RSI TPS areas. In-depth temperature measurements were found to be best achieved through the use of chromel/alumel (type K) and platinum-platinum/13 percent rhodium (type R) thermocouples contained in plugs of the RSI material measuring no more than 0.0245 meter (1 inch) in diameter with the thermocouple wire contained in a helicoil configuration. For cold wall heat flux measurements it was determined that the augmented Gardon gage concept represented the best approach based on the design criteria for ruggedness, sensitivity, repeatability, calibration, time constant, handling, and installation constraints. Testing verified both qualitatively and quantitatively that the prediction techniques employed to define the boundary layer perturbations were accurate. Under Task 2, preliminary testing was performed on the thermocouple and cold wall heat flux gage design concepts for use in the RSI material and to a lesser extent on thermocouple temperature measurement concepts for use on the RCC material. Testing and analysis indicated that for monitoring transient temperature histories on RCC, the flame sprayed alumina attachment technique is preferred. RCC testing further demonstrated a surface catalycity efficiency of approximately 50 percent. The recommended thermocouple material for the RCC measurements is platinum-platinum/13 percent rhodium (type R), with leads insulated with aluminum oxide in an inconel sheath. Finally, testing revealed the damage to the RSI TPS coating would easily occur if extreme care were not exercised in instrument installation. Vibration and acoustic environmental effects upon calorimeter installations were not addressed in this program. Recommendations were made to address these and other related design constraint problems and to integrate this into the overall shuttle TPS development activity.

TABLE OF CONTENTS

LIST OF ILLUSTRATIONS

LIST OF ILLUSTRATIONS (Continued)

LIST OF ILLUSTRATIONS (Concluded)

LIST OF TABLES

SECTION 1

SUMMARY

With the development of advanced reusable heat shield materials for space shuttle application, it became apparent that existing instrumentation used for previous thermal protection systems was not adequate for the requirements of a shuttle vehicle which was being designed for a minimum 100 mission life time capability. Existing instrumentation had been developed primarily for use in reentry heat shields on spacecraft such as Mercury and Apollo with no reuse requirement. The Space Shuttle Orbiter, however, must survive a multiple number of reentries without significant change in the characteristics of the heat shield materials. The concept of a fully reusable thermal protection system established the need for advanced instrumentation to (1) be used in the development and qualification of the heat shield and (2) to monitor the performance of the heat shield system during operational flights. The stringent requirements for the shuttle application made it clear that additional development was required. This program was initiated to address those problems.

The primary objective of this program was to develop and determine the adequacy of thermal and flow sensor instrumentation which are an integral part of the orbiter reusable TPS. The ultimate objective of the effort was to recommend to NASA the type of sensors to be used, the installation procedure, and the accuracy of the measurements expected for the orbiter TPS instrumentation.

The program consisted of three basic tasks:

- Task 1 - Instrumentation Installation Study
- Task 2 - Testing
- Task 3 - Data Reduction and Analyses

The objective of Task 1 was to perform a study to determine the optimum instruments and instrument installation for the Shuttle Orbiter TPS. The study considered (a) heat flux sensors for use with RSI materials, (b) high temperature coated and uncoated thermocouples for use in RSI and (c) high temperature coated thermocouples to be used with RCC. A detailed review of existing state-of-the-art instumentation in industry was performed to determine the baseline for departure of the research effort. Both government and industry sources were surveyed to determine

current experience and background directly related to the orbiter TPS instrumentation requirements. During this phase of the program, detailed criteria for a thermal protection system instrumentation were developed. A preliminary design study was conducted on heat flux, temperature and pressure measurements. Measurement error analysis was conducted to support this activity by quantifying the effects of various environmental parameters on the performance of the candidate systems. The effects of installation constraints and other factors were reviewed with the objective of determining whether or not such instrumentation could be adequately incorporated in the RSI and RCC TPS. The results of the design and installation study identified several approaches for space shuttle TPS instrumentation

The objective of Task 2 was to perform tests and supportive analyses on the selected candidate TPS instrumentation concepts. The test program was designed and performed in support of the Task 1 installation study. Boundary conditions for the test program were defined from the shuttle flight envelope, and specific test conditions were selected to simulate critical areas for the instrumentation. Preliminary analyses were conducted to predict the performance characteristics of the shuttle TPS materials and installed instrumentation to the test environments. Limited tests were conducted on the RCC materials due to the unavailability of test material, however, extensive testing was conducted on the RSI materials utilizing the various measurement concepts. The instrument system performance was evaluated through comparisons of analytical performance predictions and available test data. These analyses considered surface catalycity effects, test facility data reduction capabilities, heat leak effects, and other installation/facility related errors. Instrumentation installation problems were identified, and a number of procedures were developed to overcome these problems.

The final task of the program was to reduce the test data and to evaluate the analytical methods developed during the design phase of the program. The overall result of the program was to identify specific instrumentation concepts for use in both the RSI and RCC TPS for the shuttle orbiter: (1) A calorimeter concept was identified for measuring HRSI surface heat flux, (2) surface and in-depth temperature measurement techniques were defined for the HRSI TPS, and (3) a temperature measurement technique for monitoring RCC performance was recommended. A description of the expected errors, installation constraints/techniques, and lifetime expectancy for each of the recommended instrumentation systems were developed under this task. It was demonstrated through arc plasma testing that penetration of the HRSI and HRSI coating by pressure ports or heat flux transducers was not detrimental to the thermal performance of the heat shield material. Testing revealed that damage to the TPS coating would easily occur if extreme care were not exercised in the instrument installation. Vibration and acoustic environmental effects upon calorimeter installations have not been addressed. Based upon the results of the program, specific recommendations were identified for the advanced developments of flight system hardware.

SECTION 2

TECHNICAL DISCUSSION OF TASKS

2.1 INTRODUCTION

This final report describes the work performed in NASA Contract No. NAS9-13543, "Development of TPS Flight Test and Operational Instrumentation." The orbital stage of the manned space shuttle will have a reusable thermal protection system consisting primarily of an oxidation resistant reinforced carbon/carbon nosecap and leading edges and a coated silica surface insulation covering all other vehicle surface areas.

In the last three years considerable research has been directed towards the development of these reusable thermal protection materials to meet the minimum 100 mission lifetime requirement. During this period little attention was given to the development of reusable TPS instrumentation, a unique requirement. Considerable work, however, had been accomplished in the testing and evaluation of the reusable TPS materials resulting in the indirect evaluation of existing state-of-the-art instrumentation. The use of such off-the-shelf instrumentation with the reusable TPS materials was proven to be inadequate for the thermal environments and the reuse capabilities for which materials were designed and are being tested. Considering the shuttle flight instrumentation requirements for both development flights and operational flights, there is a need for establishing instrumentation for reusable surface insulation (RSI) for major surface areas and reusable carbon/carbon (RCC) for leading edges. This program was initiated on June 25, 1973. The program consisted of three tasks. The objectives of these tasks were to:

- Task 1 - perform a study to determine the optimum instruments and instrument installations for the Space Shuttle Orbiter RSI and RCC TPS
- Task 2 - perform tests and/or analyses to determine the instrument installations to minimize the thermal losses through conduction and radiation, the determination of material effects such as cooling and catalycity and other sources of error that are inherent with arc heater environments
- Task 3 - conduct a program analysis using data from the test program and compare to analytical methods

2.2 TASK 1 - INSTRUMENTATION INSTALLATION STUDY

This task consisted of a study to determine the optimum instruments and instrument installations with consideration of all factors affecting accuracy, reliability, maintainability and TPS performance. The study defined requirements for the Shuttle Orbiter TPS instrumentation, considered all sensors and installation concepts which met the requirements and performed complete evaluation of each concept, identifying optimum approaches.

2.2.1 Review of Existing Instrumentation

A review of the existing instrumentation used in the thermal protection subsystems of previous vehicles, such as Apollo, and more recently in the test and development of Shuttle TPS materials, was performed. Contacting NASA Ames Research Center, Rockwell International, Lockheed Missiles and Space Co., Sandia Laboratories, and LTV Aerospace, a survey of current information on instrumentation techniques and requirements not generally available in the open literature was conducted. The pertinent information assimilated in this review is summarized below for the typical Shuttle TPS types (i.e., HRSI and RCC).

2.2.1.1 HRSI Instramentation Review

A review of literature concerned with HRSI properties, testing and development, was conducted to assimilate all of the pertinent information available which might impact instrumentation system design. A summary of this information is presented below.

Thermocouples have previously been selected on several criteria. First, the types of thermocouple materials selected must be compatible with both the HRSI and the temperature range required (i.e., for a given surface temperature, various depths may use different thermocouples). Another consideration in thermocouple designation is the handling characteristics. Previous testing has used four thermocouple materials: chromel-alumel, platinum-platinum/10 percent rhodium, platinum-platinum/13 percent rhodium, and tungsten-tungsten/rhenium. It has been found that the tungsten-rhenium thermocouple embrittles when the thermocouple junction is made, and consequently this type of thermocouple is not recommended. The platinum-rhodium thermocouples are easy to handle, and testing has indicated that a lifetime in excess of 30 cycles may be expected with reproducible results.

NASA Ames' experience has indicated that 0.000127 m (0.005 inch) is the appropriate wire size to minimize heat leaks and the temperature distortion within the material due to the heat sink effect of the thermocouple wire. Ames personnel also believe that the thermocouple junction should be made from a butt weld for two reasons: to minimize the heat sink effect, and because larger junctions are more difficult to locate accurately within the RSI.

The only NDE method Ames has implemented to observe the thermocouple location was the use of X-ray techniques. Parallax appeared to be the worst problem with evaluating the X-rays, and the estimated best accuracy obtainable in locating the thermocouple is to within 0.000127 m (0.005 inch).

Two thermocouple installation techniques have been used extensively by NASA Ames. A needle technique (Ames developed) uses a 0.000254 m (0.010 inch) stainless steel needle as a lance to punch a hole through the RSI for each thermocouple lead. This technique may be used for surface as well an in-depth temperature measurements. In the case of surface temperature measurements, a 0.000508 m (0.020 inch) deep cut is made on the surface of the material. Then the puncture holes are made on each end of the slit to the backside of the material. The leads are then fed through the holes and the thermocouple is pulled into the slit. The coating is then applied (sprayed on) with care being taken to assure that the groove is filled in and a uniform surface results. This installation technique is highly desirable from a thermal standpoint since X-rays have indicated intimate contact between the thermocouple bead and the coating. However, the thermostructural effects upon the coating present a major disadvantage which must be assessed to insure that this type of thermocouple installation will not compromise the tile integrity.

The needle technique has also been used in plugs with the thermocouple lead wires run through slits in the side of the plug. Another technique is to have segmented or randomly located plugs over which a thermocouple is stretched prior to insertion into the RSI specimen. Concern has appropriately been expressed by NASA Ames over the possible errors induced at the interface of these plugs inserted into the RSI. This error has not been quantitatively addressed to date by Ames. Comparisons have been made between optical pyrometer data and surface thermocouples. For a pressed-in technique of thermocouple mounting, less than a 27.8 K (50°F) temperature difference has been observed. This comparison may be made as long as the coating is opaque. It is believed that the "pulled through" technique for a surface thermocouple location will result in an even better agreement between optical pyrometer data and thermocouple data.

Also, as yet problems have not been encountered in running the leads through the bond, stress reliever, and structure. A hole was merely drilled through the aluminium, RTV-560 was applied, and the tile was bonded in place while pulling the thermocouple leads through the hole.

Vibration and acoustic testing have not been performed on instrumented specimens. Some instrumentation of gaps has been done; however, the accuracy of these installations has not been addressed nor, to this date, has the test data been evaluated or available for evaluation.

2.2.1.2 RCC Instrumentation Review

The instrumentation of RCC presents a problem in that the siliconized coating is highly reactive with noble metals at high temperatures. Thermocouples have been installed into notches drilled into the RCC prior to coating. The chemical incompatibility of the coating and the thermocouple is offset by utilizing a barrier of high temperature ceramic such as Astroceram; however, the lifetime of this approach has not been established. Coated iridium thermocouples with a beryllia sheath, and iridium-iridium/rhodium thermocouples have been used. Various ceramic cements have been evaluated by LTV for bonding beryllia sheathed thermocouples to RCC and the only satisfactory cement found was C-34 which is produced by the Union Carbide Corporation. This bonding technique has been used by LTV in various testing programs.

Spring loaded thermocouples have had fairly widespread use in the various RCC development testing programs and offer the advantage of accommodating the expected large thermal expansions. The conduction error associated with their use however has usually been ignored. The fragility of this type of thermocouple probe must be considered and in fact has been a problem in the relatively mild (mechanically) ground test environment.

Various techniques in use at Sandia Laboratories for high temperature thermal instrumentation include a flame spray attachment technique used for strain gage and thermocouple installations on carbon/carbon and graphite materials. The flame spray material is high purity alumina, offering a high temperature (> 1922 K (3000°F)) capability for such an installation. Experience to date has shown this technique can be very successful if properly applied, i.e., proper thermocouple configuration and spraying techniques are used and if the sources of error, i.e., thermocouple/substrate contract resistance and local effect of coating material are recognized.

2.2.2 Design Criteria

Being fundamental to the operation and survival of various instrumentation concepts, the environmental and operational design constraints were defined. A summary of some of the design criteria integrated into the shuttle instrumentation review includes:

- Ascent environments
- On-orbit environments
- Once around mission environments
- Reentry environments
- Maintainability requirements

- Lifetime requirements
- Material compatibility constraints
- Material thermal properties

Five vehicle locations were identified by NASA as being representative of the range of conditions encountered by the TPS as follows:

Body Point(B.P.)A., X/L = 0.025, lower surface, fuselage

B.P.B., X/L = 0.1, lower surface, fuselage

B.P.C., X/L = 0.3, lower surface, fuselage

B.P.D., X/C = 0.5, 50 percent span, vertical stabilizer

B.P.E., X/C = 0.15, 60 percent halfspan, upper surface, wing

These locations are shown in Figure 1. The first point, B.P.A., is a RCC location while the remainder represent HRSI positions. The reentry conditions at these five locations are presented in Figures 2 through 16. This data was supplied by Rockwell International and is for Reference Trajectory 8921, 147B vehicle. The ascent, on-orbit and once around mission environments were also supplied by Rockwell International along with a predicted vibration spectra for various locations on or in the vehicle. Although all the above environments were considered in the design process, the primary design criteria was developed from the reentry environment with equal weighting for the lifetime requirements and the material compatibility constraints. A 100-mission lifetime was the criteria for all operational flight instrumentation. A 15-mission lifetime for the development flight instrumentation was considered adequate. In all cases the material compatibility constraint was interpreted to include not only the lifetime effects of the TPS materials on the instrumentation but also the effects of the instrumentation upon TPS subsystem performance, i.e., lifetime and integrity.

The material property data fundamental to the data reduction and analysis phases of the program are presented in Tables 1 and 2 for the HRSI (LI-900) and HRSI coating as supplied by LMSC.

2.2.3 Design

A design effort was performed to select instrumentation and instrumentation systems compatible with the required shuttle design constraints. These design constraints include:

- Measurement range
- Operation environment
- Accuracy

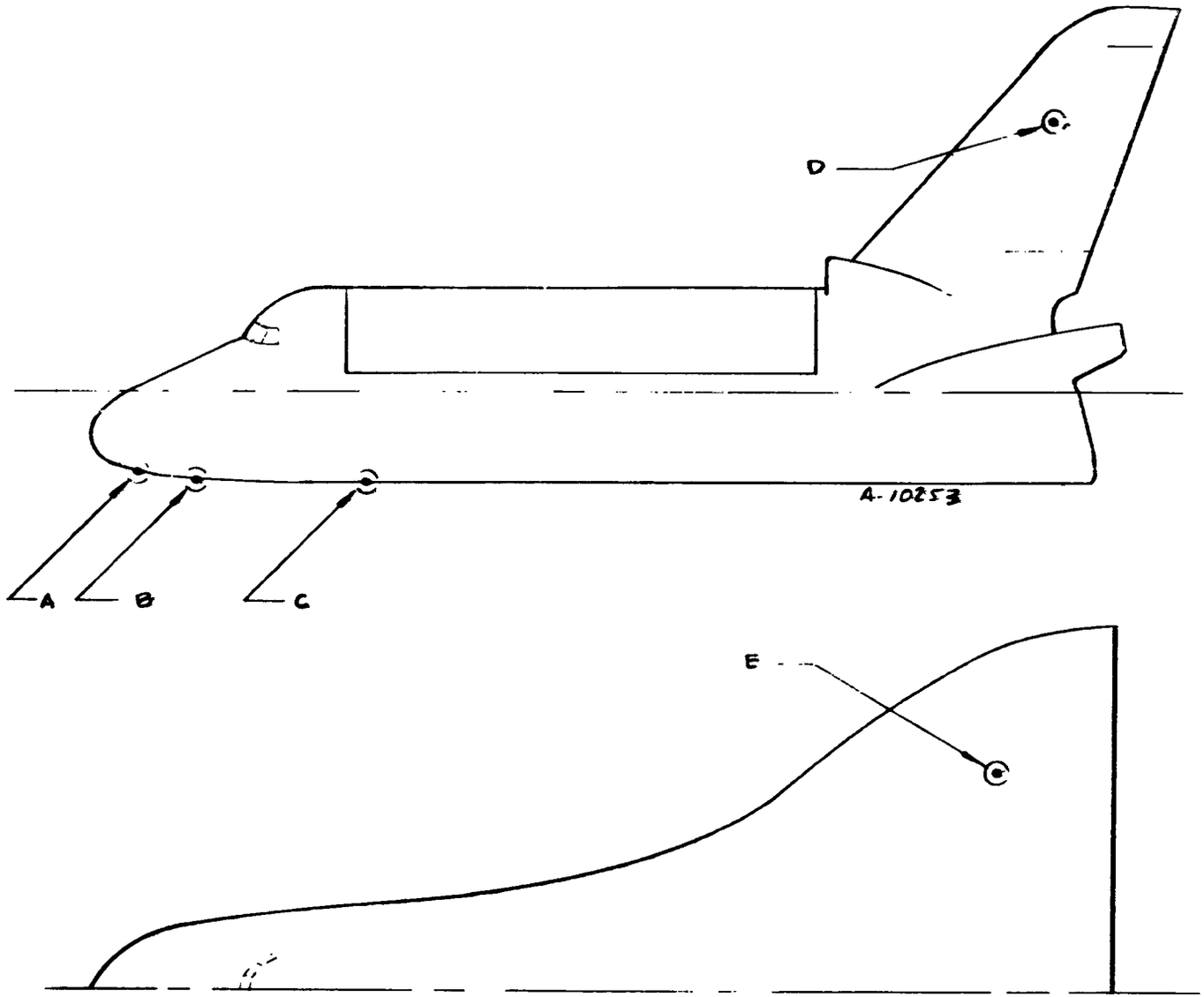

Figure 1. Reference shuttle body locations.

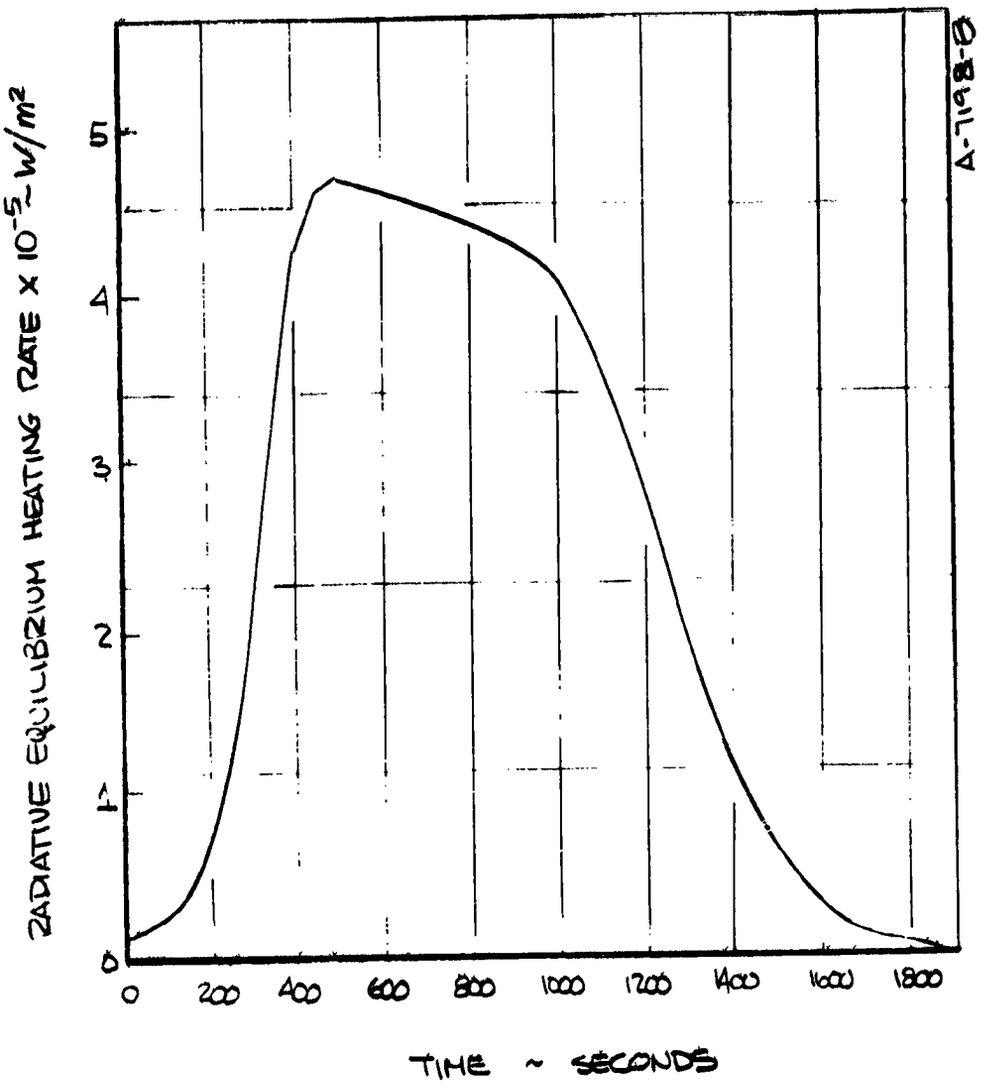

Figure 2. Reentry profile.

(Ref. trajectory 8921, 147B vehicle, B.P. A, X/L = 0.025 lower surface, fuselage)

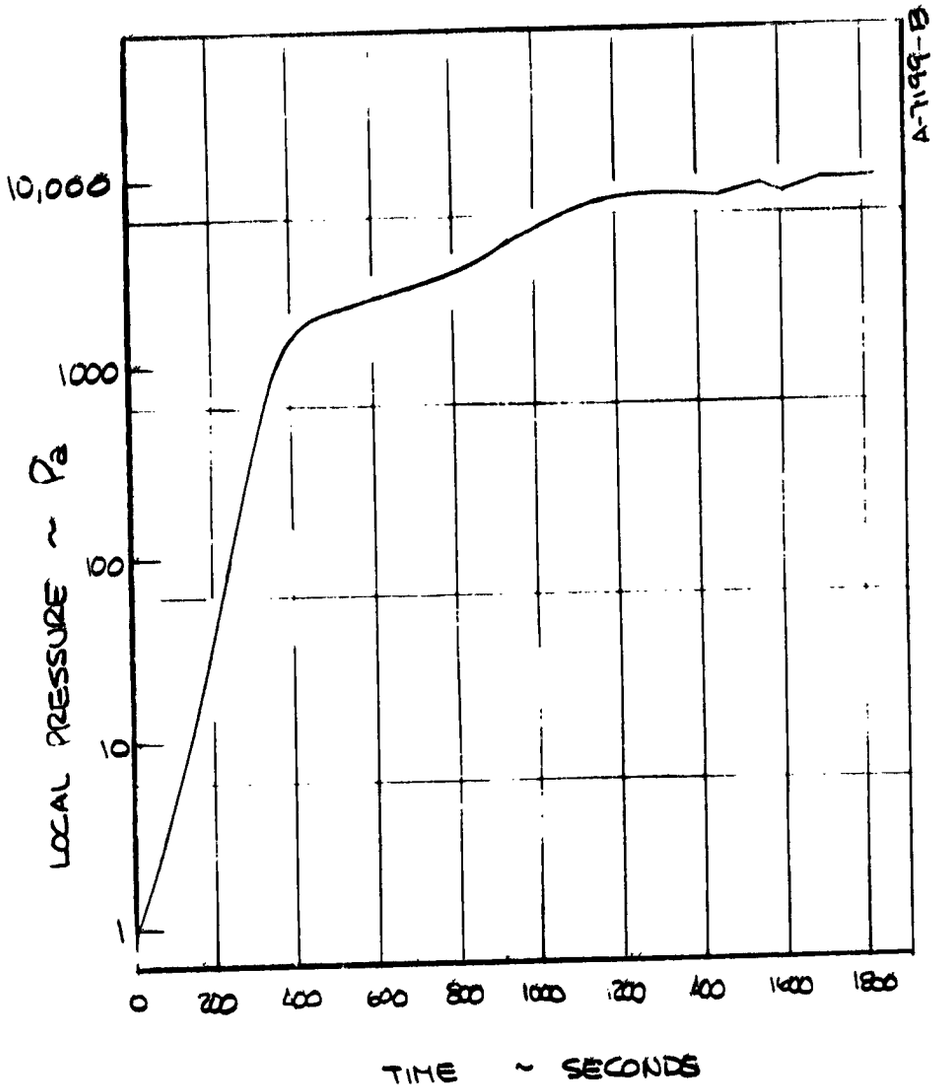

Figure 3. Reentry profile.

(Ref. trajectory 8921, 147B vehicle, B.P. A, X/L = 0.025, lower surface, fuselage)

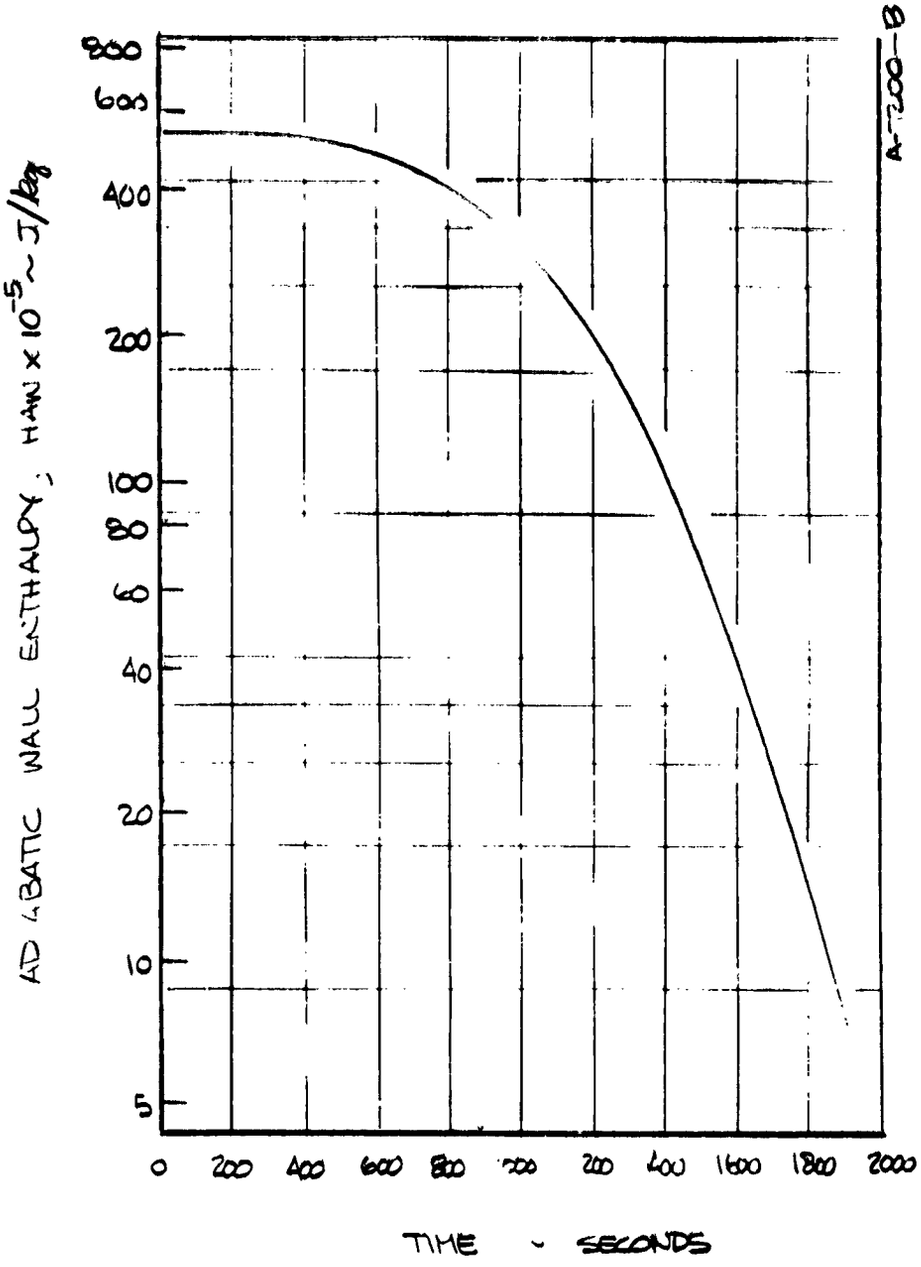

Figure 4. Reentry profile.

(Ref. trajectory 8921, 147B vehicle, B.P. A, X/L = 0.025 lower surface, fuselage)

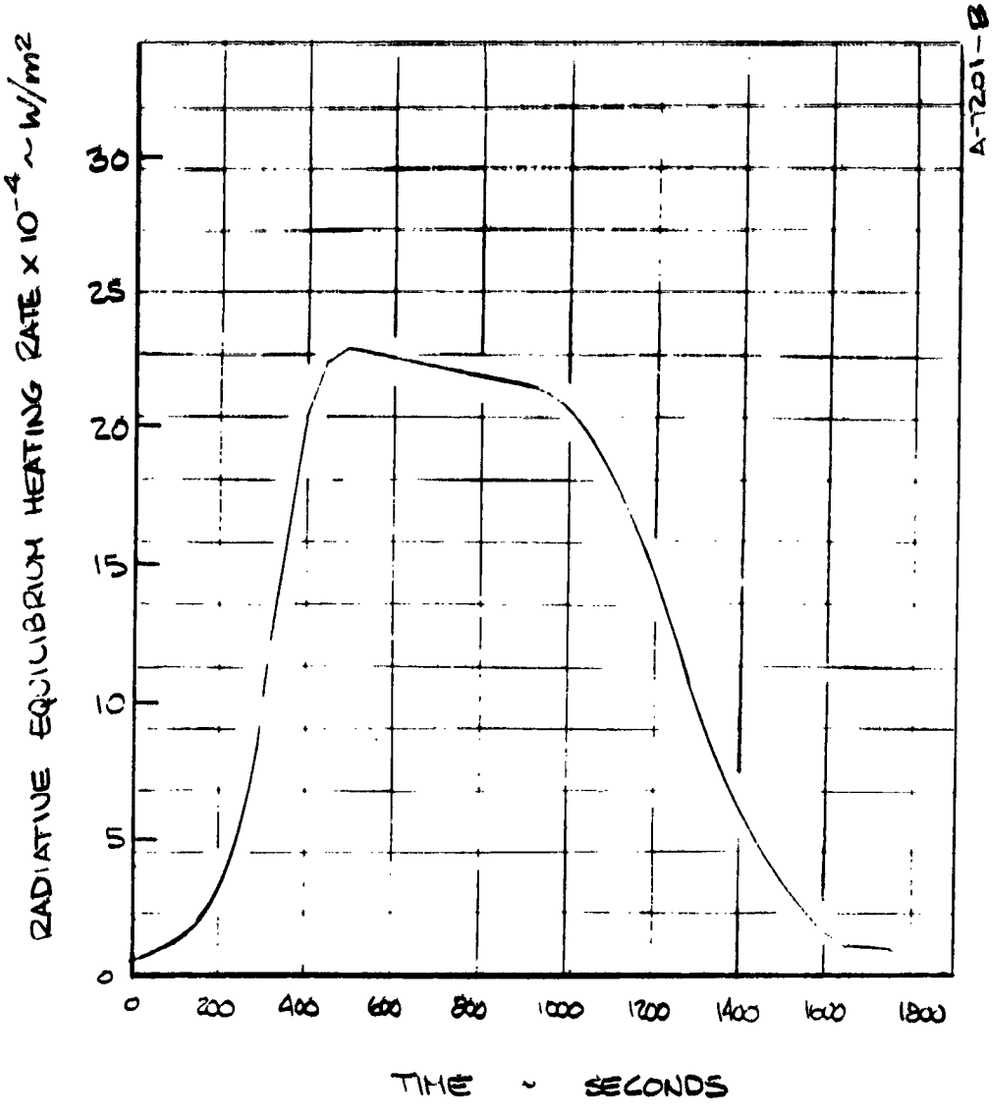

Figure 5. Reentry profile.

(Ref. trajectory 8921, 147B vehicle, B.P. B, X/L = 0.1 lower surface, fuselage)

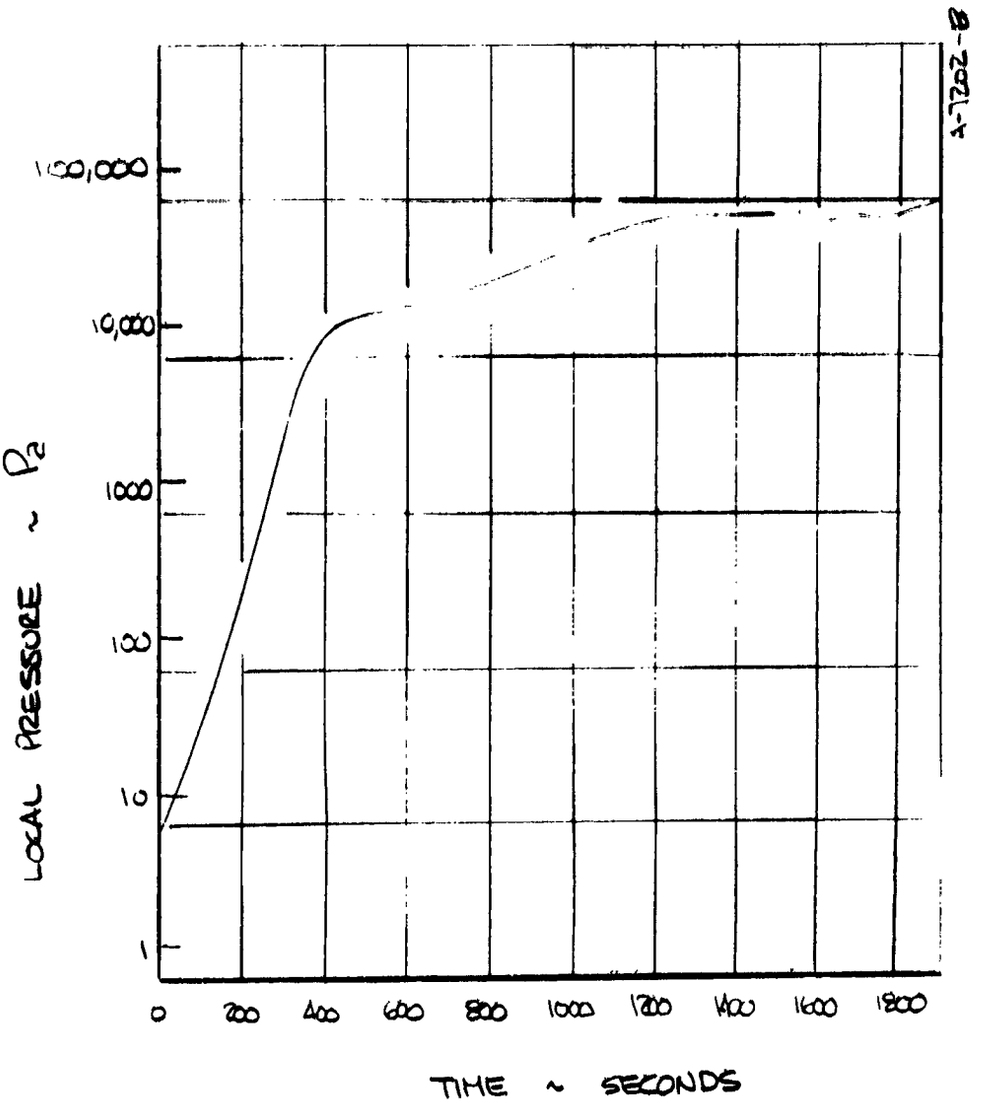

Figure 6. Reentry profile.

(Ref. trajectory 8921, 147B vehicle, B.P. B, X/L = 0.1 lower surface, fuselage)

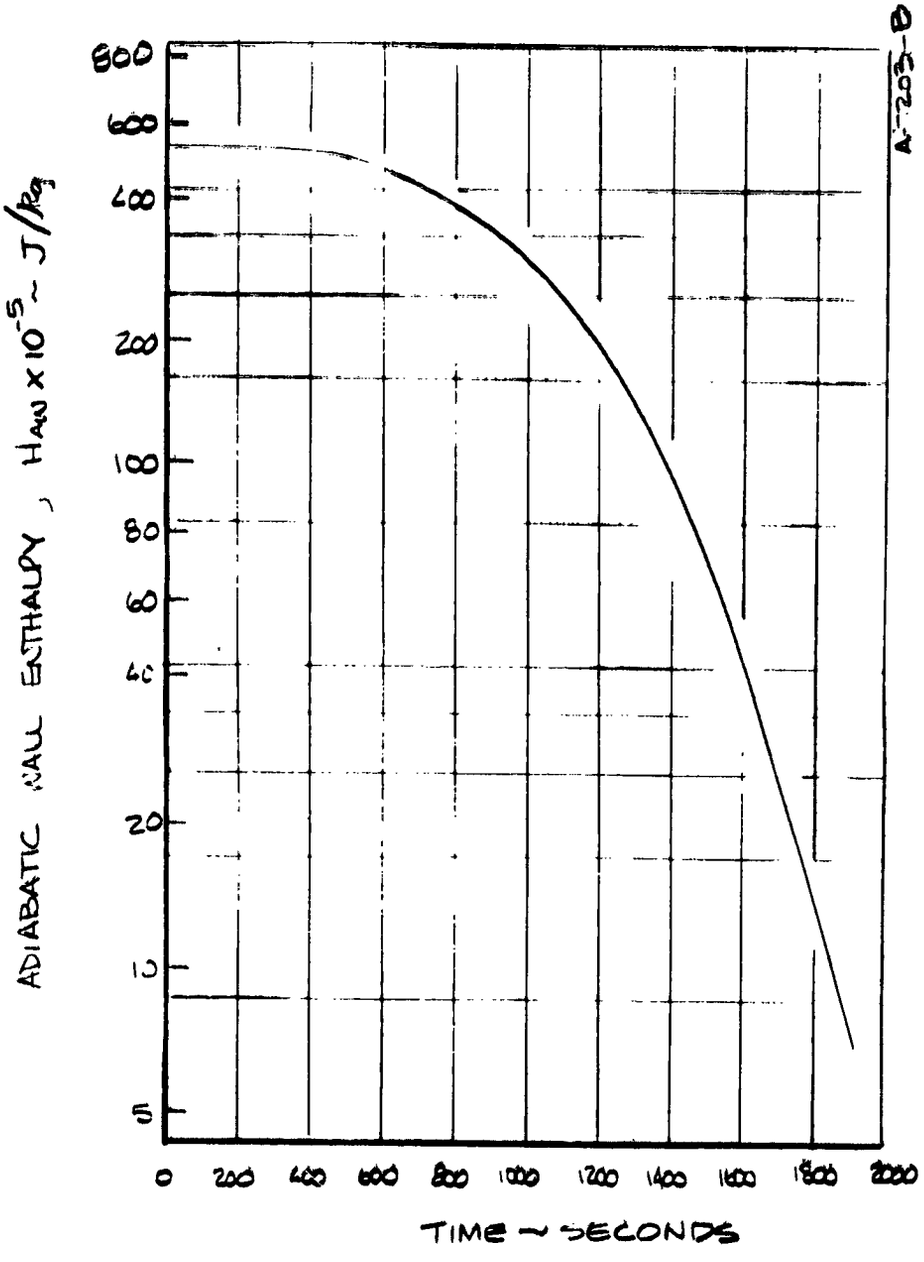

Figure 7. Reentry profile.

(Ref. trajectory 8921, 147B vehicle, B.P. B, X/L = 0.1 lower surface, fuselage)

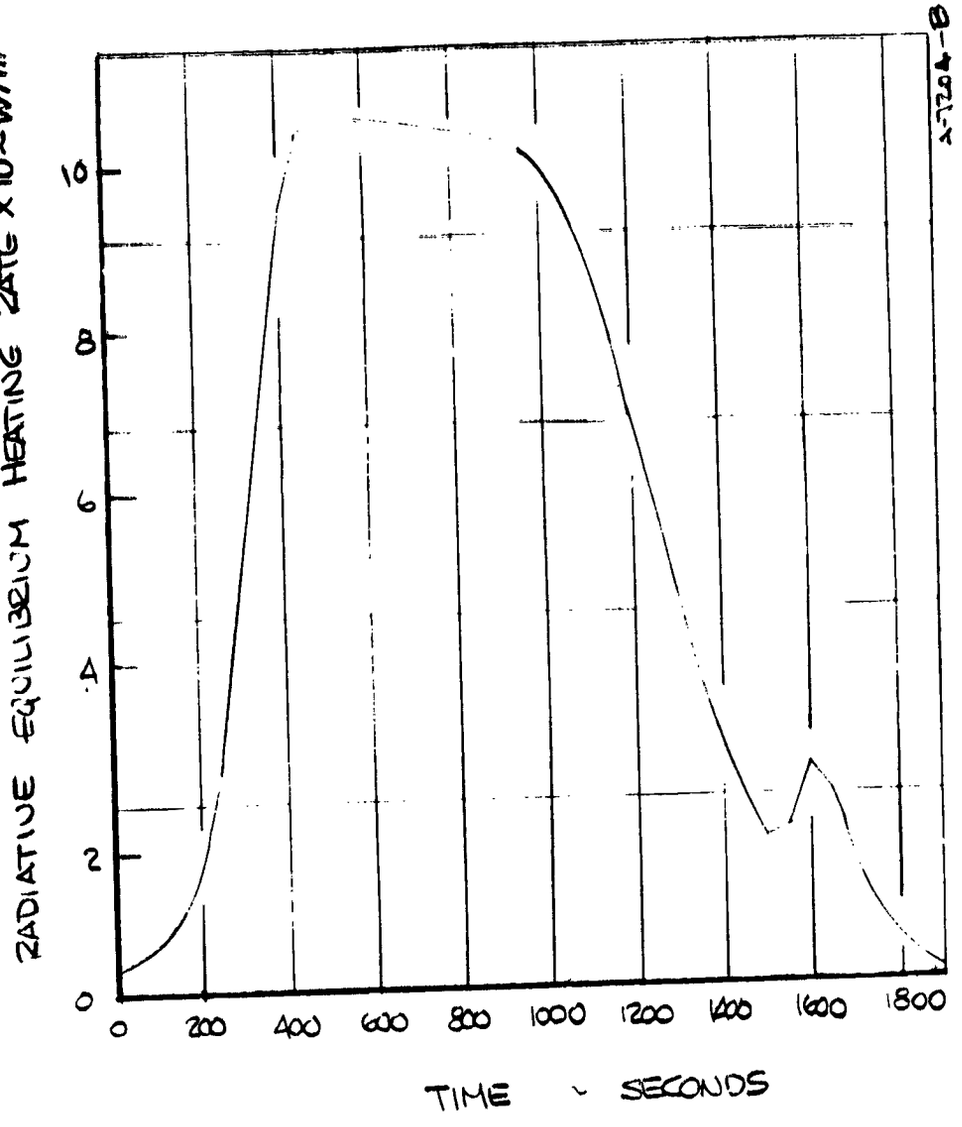

Figure 8. Reentry profile.

(Ref. trajectory 8921, 147B vehicle, B.P. C, X/L = 0.3
lower surface, fuselage)

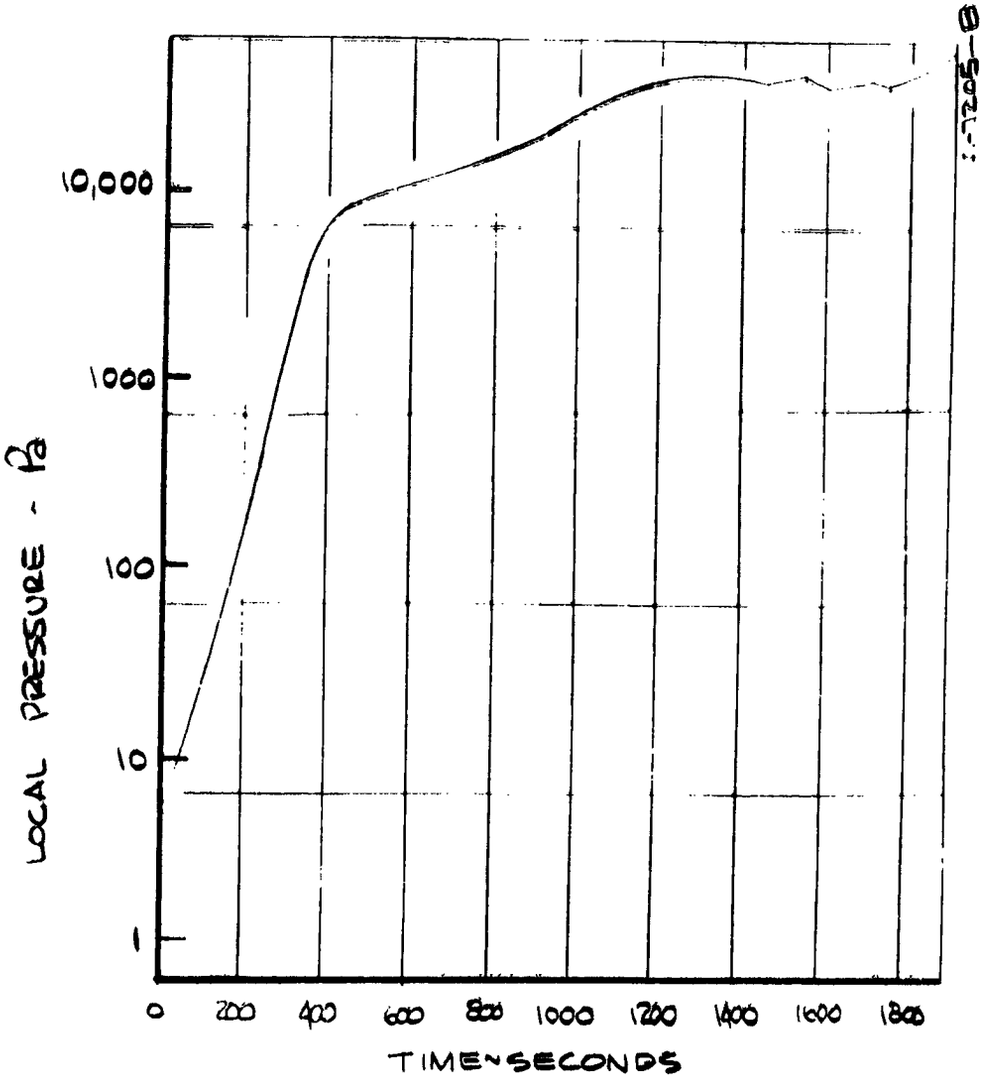

Figure 9. Reentry profile.

(Ref. trajectory 8921, 147B vehicle, B.P. C, X/L = 0.3 lower surface, fuselage)

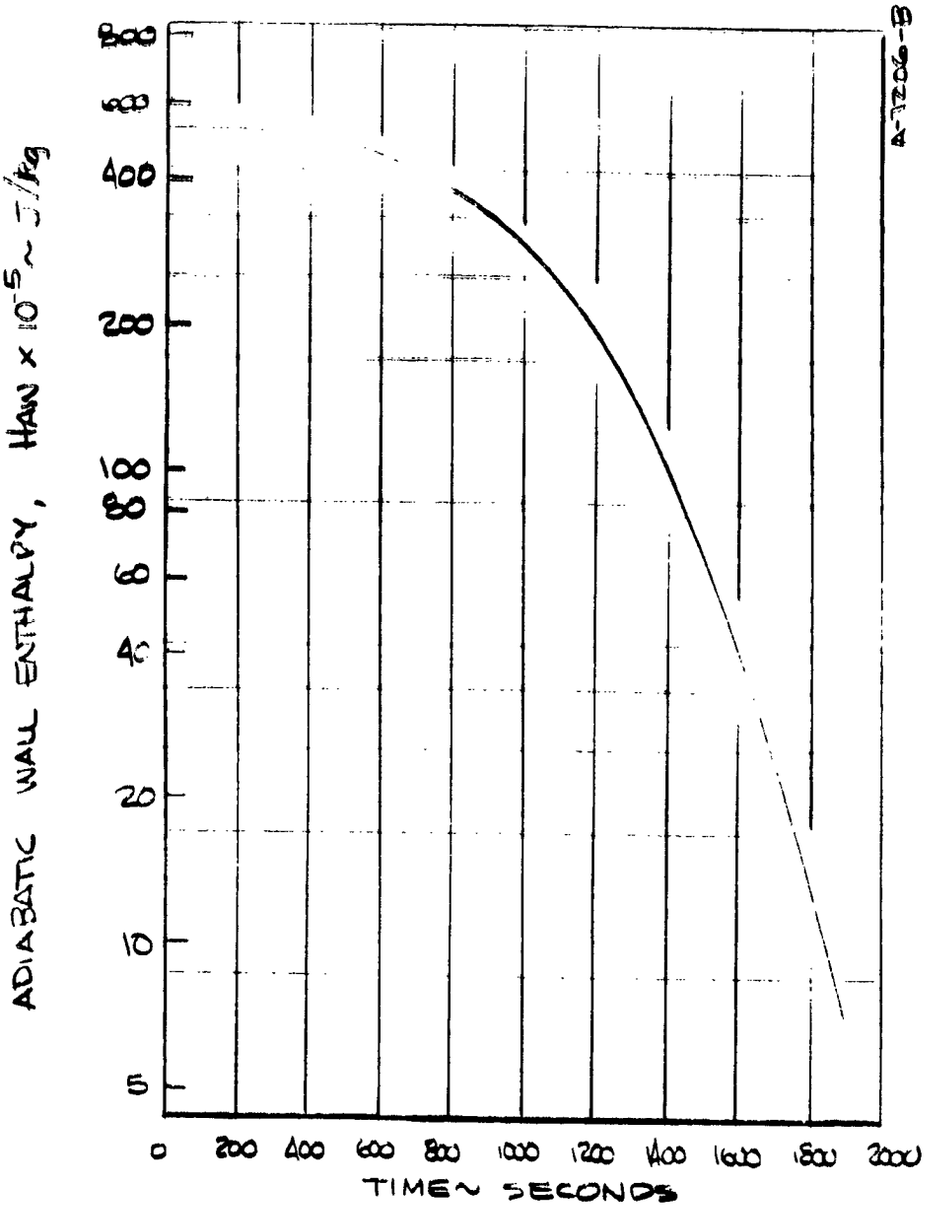

Figure 10. Reentry profile.

(Ref. trajectory 8921, 147B vehicle, B.P. C, X/L = 0.3 lower surface, fuselage)

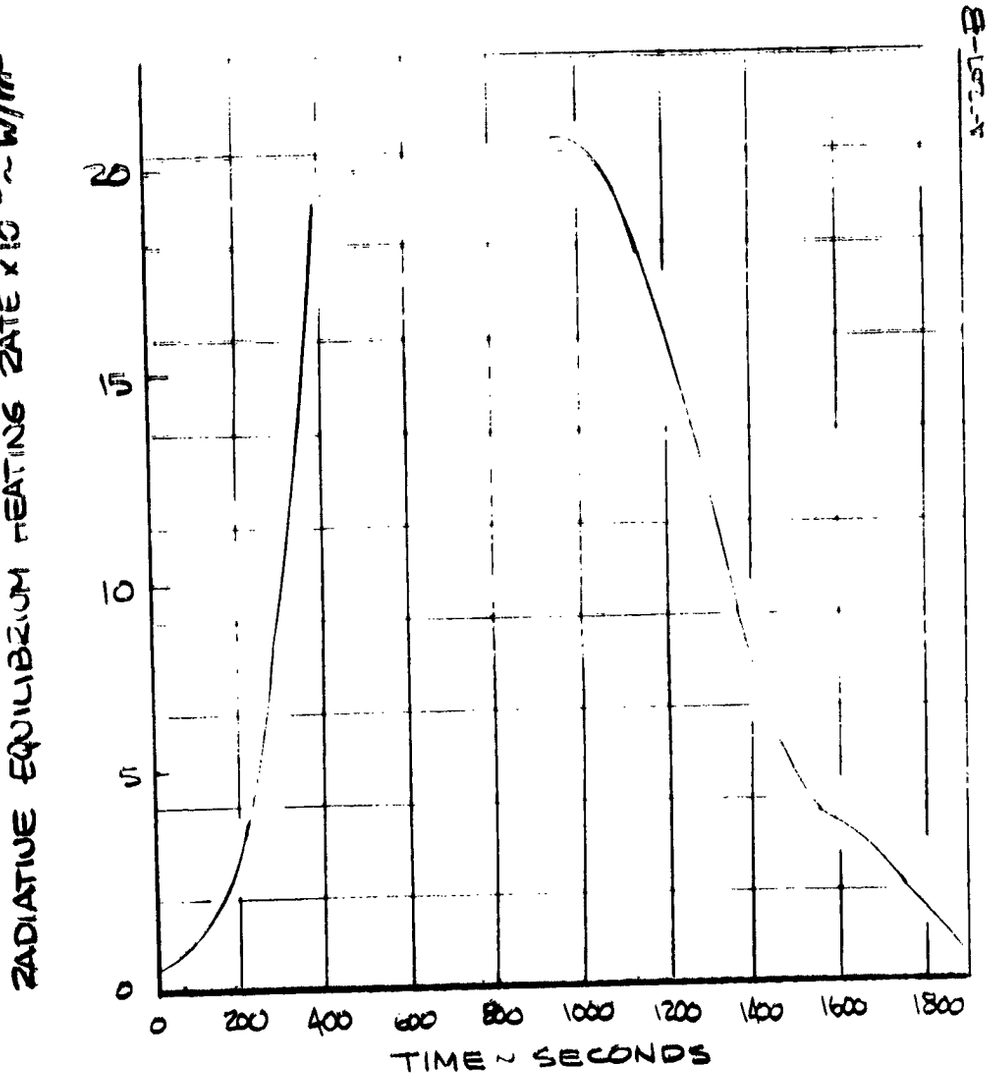

Figure 11. Reentry profile.

(Ref. trajectory 8921, 147B vehicle, B.P. D, X,C = 0.5, 50" span vertical stabilizer)

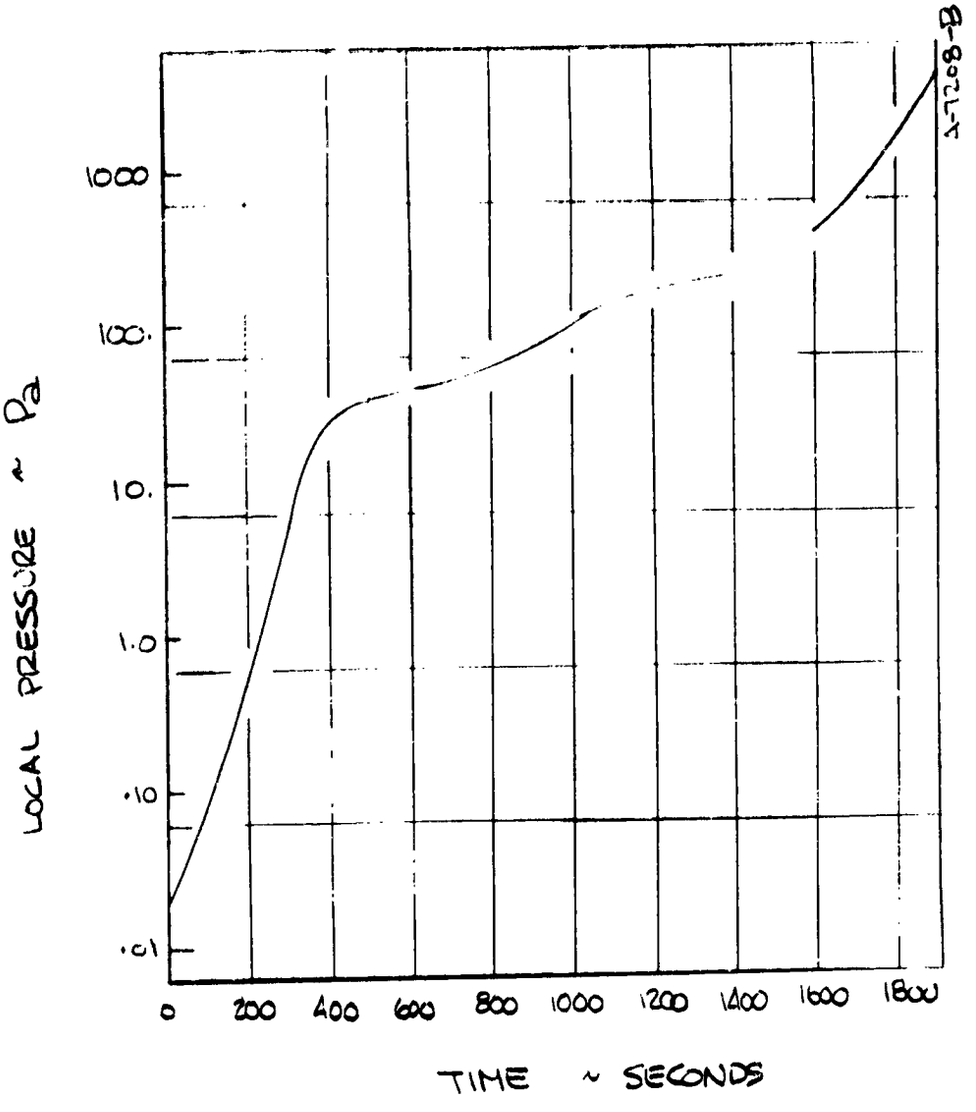

Figure 12. Reentry profile.

(Ref. trajectory 8921, 147B vehicle, B.P. D, X/C = 0.5, 50" span vertical stabilizer)

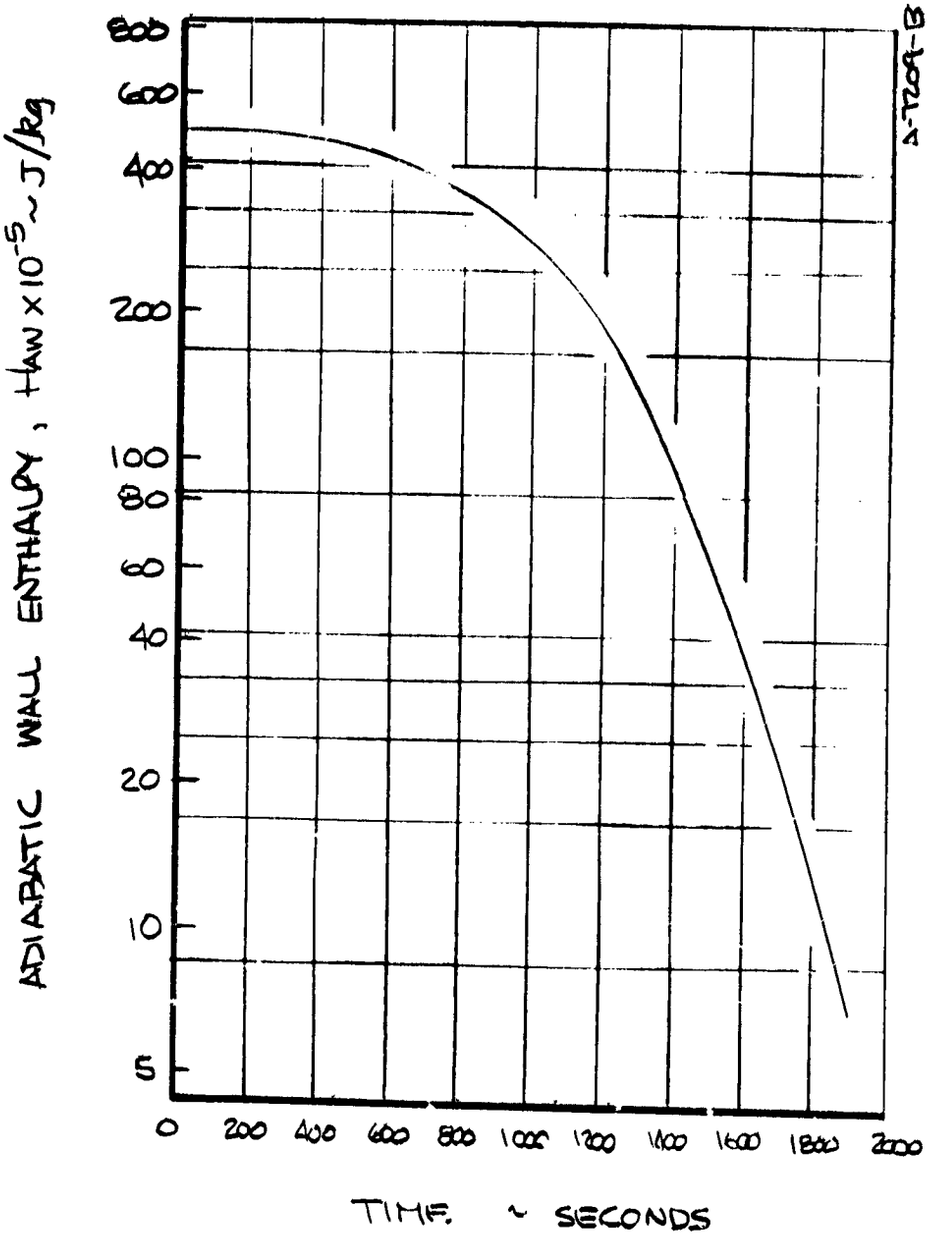

Figure 13. Reentry profile.

(Ref. trajectory 8921, 147B vehicle, B.P. D, X/C = 0.5, 50 span vertical stabilizer)

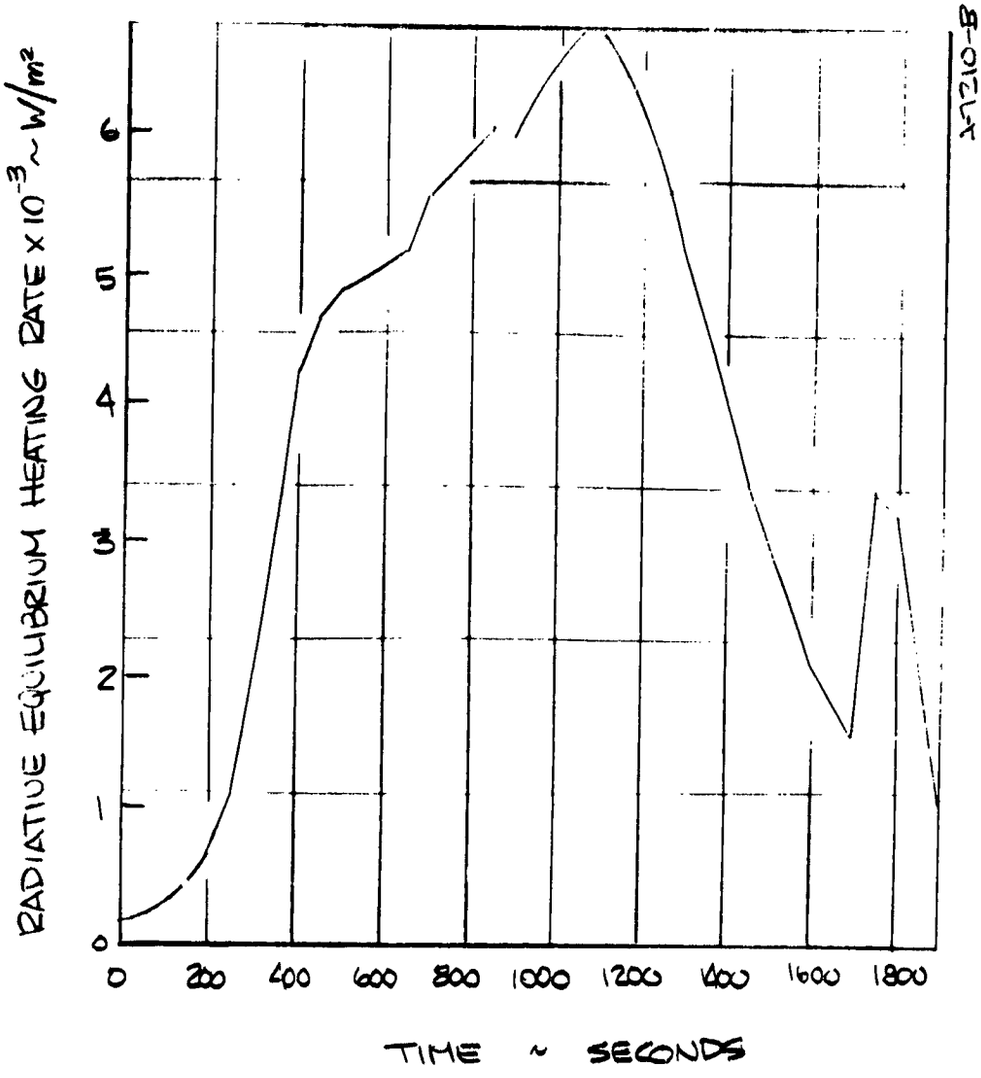

Figure 14. Reentry profile.

(Ref. trajectory 8921, 147B vehicle, B.P. E, X/C - 0 15, 60% halfspan upper surface, wing)

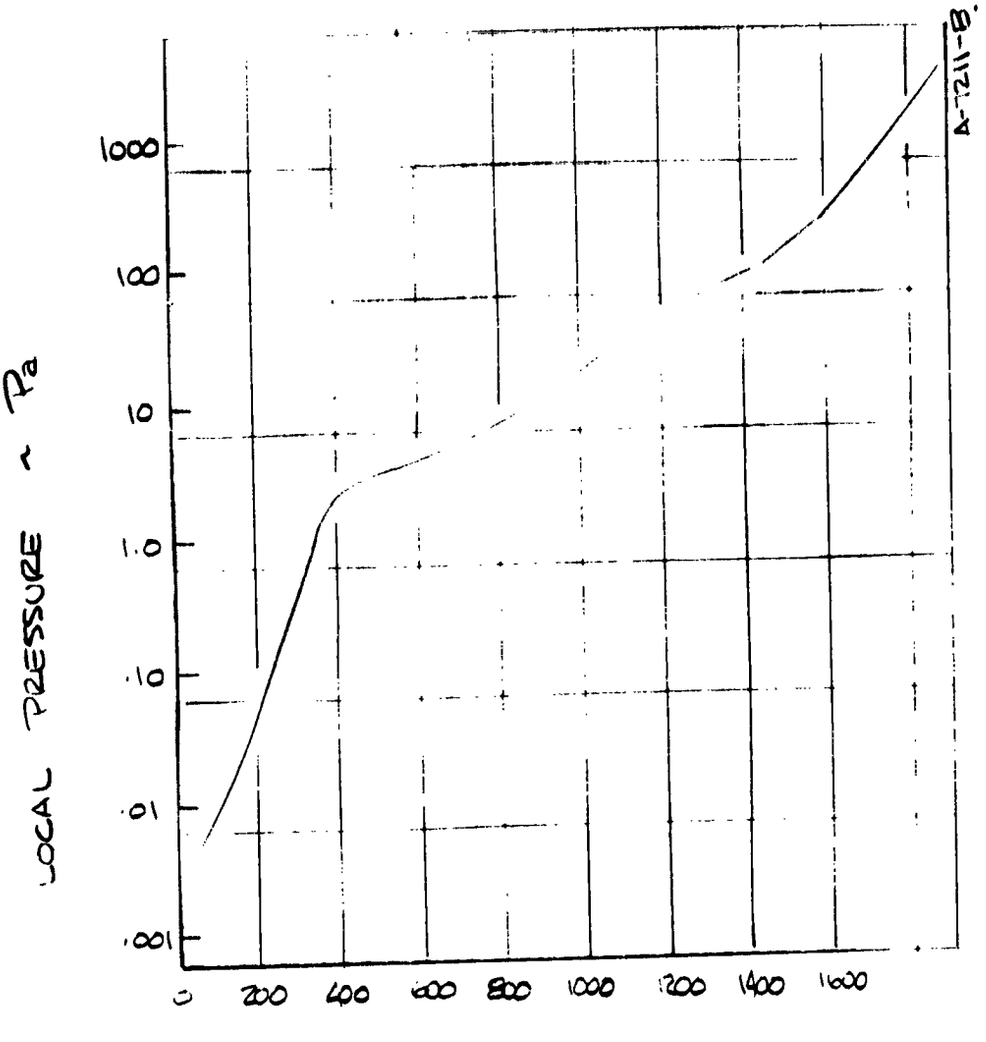

Figure 15. Reentry profile.

(Ref. trajectory 8921, 147B vehicle, B.P. E, X/C = 0.15, 60° halfspan upper surface, wing)

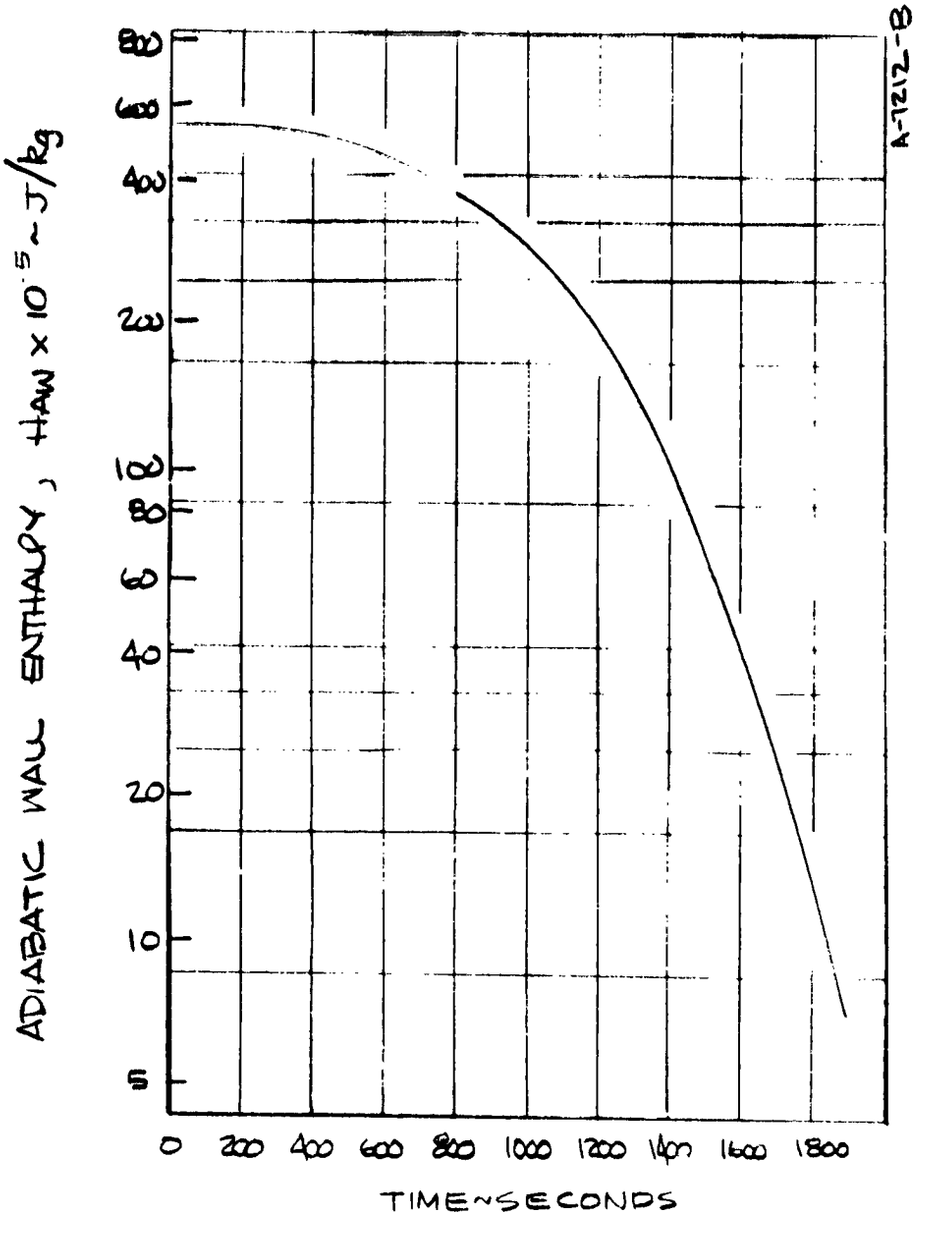

Figure 16. Reentry profile.

(Ref. trajectory 8921, 147B vehicle, B.P. 1, X/C 0.15, 60° halfspan upper surface, wing)

TABLE 1. HRSI COATING THERMOPHYSICAL PROPERTIES

$\rho = 1665/kg/m^3$

Temperature (K)	Thermal Conductivity (W/m-K)	Specific Heat (J/kg-K)	Thermal Expansion ($\Delta L/L_o$)
117	0.735	628	-1.3×10^{-4}
172	0.788	711	-1.1×10^{-4}
256	0.843	795	-0.3×10^{-4}
394	0.951	900	$+1.1 \times 10^{-4}$
533	1.045	1004	2.4×10^{-4}
672	1.131	1088	3.8×10^{-4}
811	1.218	1192	5.1×10^{-4}
950	1.297	1355	6.3×10^{-4}
1089	1.376	1318	7.1×10^{-4}
1200	1.434	1360	7.4×10^{-4}
1228	1.449	1381	7.3×10^{-4}
1339	1.506	1423	7.0×10^{-4}
1367	1.528	1444	6.8×10^{-4}
1422	1.549	1464	-0.4×10^{-4}
1450	1.564	1477	—
1533	1.614	1506	—

TABLE 2. HRSI THERMOPHYSICAL PROPERTIES

ρ = 144 kg/m^3

Temperature (K)	Transverse Thermal Conductivity (W/m-K)					Specific Heat (J/kg-K)	Thermal Expansion ($\Delta L/L_o$)
	Pressure (Pa)						
	10.13	101.3	1013	10132	101325		
117	0.009	0.013	0.026	0.038	0.040	293	-0.5 x 10^{-4}
172	0.010	0.014	0.029	0.040	0.043	439	-0.3 x 10^{-4}
256	0.013	0.017	0.032	0.043	0.048	628	-0.1 x 10^{-4}
394	0.016	0.022	0.039	0.055	0.059	879	+0.7 x 10^{-4}
533	0.022	0.029	0.048	0.069	0.075	1054	1.5 x 10^{-4}
672	0.030	0.038	0.056	0.085	0.092	1151	2.9 x 10^{-4}
811	0.040	0.048	0.068	0.104	0.114	1205	3.8 x 10^{-4}
950	0.053	0.060	0.085	0.125	0.135	1238	4.4 x 10^{-4}
1089	0.072	0.079	0.107	0.151	0.163	1256	5.0 x 10^{-4}
1200	0.092	0.100	0.127	0.176	0.189	1264	5.0 x 10^{-4}
1228	0.098	0.105	0.133	0.183	0.196	1268	5.7 x 10^{-4}
1339	0.121	0.130	0.156	0.212	0.226	1268	6.3 x 10^{-4}
1367	0.127	0.135	0.163	0.219	0.235	1268	6.2 x 10^{-4}
1422	0.140	0.148	0.174	0.235	-.252	1268	3.5 x 10^{-4}
1450	0.147	0.156	0.187	0.244	0.261	1268	-0-
1533	0.167	0.177	0.200	0.268	0.288	1268	—

- Sensitivity
- Response time
- Compatibility with TPS
- Ruggedness and reliability
- Lifetime and maintainability
- Calibration requirements
- Data handling and reduction requirements
- Cost
- Weight

The operating environment includes preflight, ascent, orbit, reentry, and lower atmospheric flight. In addition, consideration must be given to the effects of (1) humidity, temperature, and handling during preflight, and (2) vibration and acoustical noise during ascent and reentry.

2.2.3.1 Heat Flux Sensors

In order to evaluate the various calorimeters under review, a comprehensive evaluation criteria list was generated covering those calorimeter characteristics which impact on the present application. A somewhat condensed listing of these criteria is shown on the left side of Table 3. The following paragraphs elaborate upon the information presented in the table. Following a discussion of each gage, a summary is presented together with the recommended selection.

Gardon-Type (Asymptotic) Calorimeter

The circular foil (Gardon-type) gage has been widely used since its initial development by Gardon in 1953. Its steady state and transient response have been thoroughly analyzed in the past, and the second order effects upon performance and the gage effect upon local heat transfer (boundary layer perturbation) has also been examined in detail. The past development of the gage has resulted in a device well proven in many ground and flight test environments. Primary advantages of the Gardon-type gage are a signal output directly proportional to heat flux, good accuracy, comparative freedom from drift, potential for fairly high temperature use (811 K - 978 K (1000°F - 1300°F)), ruggedness in shock, vibration and acoustic environments, and depending upon sizing of foil diameter and thickness, use over a wide range of heat flux environments.

The primary problem associated with the Gardon gage in the present application is the low level of signal generated in low flux environments. The only thermocouple

TABLE 3. CALORIMETER EVALUATION

	Gardon Gage	Thermopile Gardon Gage
Performance		
Time Constant	Variable - 0.3 sec typical	Variable - 0.1 sec for .0047/6-m dia. typical
Linearity	Better than 1 for copper-constantan	Poor - Alloy T/C's not generally possible
Sensitivity	Variable - Generally for 56/45 W/m²	Generally 10-20 times Gardon Gage
Repeatability	Good - ? = copper oxidation?	? observed for 1 run
Calibration Drift	Stable - Coating changes possible	?±1 observed per run in tunnel
Ruggedness		
Handling	Good for small gages, .00005 m foils	Fair-Good-Shock Sensitive
Shock	Good - 20 to 100g typical	Unknown - lead wires shock sensitive
Vibration	Good - 20 to 50g rms typical	Unknown - possible lead wire failure
Acoustic	Good - 160 db typical	Unknown - used in M - 5 tunnels
Decompression	Good - 33.8 Pa in 160 sec typical	Probably same as Gardon Gage
Temperature Cycling	Good - copper oxidation?	Unknown - possible insulation failure
Vacuum Outgassing	Good - materials stable	Unknown - probably controllable
U.V. Degradation	Depends only on coating	Depends only on exterior coating
Peak Survival Temperature	Good - 811 K typical if copper protected	limited by electrical insulation (533 K typ.)
Moisture Resistance	Good - 10 days MIL-E-5272C typical	Probably like Gardon Gage if sealed
Installation		
Thermal & Structural Perturbation	Variable depending on heat load, size. Large size for low flux	Variable, but smaller than Gardon Gage because of increased sensitivity
Wiring output	Copper wire pair	Copper wire pair
Calibration		
Technique	Coating/radiant heat	Coating/radiant heat
After Installation	Coating/radiant heat (portable lamp)	Coating/radiant heat (portable lamp)
Error Analysis		
Boundary Layer Perturbation	Calculate - 50% error in hot wall	Comparable to Gardon Gage
Catalycity effects	Dependent upon coating	Dependent upon coating
Previous History		
Usage	Extremely widespread including space	Limited - few tunnel runs, flight
Data availability	Excellent including analytical development	Limited to some tunnel work
Device availability	Excellent - off-the-shelf sources	Poor - essentially custom only
Other Comments	Possible problems with oxidation of copper center wire can be handled by N_2 fill and sealing back. Coating effects can show up on thin foil gages. Possible nonlinearity due to poor grade constantan.	Variable sensitivity requires monitoring thermocouple output. Primary problems relate to electrical insulation - Stability and quality of vapor deposition bonds.
Summary	Most extensive background of all gages. Fragility of thin foils makes gage useful only in high flux location. Large ΔT required for sensitivity means (1) large size, (2) thin foil, (3) large sink, (4) compromised reliability of center wire. No monitoring T/C required for data reduction. Must protect copper from oxidation - then overtemperature survival is excellent. Cost is moderate ($150 typical).	Limited background. Complexity justified only for low flux locations. Good sensitivity, but monitoring T/C required to reduce data. Numerous unknowns require much testing. Need materials evaluation. Overtemperature capability limited by insulation. Good sensitivity gives high level signal without need of amplifier. Gages alone are expensive ($500-$1000 each).
Data Reduction	Simple - output proportional to flux, but different calibration curves required for different gages.	Linear or nonlinear output. Need monitoring T/C data to reduce flux data; real time data reduction difficult.

TABLE 3 (continued)

	OP-AMP Gardon Gage	Schmidt-Boelter Gage
Performance		
Time Constant	Variable 0.1-0.5 sec typical	0.3 sec typical
Linearity	Better than 3% for copper-constantan	Good - sensitivity shift w/temp.
Sensitivity	Dependent on amp gain - 10X Gardon Gage typical	Very good - usually for ~56/45 W/m²
Repeatability	Good - lower T possible than Gardon	Good if not overtemperatured
Calibration Drift	Stable - thick foil reduced coating effect	Stable with Kapton film
Ruggedness		
Handling	Good (thicker foils, smaller diameter)	Fair unmounted, very good mounted
Shock	Good - 20 to 100g typical	Very good - 100g 4 routinely
Vibration	Good - 20 to 50g RMS typical	Very good
Acoustic	Good - Comparable to Gardon Gage	Very good
Decompression	Good - Thick foil; smaller diameter	Very good
Temperature Cycling	Good - reduced oxidation - lower T	Good with kapton below 533 K
Vacuum Outgassing	Good - materials stable	Good with kapton, polyimides
U.V. Degradation	Depends only on coating	Good with kapton
Peak Survival Temperature	Good - 811 K+ if copper protected	Max. 533 K for stability, 644 K abs. max.
Moisture Resistance	Good - comparable to Gardon Gage	Good for glass, possibly Kapton
Installation		
Thermal & Structural Perturbation	Variable, but should be good because of small possible size	Depends upon size - generally larger for larger flux
Wiring Output	Copper wire pair, shielded	Wire pair
Calibration		
Technique	Coating/radiant heat	Radiant heat or graphite block
After Installation	Coating/radiant heat (portable lamp)	Radiant heat (coated) (portable lamp)
Error Analysis		
Boundary Layer Perturbation	Comparable to Gardon Gage	Unknown - expect comparable to Gardon Gage
Catalicity Effects	Dependent on coating	Generally minimal
Previous History		
Usage	Arc jets (2 years)	Widespread, space qualified
Data Availability	Good (arc jet use)	Excellent - extensive data available
Device Availability	Off-the-shelf sources	Excellent - off-the-shelf
Other Comments	Primary problem is amp zero drift with temp. (must zero check or compensate amp). Some possible problem with copper oxidation, but less so than Gardon Gage because of lower operating ΔT.	While organics appear stable, questions remain about long term stability. Excellent sensitivity possible, but monitoring thermocouple is mandatory. Small diameter possible in low flux areas.
Summary	Gage head is small, tough Gardon, and has all attributes of Gardon, but much smaller size. Can use same gage in all locations. Data indicates no susceptibility to noise. Minimum tile perturbation because of small size. Same copper oxidation problem as Gardon Gage but to lower degree. Better overtemperature survival than Gardon because of small ΔT. Cost moderate ($300/channel).	Extensive background available in low flux applications. Size of sink required forbids use in high flux areas. Biggest drawback is requirement for monitoring thermocouple. No margin for overtemperature because of organic materials behavior. Long term stability questionable. No amps required in low flux locations. Low cost ($50-$100).
Data Reduction	Simple - output proportional to flux. Amp gain can be adjusted to compensate for gage-to-gage sensitivity variation.	Requires reference to monitoring T/C output; real time data reduction difficult.

TABLE 3 (concluded)

	Equilibrium Slug	Thermocouple
Performance		
Time Constant	Temp dependent: 2 to 40 sec	Depth dependent - 2 to 200 sec typ.
Linearity	Nonlinear device	No direct reading of flux
Sensitivity	Excellent, particularly at low temp.	Depends on depth - can be good
Repeatability	Good	Excellent if silica compatible
Calibration Drift	Stable	Excellent if silica compatible
Ruggedness		
Handling	Good	Good after installation
Shock	Good	Good after installation
Vibration	Good	Excellent
Acoustic	Good	Excellent
Decompression	Good	Excellent
Temperature Cycling	Good - materials stable	Excellent
Vacuum Outgassing	Good - materials stable	Good - possible alloy volatilization
U.V. Degradation	Depends only on coating	Excellent - no exposure
Peak Survival Temperature	1533 K	1922 K+ possible
Moisture Resistance	Good	Excellent
Installation		
Thermal & Structural Perturbation	Good - no sink required - no thermal path through tile	Minimum - no thermal sink required; minimum possible lead
Wiring Output	T/C wire pair - ref. T/C required	Thermocouple pair
Calibration		
Technique	Coating/radiant heat	RCS calibration data
After Installation	---	Not possible for heat flux
Error Analysis		
Boundary Layer Perturbation	Minimum - approximately at wall temp	None
Catalycity Effects	Dependent on coating	None - no exposure
Previous History		
Usage	Thermal-vacuum tests at Aerotherm	Apollo, ground test
Data Availability	Limited	Good
Device Availability	Custom device	Excellent
Other Comments	Not off-the-shelf so development program required. Must minimize wafer thickness to reduce time constant.	Silica compatibility of some T/C materials uncertain. Possible alloy volatilization possible. Variation in RSI properties requires pressure history to reduce data.
Summary	Unique device not commercially made. Advantages: Temp. perturbation to boundary layer less severe than other gages. No sink required. Disadvantages: Development effort required. May need to calibrate out heat leak effects. Nonlinear output, long time constant. Cost should be comparable to Gardon Gage once developed.	Advantages: Rugged, simple. No boundary layer perturbation, minimum tile perturbation. Gives local temperature history. Disadvantages: Complicated data reduction requires pressure history, computer analysis. Direct flux calibration not possible. Time constant, material compatibility uncertainties. X-ray examination of each tile mandatory. Cost - $25-$50 per calibrated thermocouple.
Data Reduction	Nonlinear output, but no monitoring T/C output required.	Exceedingly complex requiring computer; real time data reduction impractical.

that gives a constant sensitivity independent of temperature in the required range is copper-constantan. Generation of a 10-millivolt signal requires a temperature differential between the center and edge of the foil of 211 K (380°F). In order to achieve this temperature difference at low fluxes it is necessary to use a large diameter and a thin foil (typically 0.0203 m (0.8 inch) diameter and 0.0000254 m (0.001 inch) thickness foil for a flux of 6809 W/m² (0.6 Btu/ft²sec)). This results in a fragile gage with susceptibility to vibration and shock. Further, the errors due to center wire conduction and coating variation can become appreciable because of the relative thinness of the foil. Finally, the heat load on the gage (total integrated flux input) is proportional to the frontal area of the gage, and the gage being large in diameter, requires that it have a large heat sink to handle the large heat load. As a result, the size and weight of the gage and heat sink assembly rapidly escalates with resulting large perturbation to the structural and thermal integrity of the tile.

The situation is somewhat different in the high flux locations (56,745 W/m (5 Btu/ft²sec)) because the required 10-millivolt signal can be obtained from a gage of small diameter and reasonable foil thickness (for example, using a foil thickness of 0.000051 m (0.002 inch) requires a diameter of 0.00483 m (0.19 inch) at a heat flux of 2.27×10^5 W/m² (20 Btu/ft²sec)). Discussions with manufacturers and users suggest that a 0.000051 m (0.002 inch) thick foil is a practical minimum to give a gage of reasonable ruggedness and reduced sensitivity to errors arising from center wire conduction losses and variable coatings. In the low flux location a 0.000051 m (0.002 inch) foil results in a foil diameter of over 0.0254 m (1.0 inch) for a 10-millivolt output. The 0.00483 m (0.19 inch) diameter at the high flux location is much more reasonable and results in a gage of greatly increased ruggedness. The small diameter also minimizes the problems of heat leaks from the hot surrounding RSI.

The Gardon gage thus appears to be a good candidate for the high flux location because of its small size, ruggedness, and good performance. However, one particular problem needs to be examined. In order to minimize the size of the heat sink associated with the gage it is desirable to allow the sink to make the largest possible rise in temperature during the heating phase. Experience indicates that the constant sensitivity behavior of the copper-constantan Gardon gage is limited to temperatures below about 478 K (400°F). The temperature difference across the foil at peak heating is 211 K (380°F) in order to obtain the desired signal condition, so that the peak temperature at the center of the foil where the copper center wire is attached is about 689 K (780°F). Discussions with some manufacturers have indicated that at these temperatures oxidation of the center wire can become a severe problem. The small size of the wire (typically 0.0000254 m (0.001 inch) diameter) implies that oxidation can destroy the wire after just one temperature cycle. One manufacturer claims that 1/2 percent repeatibility can be obtained up to a temperature

of 394 K (250°F), and 1 percent repeatibility can be obtained up to 422 K (300°F), with the limitation being copper oxidation. Higher temperatures require that steps be taken to prevent oxygen from coming in contact with the copper center wire. The procedure generally used is to minimize the cavity volume by filling most of the cavity with a high temperature potting compound leaving a small thin cavity behind the constantan disc and sealing it at the same time. This minimizes the oxygen available for oxidation and apparently provides sufficient protection as gages constructed in this way have been run in excess of 533 K (500°F) (foil center) in arc jet and radiant heat facilities and then opened for inspection after repeated temperature cycling. Examination showed bright unoxidized surfaces inside the gage cavity. An alternate procedure would be to evacuate the cavity behind the foil and then backfill and seal in an inert gas, typically nitrogen. Back-filling with helium worsens the error due to center wire conduction because of the higher thermal conductivity available with helium. The oxidation problem can thus be handled, but some care must be exercised in sealing the gages to assure a hermetic seal. A possible third approach to the oxidation problem is to vapor deposit a thin layer (1 micron) of silica inside the gage cavity. Silica has been used in the past for surface protection of a variety of materials, and performs well in severe environments.

Another problem of the Gardon gage is shared with all "cold wall" gages, and this is the problem of boundary layer perturbation and subsequent local variation in heat flux. The Gardon gage surface would run in the temperature range of 478 K (400°F) to 700 K (800°F) while located in an insulating wall which can have surface temperature as high as 1478 K (2200°F). The presence of a cold spot in the hot wall perturbs the boundary layer. Preliminary estimates of the error induced by the presence of the cold gage have been made using the BLIMP program on a simplified model which assumes a simple step change in temperature along the wall. The preliminary results indicate that the local heating rate can vary by 30 percent over the unperturbed heating rate. Consequently all cold wall gages will have to be carefully evaluated from the standpoint of boundary layer perturbation.

Catalycity effects arising from nonequilibrium conditions in the boundary layer can occur on the gage surface depending upon the nature of the surface presented to the boundary layer. With the Gardon gage catalytic or noncatalytic coatings are possible by merely applying the desired coating to the foil surface. Care must be taken to select a coating that will not affect the thermal behavior of the foil during reentry, and further that the coating be stable in the vacuum and solar heating environment encountered in orbit. The coating must also have the appropriate α/ε to prevent excessive temperature rise during exposure to solar radiation.

Calibration of the Gardon gage is normally obtained by subjecting the gage to a radiant heat source of known flux. The gage is coated with a well known high absorption layer (typically a very thin layer of colloidal graphite or soot) before

testing, and the special coating is removed after calibration. One manufacturer now produces a portable calibration standard using radiant heating that could conceivably be used to calibrate the gage in situ on the spacecraft. The only requirement is that the absorbing coating be applied before calibration and then removed afterwards. Calibration standards have been well worked out for Gardon gages and calibration is not expected to present serious problems.

To summarize, the Gardon gage is limited only to high flux areas for reasons of size and ruggedness. In the high flux areas the gage would be expected to perform well giving good linearity, high level output signal, and reasonably small size. Past experience indicates ruggedness is good in small sizes. One problem to be considered is the oxidation of the copper center wire. Possible solutions are backfill with inert gas and seal, or vapor deposition of silica to prevent oxygen contact with the copper.

Thermopile Gardon-Type Calorimeter

The thermopile Gardon-type gage consists of a Gardon gage with no center wire, an electrically insulating layer on the backside of the foil, and a thermopile vapor-deposited on the electrically insulating layer (see figure 17). The thermopile is usually a rosette type with a ring of thermocouples arranged in a small circle around the center of the foil (measuring the high temperature) and another ring of thermocouples arranged in a circle near the edge of the foil (measuring the lower temperature). Typically, 6 or 12 thermocouples are used to generate a larger signal than is possible with a simple Gardon gage. The signal level is further enhanced by using high sensitivity thermocouples (bismuth/antimony have been used) and a foil with a lower thermal conductivity than constantan (typically stainless steel). As a result signal levels 10 to 20 times that obtainable from a comparable Gardon gage are possible. This permits the gage to be used in low flux environments (less than 11,349 W/m (1 Btu/ft-sec)) and still generate millivolt level signals from a gage 0.00635 m (0.25 inch) or less in diameter. A major disadvantage of the device is that the output is not linear due to nonlinearity in the high sensitivity thermocouples used, and the sensitivity varies depending upon the device temperature. Thus in order to use the device in an environment whose temperature is changing more than several tens of degrees requires a reference thermocouple in the gage to monitor the temperature. The data must then be reduced by referring to the temperature history of the device. The data reduction process required causes some complication, but the primary problem associated with this kind of behavior is that two channels of data are required for each gage.

Another disadvantage of the gage is its limited usage in the aerospace industry. ARO Inc. has produced gages for use in hypersonic wind tunnels at AEDC, and

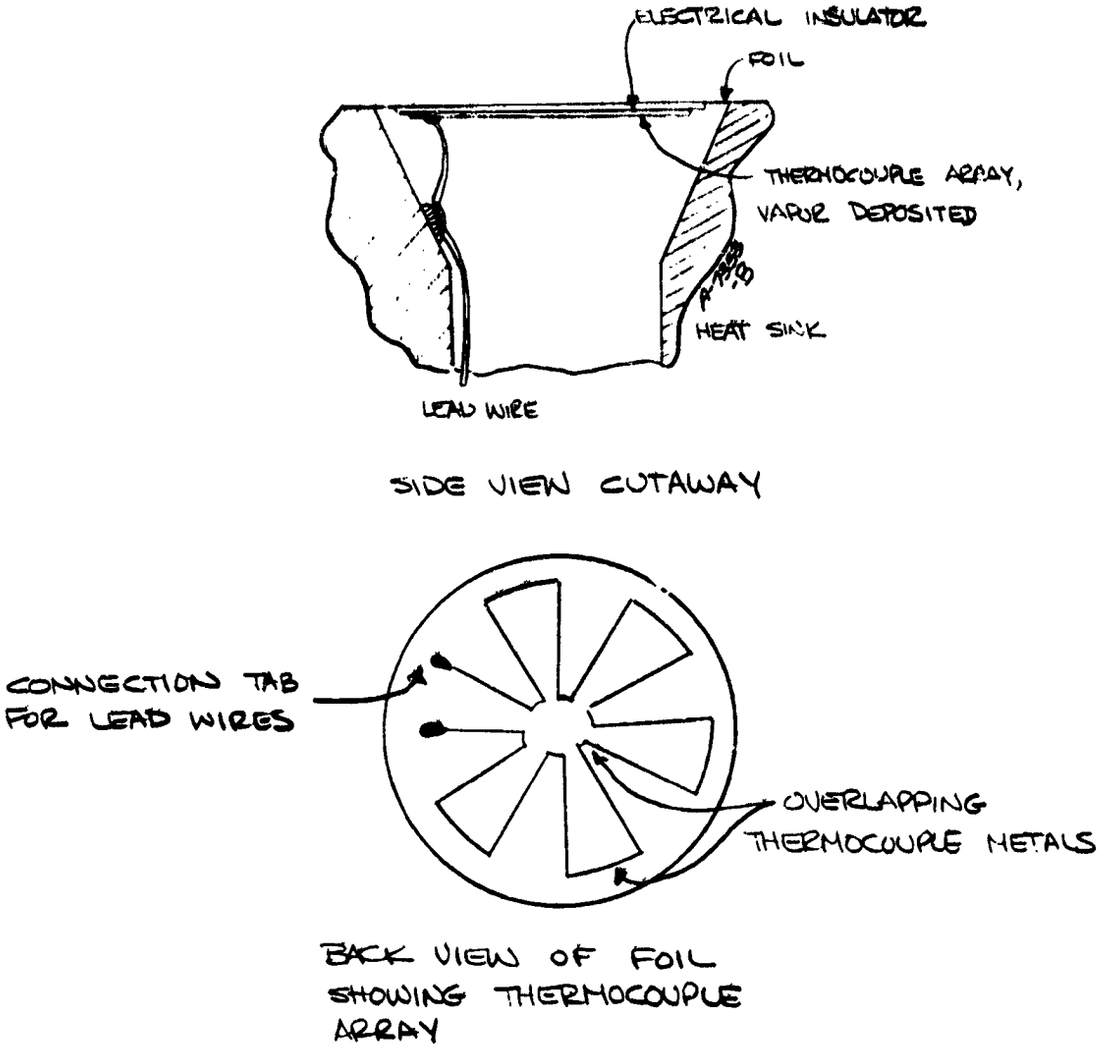

Figure 17. Thermopile-type Gardon gage.

RdF Inc. produced some on a custom basis for Martin-Denver in 1964. Because of the limited usage there is little data available on reliability. Acoustic and vibration ruggedness are undefined, but at least adequate for the unspecified missile work at Martin. Resistance to shock should be better than a conventional Gardon gage because of the absence of a delicate center wire (lead wires in thermopile Gardon gages are usually bonded down). The area of major uncertainty is the insulating layer deposited on the back of the foil. High temperature organics are usually used, and these are stable up to about 533 K (500°F). It is necessary to protect the organic from moisture to prevent properties from changing. Peak survival is expected to be 644 K (700°F), again determined by the organic layer. Recalibration would probably be required after an overtemperature condition because of possible property shifts in the electrical insulator.

Catalycity effects are the same as conventional Gardon gages, and are dependent upon the coating selected to cover the foil. Calibration is also handled the same as a Gardon gage using a special removable coating in conjunction with a radiant heat source. It appears that the thermopile Gardon gage can also be calibrated after installation in the spacecraft by use of a portable radiant source. Boundary layer perturbation effects are also the same as with the Gardon gage. The primary advantage over the Gardon gage is high sensitivity which allows use of a small gage without amplifiers in low flux locations.

Primary disadvantages include variable sensitivity requiring use of a reference thermocouple, limited overtemperature capability, limited usage and large numbers of unanswered questions about the electrical insulation layer required on the foil. At present there are no suppliers producing these types of gages in any volume, although a custom design and fabrication capability does exist in the industry.

Gardon-Type Gage with Operational Amplifier

The combination of Gardon-type gage with a high gain operational amplifier (Op-amp Gardon gage) is discussed as a separate type of device because its behavior and impact are substantially different from either of the two Gardon gages discussed above. The heat flux sensor is a conventional Gardon gage with all the attributes of that type of gage. However, the amplifier (typically a low noise integrated circuit chip plus about a half dozen resistors) allows signals of the order of microvolts to be used, and thus a very low gage sensitivity is adequate to get the required signal level. This trarslates into a gage of very small diameter 0.00203 m (0.080 inch) foil diameter) with fairly thick foil (0.0000508 m (0.002 inch) typical) being used even in regions of low flux. The small gage is exceptionally rugged, and the small size minimizes the heat load both directly from the boundary layer and from heat leaks from the hot RSI.

The reliability of the gage itself should be better than a conventional Gardon gage of larger size because of the extreme ruggedness mentioned above, and because low temperature differences across the foil give satisfactory response. Whereas a conventional Gardon gage using copper-constantan thermocouples requires a temperature difference of 211 K (380°F) to generate a 10-millivolt output signal, a small gage together with an amplifier having a gain of 100 requires a temperature difference across the foil of only 2.11 K (3.8°F). The gain requirement is not excessive; the same amplifier mentioned above can routinely be used with a gain of 1000. As a result, the temperature of the foil center is only slightly above the foil edge temperature, with peak temperatures of 478 K (400°F) being typical (compared to the 700 K (800°F) temperatures possible with conventional Gardon gages). The reduced temperature would be expected to increase reliability because of reduced copper oxidation if oxygen were to leak into the gage cavity.

In the discussion of devices with microvolt level output the question of signal-to-noise ratio immediately arises. Because of the low signal level, there exists the concern that spurious noise arising from electrical activity in the boundary layer or electromagnetic pickup from the environment will become superimposed on the desired output signal of the gage, and thereby generate errors or mask the output signal entirely. The problems appear to be easily handled based upon experience with these types of devices in arc jet applications. Martin-Denver has had over a year of experience with 30 channels of small Gardon gages together with high gain operational amplifiers of the type described in low flux environments. Tests have been made in the arc jet facility at Martin with amplifiers using a gain of 100 and 1000 with no noise problems. Conventional shielded cable was used with all grounding at the amplifier, and no electromagnetic coupling was observed. Tests ranged from a few seconds to 1/2 hour with a total of approximately 30 runs on the equipment thus far. The data generated correlates well with other data and with theoretical predictions with the result that Martin personnel have a high level of confidence in this calorimetry system.

The chief performance disadvantage of the Op-amp Gardon gage is the tendency of the amplifier to drift with temperature. The amplifier has excellent linearity throughout its temperature range, but it has a zero drift of 3mv/10°C. Thus if the amplifier environment is changing in temperature during the reentry (as one would expect it would) the zero drift would have to be monitored. Numerous approaches can be taken with this problem, and all would have to be examined.

Another disadvantage of the Op-amp Gardon gage is the increased complexity arising from the need for the amplifier. The output from several gages would have to be run to zone boxes containing the amplifiers. An amplifier assembly is expected to be quite small with 20 amplifiers requiring one printed circuit card

approximately 0.102 by 0.152 m (4 by 6 inches) in size. Powers would have to be supplied to the zone box to drive the amplifiers (probably 5 or 10 volts DC). However, the small additional weight penalty of the amplifiers would be more than offset by the large expected reduction in sensor heat sink weight.

It is anticipated that reliability and quality control constraints necessary with the semiconductor amplifier could be easily satisfied (if they are not already satisified) by utilization of the specifications and procedures outlined by military specifications (MIL SPECS). It is thus felt that if the necessary components comprising the amplifier assembly can be purchased to appropriate specifications, the reliability and performance standards required will be obtained. In short, the amplifier is not felt at this time to jeopardize the reliability or performance of the calorimeter data channel.

It should be noted that the amplifier has a significant advantage to offset its complexity in that the gain can be adjusted to compensate for variations in gage sensitivity. Gardon gages of a particular size and method of manufacturer vary in sensitivity as much as 15 percent from gage to gage because of variations in manufacturing and assembly tolerances. Each gage then requires its own calibration curve in order to reduce data. By use of the variable gain amplifier, the gain can be adjusted to compensate for these differences, and thus all gages can have the same overall sensitivity, or conversely, the sensitivity of a channel can be tailored to the location of the gage, and made compatible with the data recording system. It is expected that this allowance for adjustment can greatly reduce the complexity of data reduction, and simplify the problems associated with real time data readout.

Like the other two Gardon gages discussed previously, the Op-amp Gardon gage is best calibrated using a special removable coating in conjunction with a radiant heat source. This means that it can probably be calibrated after installation in the spacecraft if necessary. Catalycity effects are controlled by the use of coatings applied to the foil face. Boundary layer perturbation effects are expected to introduce errors similar to the other cold wall gages, but the effect of the small gage size needs to be examined more carefully.

To summarize, the Op-amp Gardon gage has all the advantages of the conventional Gardon gage but with the additional advantages of increased ruggedness, smaller size (with attendent size reduction of heat sink), adjustable sensitivity for use in low or high flux regions, and lower foil center temperature. Primary disadvantages include zero drift in the amplifier, and the increased complexity associated with the amplifier.

Schmidt-Boelter (Gradient-Type) Calorimeter

The Schmidt-Boelter type calorimeter is probably the most widely used calorimeter presently in use, with applications in aerospace (flight and ground test), industry, and even in architecture. The gage operates by measuring the temperature drop across a thickness of material using a thermopile arrangement which can give excellent sensitivity if a sufficient number of thermocouple pairs are used in the thermopile. By careful selection of materials gage linearity can be very good (1 percent), and sensitivity can be held constant over a narrow range of temperatures near room temperature. However, if temperatures exceed approximately 325 K - 339 K (125°F - 150°F), the variations in thermocouple EMF and substrate material thermal conductivity combine to change the gage sensitivity. The most common materials used over extended temperature ranges are Kapton bonded with particular types of polyimide adhesives together with chromel-constantan thermocouples. This combination is linear and exhibits constant sensitivity over the range noted above, but the sensitivity changes approximately 20 percent as the temperature approaches 533 K (500°F). The change in gage sensitivity requires that a thermocouple be carried in the gage to monitor the calorimeter temperature. The temperature history is then referred to together with a temperature-sensitivity variation curve in order to reduce the data. One manufacturer recommends that the monitoring thermocouple be within 2.2 K - 2.8 K (4°F - 5°F) of the thermopile temperature in order to get 1 percent accuracy in the data reduction. It thus becomes mandatory to install a second data channel (for temperature) in order to reduce the heat flux if this type of gage is used.

The Schmidt-Boelter gage offers excellent resistance to shock, vibration, and acoustic excitation because there are no foils or small diameter wires to be damaged. Kapton offers good moisture resistance, ultraviolet radiation resistance, and good general long term stability. Peak survival temperature is limited, however, by the polyimide adhesives used to bond the gage together. At temperatures above 533 K (500°F) the adhesives may begin to change their thermal properties with a possible calibration shift resulting. There also exists the possibility of delamination and the subsequent appearance of gaps on the gage that would also change its performance. As a result a maximum temperature of 533 K (500°F) is recommended, and this is recommended for only periods of tens of minutes at best. As a result the gage has only limited overtemperature capability.

The Schmidt-Boelter type calorimeter makes a cold wall measurement (like the Gardon-type gages) and thus requires a heat sink. A survey of the literature and review of manufactured products indicates that in general the smallest possible Schmidt-Boelter gage is considerably larger than the smallest practical Gardon-type gage with the result that the Schmidt-Boelter type must handle a larger total integrated heat load than a comparable Gardon gage (comparison on the basis of sensitivity). This requires a larger heat sink and indicates a greater susceptibility

to heat leaks in high flux locations. However, the situation changes in low flux locations where the large size required and the fragility of the Gardon-type gage makes the Schmidt-Boelter preferable for reasons of ruggedness and size. However, the Schmidt-Boelter is comparable to the Gardon gage in the respect that a cold wall measurement is being made, and there thus exists a boundary layer perturbation expected to be comparable to that caused by the presence of a cold Gardon gage in the hot RSI wall.

Before installation on the heat sink, the Schmidt-Boelter calorimeter can be calibrated by mounting on a slug type calorimeter and then comparing the data derived from the slug with the data of the test calorimeter. After installation, calibration is best accomplished in the same means as the Gardon-type gages, that is, the calorimeter is coated with a removable coating of known absorptivity, and then calibrated using a radiant source of known flux. It is thus possible in theory to calibrate the gage after installation in the spacecraft, if required.

To summarize, the Schmidt-Boelter type gage is best suited to low flux locations where the high sensitivity possible with this type of gage permits signals to be used without amplification. Size considerations preclude its use in high flux locations. Heat flux is read out directly. However, variable sensitivity as a function of temperature requires that a monitoring thermocouple be carried in the gage, and this in turn requires another data channel for each calorimeter. Finally, overtemperature capability is limited, and long term stability of the organic materials at high temperatures needs examination and possible development.

Equilibrium-Slug Type Calorimeter

The equilibrium slug calorimeter operates on the principle than an isolated body which has negligible conduction heat leaks will achieve a temperature which depends on the convective heat transfer into and reradiation away from the body. If the body is of low thermal mass such that its time constant is small relative to the rate of change of convective heat flux, then it will be essentially in equilibrium at all times with its environment. By monitoring the body temperature and accurately knowing its surface emittance, the convective heat flux is calculated from the expression, $\varepsilon\sigma T^4$, where ε is the emittance, σ is the Stefan-Boltzmann constant and T is the temperature (absolute).

Although application of this principle as a means of calorimetry has not been found in the literature, it has been used successfuly by Aerotherm in thermal-vacuum testing to monitor the temperature of an earth radiation simulator.

Preliminary consideration of the equilibrium slug as a candidate heat flux sensor for the RSI has focused on performance characteristics. Considerations of flight worthiness are difficult to assess because the device has no previous flight

history. In fact, lack of experience with the equilibrium slug becomes its major drawback. It is expected that a significant development effort would be required to achieve the same confidence factor found in other calorimeters. On the other hand, the major advantages of the equilibrium slug are: (1) it does not need the heat sink required by all other candidate calorimeters and (2) its temperature approximates that of the surrounding insulation minimizing the local influence on the boundary layer previously mentioned in connection with the other calorimeters.

To minimize the mass of the equilibrium slug, it should be a thin wafer. At peak HRSI heat flux, the peak temperature of the slug may be 1478 K (2200°F), therefore it must be made of a high temperature alloy or a refractory metal. Mounting the slug flush with the HRSI surface yet thermally isolated suggests that it might be bonded directly into a counterbored cavity in the HRSI. The attachment would be made only at the wafer perimeter. Since the HRSI surface temperature approximates radiation equilibrium temperature, the temperature difference across the slug mounting interface and therefore the heat leak is kept to a minimum. High temperature cement could be used to attach the wafer to the insulation. However, differential thermal expansion between the various materials might prove to be a problem.

Figure 18 shows the mounting configuration described above. A chromel-alumel or platinum-platinum/10 percent rhodium thermocouple is attached to the center of the wafer. Heat leak by radiation from the backside is theoretically controlled by a low emittance finish. However, in practice, low emittance may be difficult to retain because of oxidation of the metallic wafer at high temperature. By calibration in a radiant source in the mounted configuration and at operating temperatures the heat leak effects, if they prove to be significant, can be calibrated out. The calibration procedure, however, is not simple.

Since the output signal from the equilibrium slug varies as the fourth root of heat flux, it is highly nonlinear. However, it has excellent sensitivity. Consider a resolution requirement of 1 percent of full scale and a full scale of 2.27 x 10^5 W/m^2 (20 Btu/ft^2sec). The signal increment corresponding to 1 percent heat flux resolution is 8.2 mV at 367 K (200°F) and 0.15 mV at 1367 K (2000°F).

An examination was made of the time constant of the equilibrium slug. Neglecting heat leaks to the HRSI, the transient energy balance on the calorimeter wafer is:

$$\dot{q} - \varepsilon\sigma T^4 = b\rho c_p \frac{dT}{dt}$$

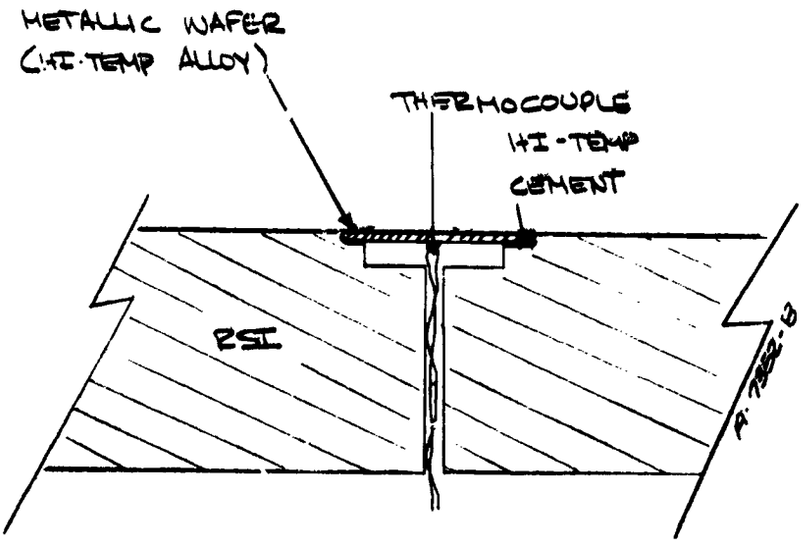

Figure 18. Equilibrium slug, possible mounting configuration.

where

$\dot{q}$ = Incident convective heat flux

T = Wafer temperature

$b\rho c_p$ = Wafer thickness, density and specific heat, respectively

ε = Surface emittance

σ = Stefan-Boltzmann constant

t = Time

Starting from an initial equilibrium temperature, T_0, and suddenly imposing a constant heat flux, the time constant is defined as the duration required for the wafer to achieve 63 percent of its total temperature transition, ΔT_{ss}, to a new steady state condition, T_{ss}. Integration of the energy balance equation yields the following equation for time constant, τ.

$$\tau = \frac{t\rho c_p}{2\varepsilon\sigma T_{ss}^3}\left[\tan^{-1}\left(\frac{T_0 + 0.63\Delta T_{ss}}{T_{ss}}\right) + \tanh^{-1}\left(\frac{T_0 + 0.63\Delta T_{ss}}{T_{ss}}\right)\right.$$

$$\left. - \tan^{-1}\left(\frac{T_0}{T_{ss}}\right) - \tanh^{-1}\left(\frac{T_0}{T_{ss}}\right)\right]$$

The calculated time constant is sensitive not only to the initial temperature, T_0, but also to the heat flux step implied in ΔT_{ss}. Therefore the ΔT_{ss} chosen was that which corresponds to 1 percent resolution on a 2.27 x 10^5 W/m^2 (20 Btu/ft^{2}sec) full scale. The resulting time constants computed for 0.000762 m (0.03 inch) and 0.000254 m (0.01 inch) thick equilibrium slug wafers appears in Figure 19. Heat leak effects will lengthen these time constants. Previous analysis of the calorimeter time constant requirement for a typical shuttle HRSI heating pulse has shown that the time constant must be less than 2 seconds if the error due to thermal lag is to be less than 1 percent of full scale. Thus, unless the wafer thickness can be made only a few mils, the equilibrium slug will suffer from significant thermal lag errors.

In summary, the equilibrium slug has the advantages of no heat sink requirement, a hot wall measurement, and good sensitivity. However, since the device has little history, a major development is required to define the best mounting technique, evaluate heat leak effects, and determine the calibration technique. Thermal lag has been identified as a potential weakness. The device is nonlinear and data reduction would be best implemented on a computer.

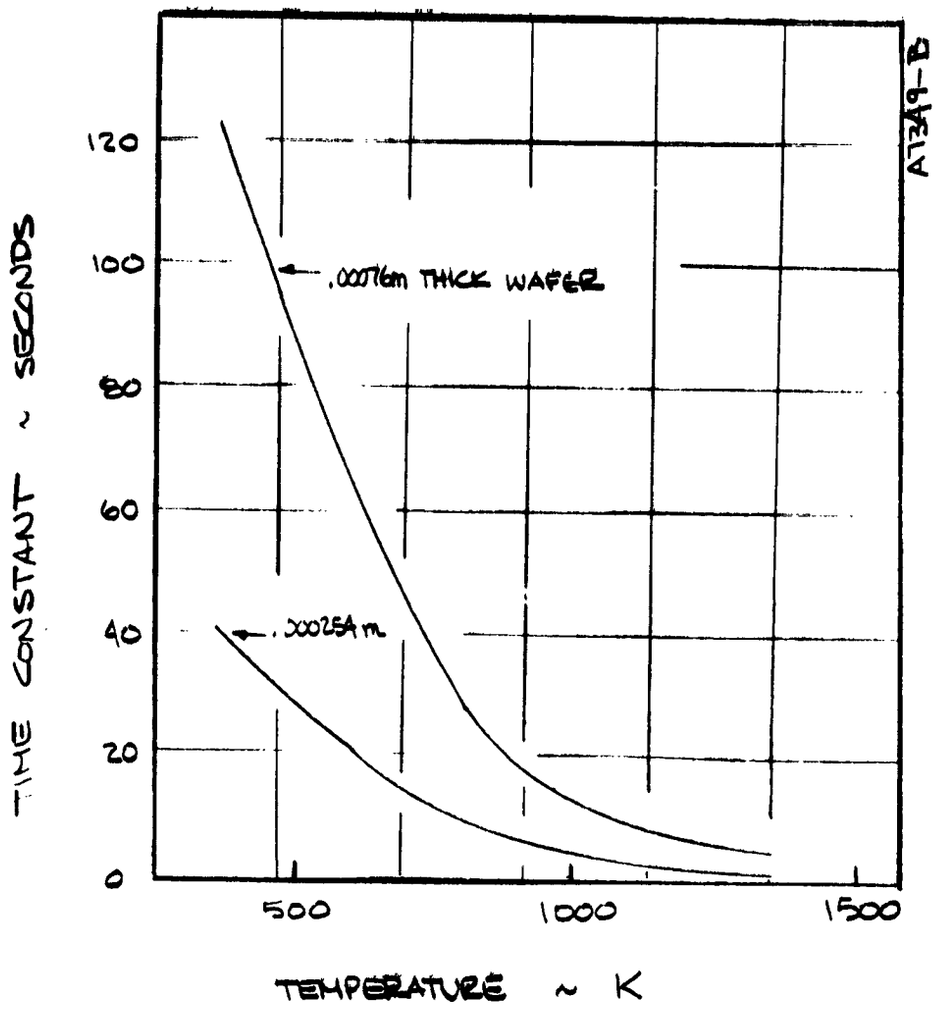

Figure 19. Equilibrium slug time constants.

Thermocouple Calorimetry

Thermocouple calorimetry consists of placing one or more thermocouples in the wall (at varying depths in the case of multiple thermocouples) and then deducing the heat flux history from the temperature history recorded by the thermocouples. In the case of a single thermocouple in intimate contact with the surface, this type of measurement is similar to null-point calorimeters used for transient heat transfer measurements at high fluxes in arc jet facilities. In null-point calorimeters the position of the thermocouple is very accurately known and the wall material is usually copper so that the thermal properties are well known. Further, the temperature range is generally limited so that thermal property variations are minimized. Even so the problem of data reduction requires a computer to back out the heat flux data from the temperature history recorded by the thermocouple.

The determination of heat flux using a thermocouple mounted in the HRSI is considerably more complicated than that encountered with null-point calorimeters because of the variations in thermal properties of the HRSI with respect to temperature and local pressure. Data reduction then requires that pressure be monitored and input to the data reduction scheme in order to accurately reduce the data.

In theory one could build a gradient-type calorimeter within the HRSI using the HRSI as the material through which the gradient is measured. If the thermocouples were connected electrically so that the temperature difference were measured rather than the temperature, then the output would be proportional to the heat flux. However numerous complications spoil the performance of this arrangement. Variations in HRSI properties result in a gage with nonlinear output and variable sensitivity depending upon local temperature and pressure. The thermocouples must be close together to minimize the effects of nonuniformities in the temperature distribution. Finally, both thermocouples must be very close to the surface to prevent significant time delay between heat flux input and data output.

Previous analysis indicates that a thermocouple placed 0.000254 m (0.010 inch) from the surface (assuming no coating) has a 2 second "time constant", while a thermocouple placed 0.000254 (0.010 inch) from the surface has a "time constant", of 260 seconds. The small dimensions encountered (necessary because the HRSI is a good thermal insulator) require careful X-ray analysis to accurately determine the location of the thermocouples within the HRSI. The complexity of the data reduction scheme indicates that real time readout of heat flux is difficult or impossible to obtain.

In addition to the problems cited above, there are also problems associated with installation and errors arising from heat leaks down the thermocouple leads. Finally, some materials are attacked by the silica in the HRSI when operated at high temperatures, and some alloy thermocouples suffer calibration shift in combined

conditions of near vacuum and high temperature because one element of the alloy volatilizes with subsequent composition change of the thermocouple material. These last problems are problems associated with thermocouple installations in general and are not restricted to calorimeter usage.

In spite of the substantial problems cited above, thermocouple calorimetry offers some significant advantages over most of the other calorimeter approaches discussed previously. Foremost among these is the absence of a heat sink which is required for most other calorimeter schemes. The only thermal path through the HRSI tile is thermocouple lead wire which is typically very small with the result that the structural and thermal perturbation is minimal. There is no perturbation to the boundary layer because the wall temperature distribution along the surface is essentially undisturbed. Ruggedness is expected to be very good, and possible survival temperatures are exceptionally high, being limited only by the thermocouple materials. Calibration of the individual thermocouples is not required as NBS data are more than adequate. However, heat flux calibration in the tile is virtually impossible to do satisfactorily in the lab, and is impossible to do on the spacecraft.

To summarize, thermocouple calorimetry presents complex problems in data reduction further complicated by the variable properties of the HRSI. Numerous installation problems need to be solved, and extensive error analyses need to be performed. Real time readout of heat flux is difficult or impossible. However, with the selection of appropriate materials, reliability should be excellent, perhaps the best of all calorimeters discussed, and the thermal and structural perturbation to the tile is less than the other calorimeters discussed.

Recommended Approach

The recommended calorimetry approach is based upon a careful review of available information in the literature and from manufacturers. The previous sections indicate that an extensive list of evaluation criteria was utilized in judging the various techniques under examination, but the major considerations are that the size and weight be minimum, the data reduction straightforward, and that the concept have a high probability of success with minimum development effort. On this basis and the results of the detail evaluation procedure, it is recommended that the small Gardon gage together with operational amplifiers be used for all locations. This approach offers low system weight, linear output, and variable sensitivity direct readout of heat flux without the need of monitoring thermocouples, and further it is based on well developed and tested technology (Gardon gages and integrated circuit amplifiers). The additional complexity of the amplifier is felt to be minimum, and offset by the advantages of small gage size, low foil temperatures, and variable sensitivity which allows the calorimeter output to be tailored to the data handling

system. It is believed that the problem of zero drift in the amplifier is one for which numerous solutions exist, and that minimum development is thus necessary.

2.2.3.2 Thermocouple Temperature Measurements

The major design and fabrication requirements for a successful temperature measurement system as applied to HRSI and RCC TPS are:

- Sensor accuracy
- Minimum disturbance of the normal spatial temperature distribution
- Accurate sensor location
- Accurate data reduction procedure
- Practical and economic methods of
  - Fabrication
  - Installation
  - Calibration
  - Data acquisition
  - Data analysis

The selection of thermocouple types for the HRSI application was based on the information contained in Table 4. Both chromel/alumel and platinum-13 percent rhodium/platinum thermocouples meet the environmental and temperature requirements with each offering unique advantages as follows:

Chromel/alumel (Type K)

- High emf output

Platinum-13 percent rhodium/platinum (Type R)

- High accuracy
- High temperature limit
- Excellent stability

Both types offer a large body of previous experience of use in HRSI through various testing programs. The stability and accuracy of the Type K thermocouple can be improved through the use of special alloys as noted in the table. The higher accuracy of the Type R thermocouple may be offset by the decreased signal-to-noise ratio with its lower (by $\cdot$ 2/3) output. The stability difference between these two types under the shuttle reentry environment is presently unknown. The Type R thermocouple does, however, offer greater margin of survival in an overtemperature condition and this may influence final selection. Both types have been studied in the long term

TABLE 4. BASIC THERMOCOUPLE COMPARISON

	Chromel/Alumel [1] Type K	Platinel [4]	Platinum-13 Rhodium/Platinum Type R	Platinum-10 Rhodium/ Platinum - Type S
Category	Base Metal	Noble Metal	Noble Metal	Noble Metal
Temperature Range	4.44 to 1694 K	Same as Type K	223 to 2041 K	Same as Type R
Limits of Error Standard	±2.2 K (273 to 550 K) ±1/4 (550 to 2045 K)	Agrees with type K calibration within 2% up to 1473 K.	±1.4 K (273 to 811 K) ±1/4 (811 to 1756 K)	Same as Type R
Special	±1.1 K (273 to 550 K) 1/8 (550 to 1533 K)			
Output	54.845 mV at 1644 K	Same as type K; see above.	15.627 mV at 1644 K	14.313 mV at 1644 K
Recommended Environments	Continuous use in oxidizing or inert atmospheres at temperatures up to 1533 K.	Same as Type K	Continuous use in oxidizing or inert atmospheres at temperatures up to 1672 K or intermittently up to 1755 K.	Same as Type R
Detrimental Environments	Reducing atmospheres or alternately oxidizing and reducing. Sulfurous atmospheres-embrittlement of KN element. Vacuum-preferential vaporization in KP element. Carbonaceous materials-calibration drift. Marginally oxidizing conditions-preferential oxidation in KP element (48.9 K neg. drift after 290 hr at 1367 K), also called "green-rot" corrosion.	Phosphorus, sulfur and silicon effect life of thermocouple. Not recommended for use in vacuum.	Reducing atmospheres. Atmospheres containing metallic or nonmetallic vapors. Vacuum for long periods of time. Platinum element sensitive to excessive grain growth at high temperature resulting in mechanical failure. Negative drifts in calibration caused by contamination, diffusion of rhodium from alloy wire into platinum and volatilization of rhodium from alloy wire. Chemical contamination principle factor in useful life limit.	Same as Type R
Stability	Oxidizing atmosphere at 1273 K, 0.5 K calibration drift after 10 hr 5.0 K calibration drift after 1000 hr at 1473 K, 2.0 K calibration drift after 10 hr	Oxidizing atmosphere at 1473 K, 3 K calibration drift after 1000 hr	Oxidizing atmosphere at 1373 K, ±0.1 K calibration drift after 10 hr 2.0 K calibration drift after 1000 hr at 1773 K, 1.0 K calibration drift after 10 hr	Same as Type R
Protection Techniques	Sheathed or swaged assembly with magnesia or alumina insulation. Permit free circulation in unsealed installations.	Same as Type K	Twin bore insulating tubes of high purity alumina. Sheathed or swaged assembly with alumina insulation. Avoid rapidly moving oxidizing atmosphere.	Same as Type R
Special Alloy	Special nickel-chromium alloys are available as follows: 1. Geminol[2]-improved resistance in reducing atmospheres; requires special calibration curve. 2. Thermo-Kanthal special[3]-improved stability 1256 to 1533 K. 3. Tophel II - Nial II - improved oxidation resistance and emf stability; within type K tolerances 422 to 1367 K. 4. Chromel 3-G-345-Alumel 3-G-196-increased stability under extreme conditions; meets standard type K tolerances.	1. Platinel II - improved mechanical fatigue properties.		

[1] Trademark - Hoskins Manufacturing Co.
[2] Trademark - Driver Harris Co.
[3] Trademark - Kanthal Corp.
[4] Trademark - Ingelhard Ind. Inc.

TABLE 4. (CONCLUDED)

	Platinum-30 Rhodium/Platinum-6 Rhodium - Type B	Iridium - Rhodium/Iridium	Platinum-15% Iridium/ Palladium
Category	Noble Metal	Noble Metal	Noble Metal
Temperature Range	266 to 2093 K	266 to 2273 K	266 - 1826 K
Limits of Error Standard	±1/2% (1144 to 1978 K)	-	-
Special			
Output	8.628 mV at 1644 K	7.5 mV at 1644 K	46.0 mV at 1644 K
Recommended Environments	Continuous use in oxidizing or inert atmospheres at temperatures up to 1978 K.	Continuous use in inert atmosphere or vacuum.	Continuous use in inert or oxidizing atmospheres at temperatures up to 1644 K.
Detrimental Environments	Same as Type R or S. However, under corresponding conditions will show less grain growth and less drift in calibration.	Reducing atmospheres. Oxidizing atmosphere shortens life.	Reducing atmosphere or vacuum. Platinum - 15% iridium alloy has better corrosion resistance than platinum - rhodium alloys. Palladium is slightly less resistant to corrosion than platinum. Alternating oxidizing and reducing atmospheres produce surface blistering.
Stability	Oxidizing atmosphere at 1973 K, 4.0 K calibration drift after 10 hr.	Inert or slightly oxidizing atmospheres at 2269 K, 10 K calibration drift after 10 hr.	Oxidizing atmosphere at 1473 K, 0.5 K calibration drift after 10 hr. 5.0 K calibration drift after 1000 hr.
Protection Techniques	Same as Type R or S	-	-
Special Alloys		Iridium - 40% rhodium/iridium Iridium - 50% rhodium/iridium Iridium - 60% rhodium/iridium	

test series with special emphasis on the calibration drift problem as a function of test time. Typical installation techniques are depicted in Figure 20.

For applications requiring several in-depth thermocouples mounted within a small volume, the instrumented plug has been found to be very successful. The most recent detailed application study at Aerotherm is reported in Reference 1. Since the plug is made of the same material as the part or the HRSI panel, there is minimum disturbance of the spatial temperature distribution as long as care is exercised in bonding the plug into the port. The main disadvantage is the relatively complicated fabrication process to insure accurate thermocouple locations.

In the RCC, the platinum-platinum 13 percent rhodium thermocouples are required due to the higher temperature limitations, and these thermocouples must be coated for this application for protection from long term vacuum exposure and chemical contamination. Aerotherm experience has shown the ceramic-insulated, metallic-sheathed design to be optimum for this application. The ceramic insulation is generally magnesium oxide (MgO) good to 2144 K (3400°F), or aluminum oxide (Al_2O_3), good to 1867 K (2900°F). The sheath materials available are shown in Table 5. For the above considerations, the Inconel 702 sheath appears to be the best choice.

The metallic-sheathed thermocouple is available with overall sheath diameters as small as 0.000254 m (0.010 inch), thus minimizing the spatial temperature disturbance when installed in depth in the RCC material. Grounded or ungrounded thermocouple junctions are possible; the grounded junction, in which the junction is welded to the sheath, being most attractive from a thermal response aspect.

Sheath-type thermocouples are typically installed in depth in the material by means of drilling a small hole to the desired location along an expected isotherm, i.e., parallel to front face for the RCC tile, and holding in place with a high temperature ceramic cement.

The use of this type of thermocouple for back face temperature measurement requires either a ceramic cement or ceramic cement/retention wire installation technique. These were studies in some detail by LTV as reported in Reference 2. Preliminary results indicated a Union Carbide Corporation cement, C-34, was successful in bonding a 0.00152 m (0.060 inch) beryllia-sheathed thermocouple which was wrapped with Kreba Carbon yarn before application of the cement, through five temperature cycles with a maximum 2256 k (3600°F) soak. Due to the problems associated with penetrating the RCC oxidation inhibiting coating, testing emphasis was placed upon bonding techniques of thermocouple attachment using available cement or bonding techniques such as C-34, Astroceram or alumina flame spray.

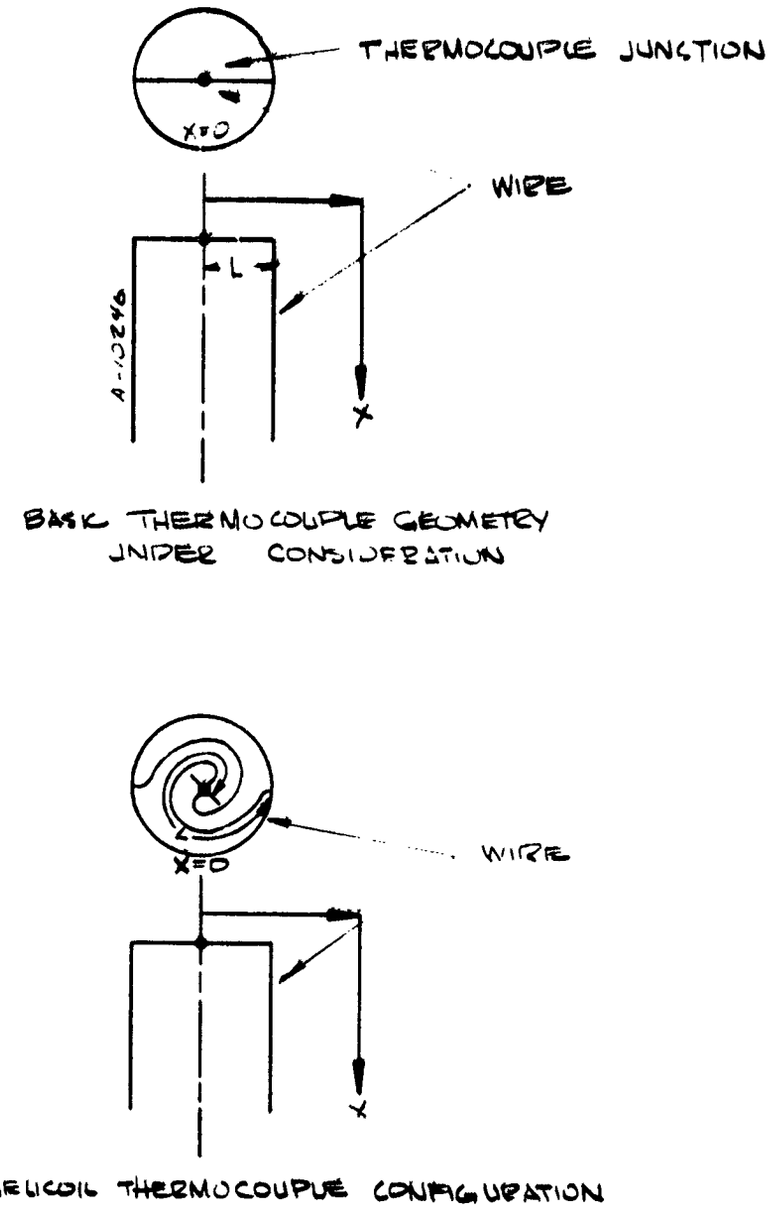

Figure 20. Typical thermocouple installation configuration.

TABLE 5. VERY HIGH TEMPERATURE SHEATH MATERIALS

Sheath Material	Rec. Useful Temp.	Melting Point	Environmental Conditions			
			Oxidizing	Hydrogen	Inert	Vacuum
Molybdenum	2478 K	2883 K	Not Rec.	Fair	Fair	Good
Tantalum	2756 K	3269 K	Not Rec.	Not Rec.	Fair	Good
Platinum	1950 K	2046 K	Very Good	Poor	Poor	Poor
Columbium	2256 K	2741 K	Not Rec.	Not Rec.	No	Good
Moly 50% Rhenium 50%	2773 K	2823 K	Not Rec.	Good	Good	Good
Inconel 702	1589 K	--	Very Good	Good	Very Good	Very Good

2.2.3.3 Radiometer Temperature Measurements

The severe environment in the void behind the RCC panels (temperatures to 1589 K (2400°F) may indicate some form of noncontact temperature measurement for the back face temperature measurement.

The various types of pyrometers that may be employed for this measurement of RCC surface temperature include:

- Total radiation pyrometer
- Single color pyrometer
- Two color pyrometer

All three types are available in an automatic operating mode with a continuous output signal for indicating and recording. All three sense radiation from the source and relate this to the source temperature. The total radiation pyrometer senses over the complete wavelength spectrum and requires a gray body source of known emissivity (independent of wavelength) for temperature measurement. The single color pyrometer senses over a narrow wavelength band and requires a source of known emissivity (at the sensing wavelength) for accurate temperature measurement. Units of this type are available which sense in the ultraviolet, visible, near infrared, and far infrared, and each has particular advantages and disadvantages. For instance, ultraviolet sensing presents measurement problems in that this radiation is attenuated by most optical and window materials, near infrared sensing avoids interference from most gas phase radiation sources, and far infrared sensing eliminates any potential transparency problems in surface temperature measurement of silica-based materials. The two color pyrometer senses over two narrow wavelength bands and requires a gray body source for accurate temperature measurement. Within this gray body requirement, emissivity need not be known since the ratio of the radiation energies at the two sensing wavelengths determines the temperature. This type of pyrometer is sensitive to any stray radiation.

Aerotherm has employed all three types of pyrometers, primarily for ablatives, with very satisfactory experience with the single color type which senses in the near infrared, 0.8 microns.

The pyrometer must be located in a relatively cool section of the RCC panel support structure; viewing the panel back face through a quartz window. Surface temperature measurements may be required at several locations; the possible approaches to accomplish this include:

- Multiple pyrometers
- Stationary pyrometer/optical switching
- Indexing pyrometer

The first approach is prohibitive from a cost standpoint. The optical switching approach while requiring an additional optical element, i.e., fiber optics, mirrors, etc., which degrades the sensitivity and accuracy of the pyrometer, may offer the least complicated method of viewing many widely separated locations. The indexing pyrometer approach provides a mechanical device for sequentially focusing the pyrometer on several locations on the surface in a continuous fashion. Such an approach has been used by Aerotherm in past test programs with up to six points being measured on a test sample. The main disadvantage of this approach is the complexity of the mechanical indexing device.

Sensor type selection has been narrowed to either photosensitive or pyroelectric devices. Both offer rapid time response and relative ruggedness. These devices are the easiest to temperature compensate, provide a size advantage over other types, and are the least expensive pyrometers available. As applied to RCC temperature measurement, these pyrometers must be calibrated as a system in the installed configuration, to the spectral shape typical of the RCC being measured. Testing experience should be used as the basis for the final development of the optical temperature measurement system based upon photovoltaic sensors. These sensors have been used successfully by Aerotherm and are readily available from Barnes Engineering Company in Stamford, Connecticut (Series T-300) and Thermogage in Frostburg, Maryland.

2.2.3.4 HRSI Pressure Measurements

The measurement of the local pressure during test flights will be used primarily to verify the analytical predictions and aid in extrapolating ground test results to full operation flight. During operational flights, the pressure measurement will serve as a check on the trajectory flown plus a warning to check material integrity if specified pressure levels are exceeded.

A pressure transducer installation similar to that used on Apollo has been studied for the Shuttle Orbiter. In choosing specific transducer types, the following must be considered.

- Pressure range
- Temperature extremes at transducer location
- Accuracy
- Data acquisition techniques
- Ruggedness/reliability
- Maintainability

In this application, the sensor response is not an important consideration due to the slow pressure transients and long flight times. The installation of the pressure port in the HRSI material is dependent upon:

- Effect the port (flaw) has on protective coating performance
- Effect of port (hole) on overall TPS performance

Testing has been performed to evaluate the effect of the pressure port defect upon the tile and protective coating performance on a configuration similar to Figure 21, but without the port lining. However, for flight systems a moisture seal isolating the port from the HRSI is required. Additional design and test activities are required to develop a viable flight configuration.

2.2.4 Measurement Error Analysis

Measurement accuracy for heat flux and temperature determination is dependent upon gage response characteristics, gage installation, inherent gage measurement errors, and data reduction inaccuracies. An analysis of these measurement errors has been performed and the results are presented below for both heat flux and temperature measurements.

2.2.4.1 Heat Flux Measurement Error Analysis

Adequate calorimeter response to the transient reentry heat pulse means that the accuracy of the measurement will not be affected by phase lag or reduction of peak amplitude. The required calorimeter response, to meet this criteria, must be defined. Following is a simplified analysis of a heat flux sensor exposed to an idealized heating profile on the shuttle insulation surface.

Assuming the sensor is a first-order system, it responds according to the equation:

$$\tau \frac{d\dot{q}'}{dt} = (\dot{q} - \dot{q}')$$

where

$\dot{q}$ = Incident heat flux

$\dot{q}'$ = Measured heat flux

τ = Sensor time constant

t = Time

Referring to Reference Trajectory 8921, 147B Vehicle heating profiles calculated by Rockwell International, the reentry radiation equilibrium heating rate, $\dot{q}$, on the Shuttle HRSI may be approximated by a trapezoidal profile with a ramped increase, a plateau and followed by a ramped decrease to zero. As a typical heating history, the profile for body point B and its approximation are shown in Figure 22. Solving the response equation, using the appropriate initial condition and $\dot{q}$ expression

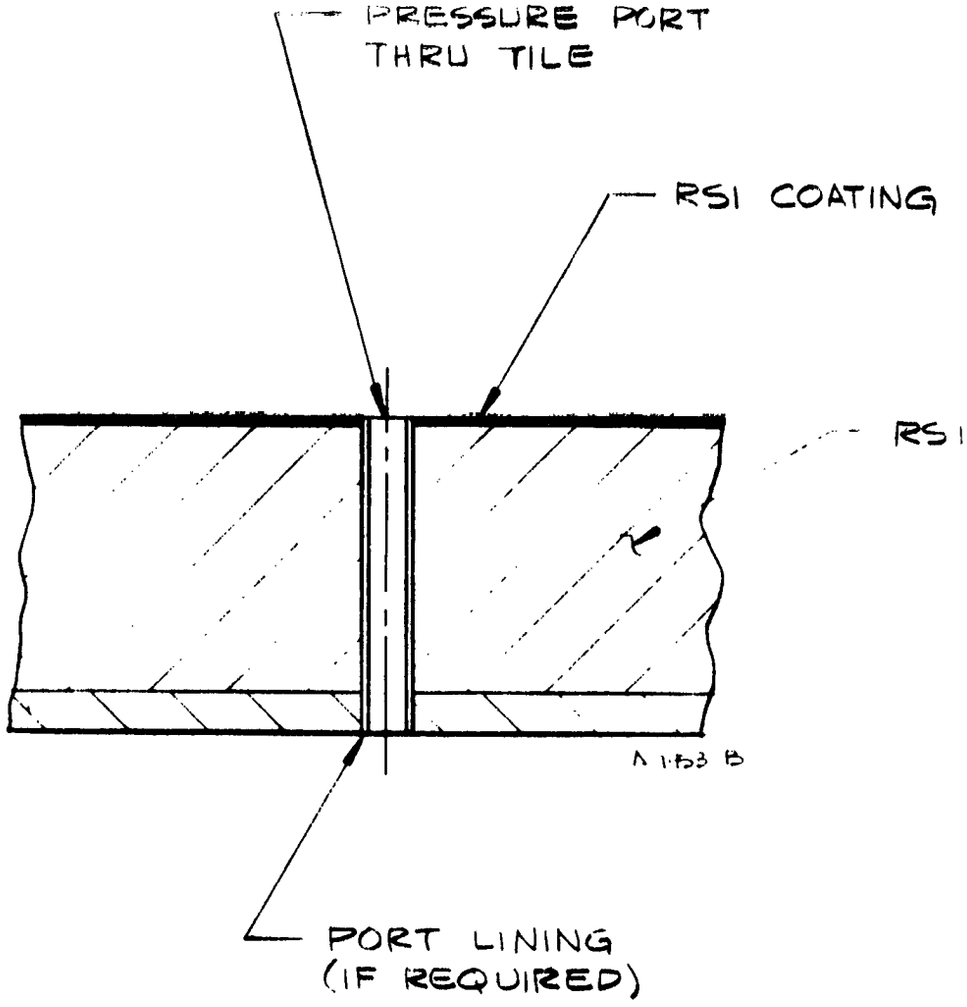

Figure 21. Proposed pressure port configuration.

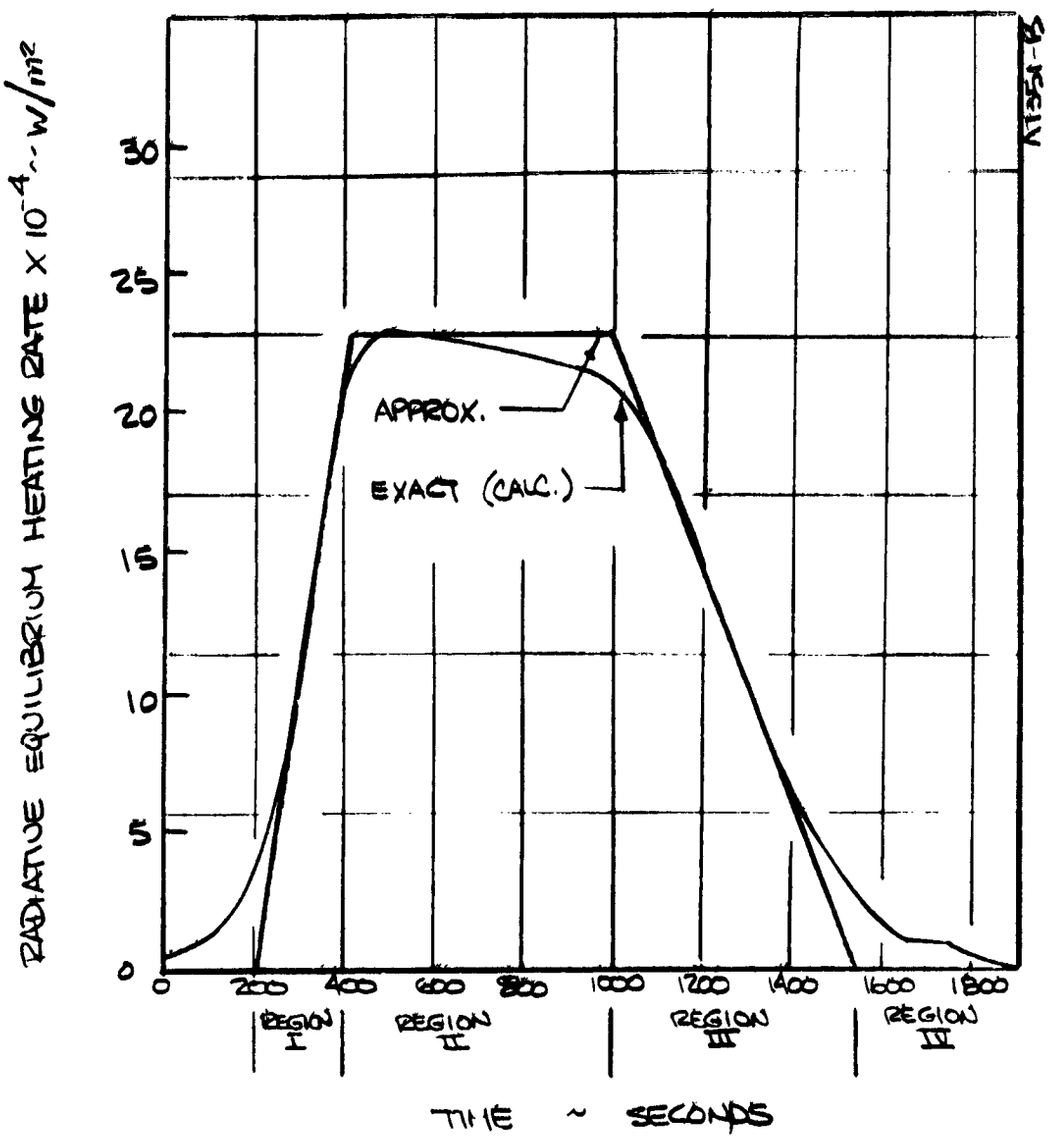

Figure 22. Reentry profile.

(Ref. trajectory 8921, 147B vehicle, B.P. B, X/L = 0.1)

for each region, an expression can be obtained for $\dot{q}'$ in each region. Of primary interest is the initial response, Region I. For the initial rise, the calorimeter response is as follows, where $\dot{q}_{max}$ is peak heat flux, t_a is the ramp duration, and τ is the sensor time constant (previously defined).

$$\dot{q}' = \frac{\dot{q}_{max}}{t_a}\left[t - \tau\left(1 - e^{-t/\tau}\right)\right]$$

Figure 23 presents the response curves for calorimeters of various time constants compared with the idealized heating input profile at body point 8. In general, for a ramped heating condition in which the period of the ramp is many times the calorimeter time constant, the calorimeter output will lag the input, after an initial transition, by one time constant. Under that situation, the measurement error due to the thermal lag expressed as a percent of $\dot{q}_{max}$ (or full scale measurement) is simply the ratio of time constant to ramp duration. Figure 24 presents the measurement error due to lag for various ramp times including the shuttle heat-up (Region I of Figure 22) which lasts about 200 seconds in the approximation.

Thermal lag is essentially a systematic error which might be corrected for in the data analysis. However the correction is not necessarily a simple matter of shifting the time base by one time constant because the degree of correction depends on fluctuations in the heating pulse. Therefore it would be preferable to select a gage with adequate response if such gages are available. For example, if the error due to lag is to be less than 1 percent then Figure 24 indicates the time constant should be less than 2 seconds. A majority of the heat flux gages considered in this study meet the preceding requirement.

Installation of calorimeters may signficantly reduce the accuracy of the measurement. For instance, copper-constantan Gardon gages lose their linearity characteristics when the calorimeter body is allowed to overheat. Consequently adequate cooling is a prerequisite of measurement accuracy. Likewise, heat leak errors associated with measurement disc mounting for equilibrium slug calorimeters provide potential error sources. However, since preliminary selections have indicated that the augmented Gardon gage is the prime candidate for the heat flux measurement systems the error analysis has been concentrated upon this particular gage and its installation. The errors associated with time constant and installation interfaces do not present a problem for this gage. However, there are errors associated with the boundary layer perturbation created by a discontinuity in the surface temperature. Perturbing the boundary layer, the cold sensor measures a flux significantly larger than the unperturbed incident flux. Two-dimensional analyses have been performed using BLIMP (Reference 3) to quantitatively evaluate this phenomenon. BLIMP is a computer code capable of analyzing a two-dimensional, multicomponent, chemically reacting, nonsimilar boundary layer. Using this analysis procedure, the effect of

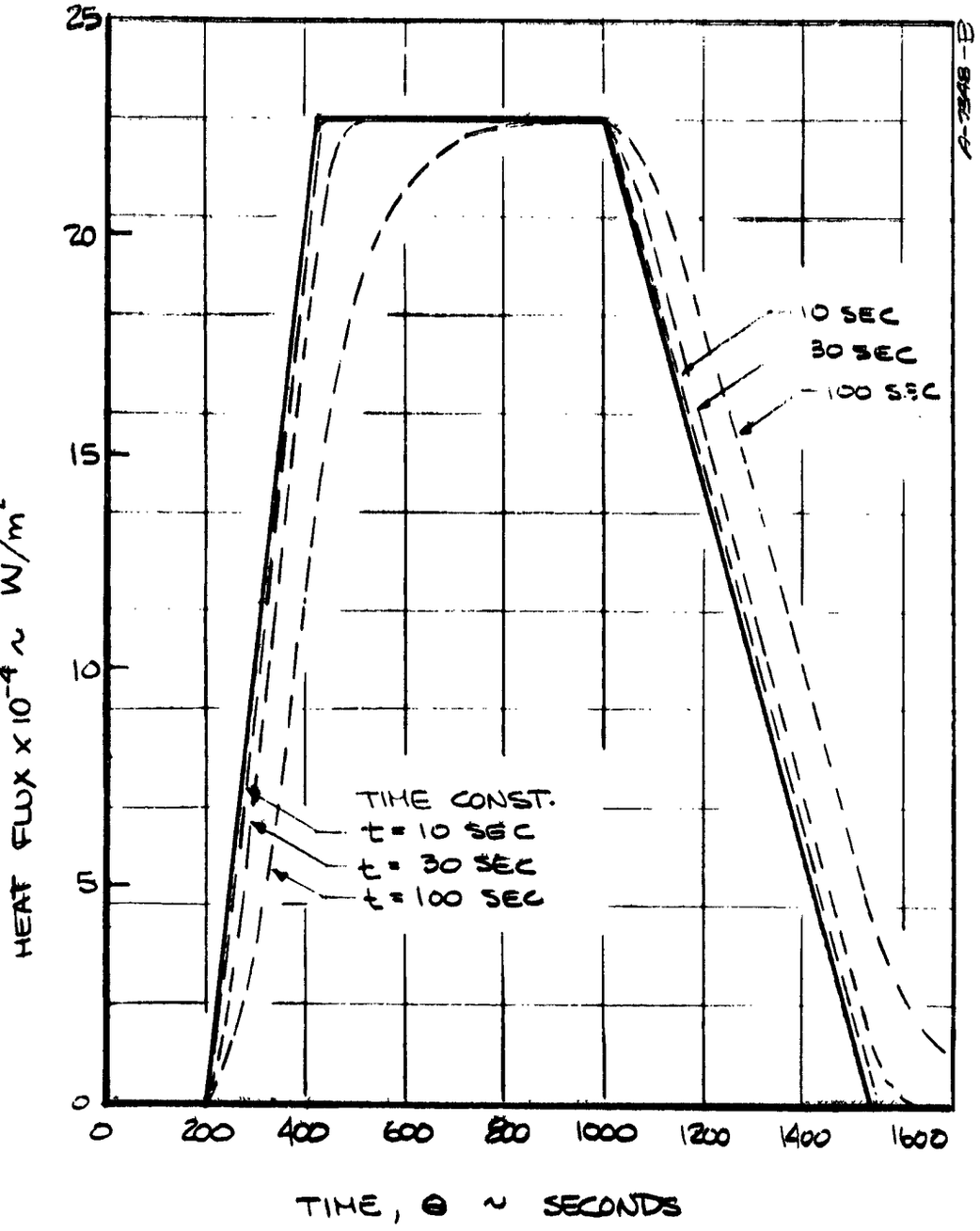

Figure 23. Calorimeter response to B.P. B idealized heating profile for various calorimeter time constants.

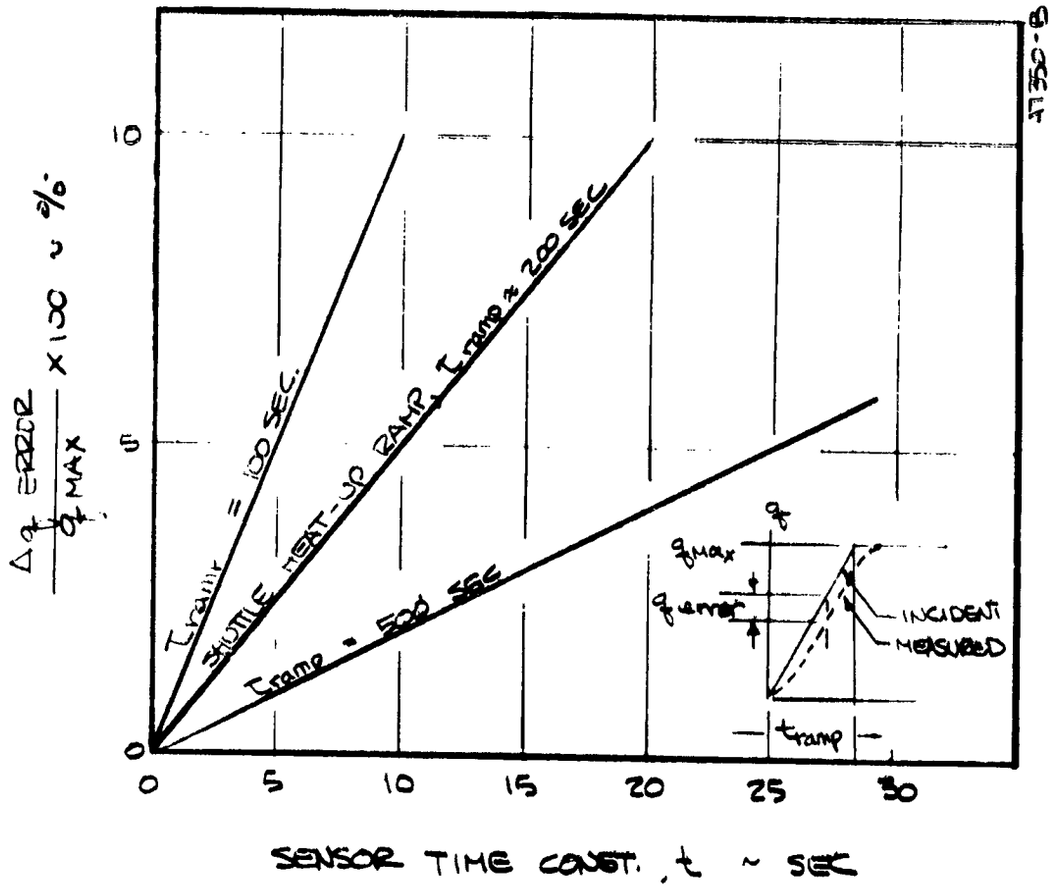

Figure 24. Sensor error due to thermal lag vs. sensor time constant for a ramped heating profile.

sensor surface temperature distribution upon the measured incident flux has also been evaluated. This sensor temperature distribution occurs in the case of unaugmented Gardon gages wherein center to edge temperature differences reach 211 K (380°F) at peak flux conditions in the case of standard copper-constantan gages. Figure 25 compares the incident flux upon the sensor face for uniform and parabolic sensor temperature distributions at a high flux condition typical of body point B. It is apparent that a sensor with a uniform temperature experiences a more uniform flux distribution across its face with the disadvantage of an increased incident heat load. With passively cooled concepts favored, the increased heat load requires larger heat sinks. This increased size and weight provide additional perturbations to the local tile response as well as creating problems in acceleration and vibration environments. A three-dimensional approximation to the measured flux level has been made using the two-dimensional results for the high flux location. A 2 percent higher total incident flux resulted from this analysis. Subsequent to the above-mentioned analysis, a low flux location (typcial of body point E) was analyzed for a uniform temperature sensor (Figure 26). A 30 percent increase in incident flux was predicted and this result is consistent with the high flux location prediction of a 32 percent flux increase. It is important to note that the boundary layer recovers within 3 sensor diameters downstream in the high flux location and within 10 sensor diameters for the low flux location.

BLIMP analyses of the effect of a cold guard ring upon the measured flux level indicate that a guard ring of on ensor diameter will produce a uniform flux distribution across the sensor. Figure 27 displays the flux distribution acorss an eight sensor diameter guard ring. However, a 10 sensor diameter guard ring will virtually allow the measurement of an unperturbed flux level.

Further boundary layer analyses have been performed at a medium flux location (body point C) for several times throughout the entry environment. These results are presented in Figures 28 through 30 wherein it is noted that heating augmentation ranges from a 60 percent increase to a 179 percent increase in the unperturbed flux. These results indicate significantly higher augmentation factors than have been predicted for the other reference body locations. Further analysis of the results indicates that the chemically reactive component of the thermal conductivity at these local pressure/enthalpy conditions becomes a controlling factor in the surface energy balance. Consequently, calorimeter location should be analyzed prior to installation to predict which locations have high probabilities for experiencing abnormal heating augmentation. This phenomena affects heat sink sizing and potentially the tile integrity (due to the downstream effect of the boundary layer perturbation). Cold wall boundary layer perturbation effects upon incident heating must also be assessed for ascent heating environments. A BLIMP analysis has been performed for a reference body point (body point C) at a point in the ascent trajectory near peak

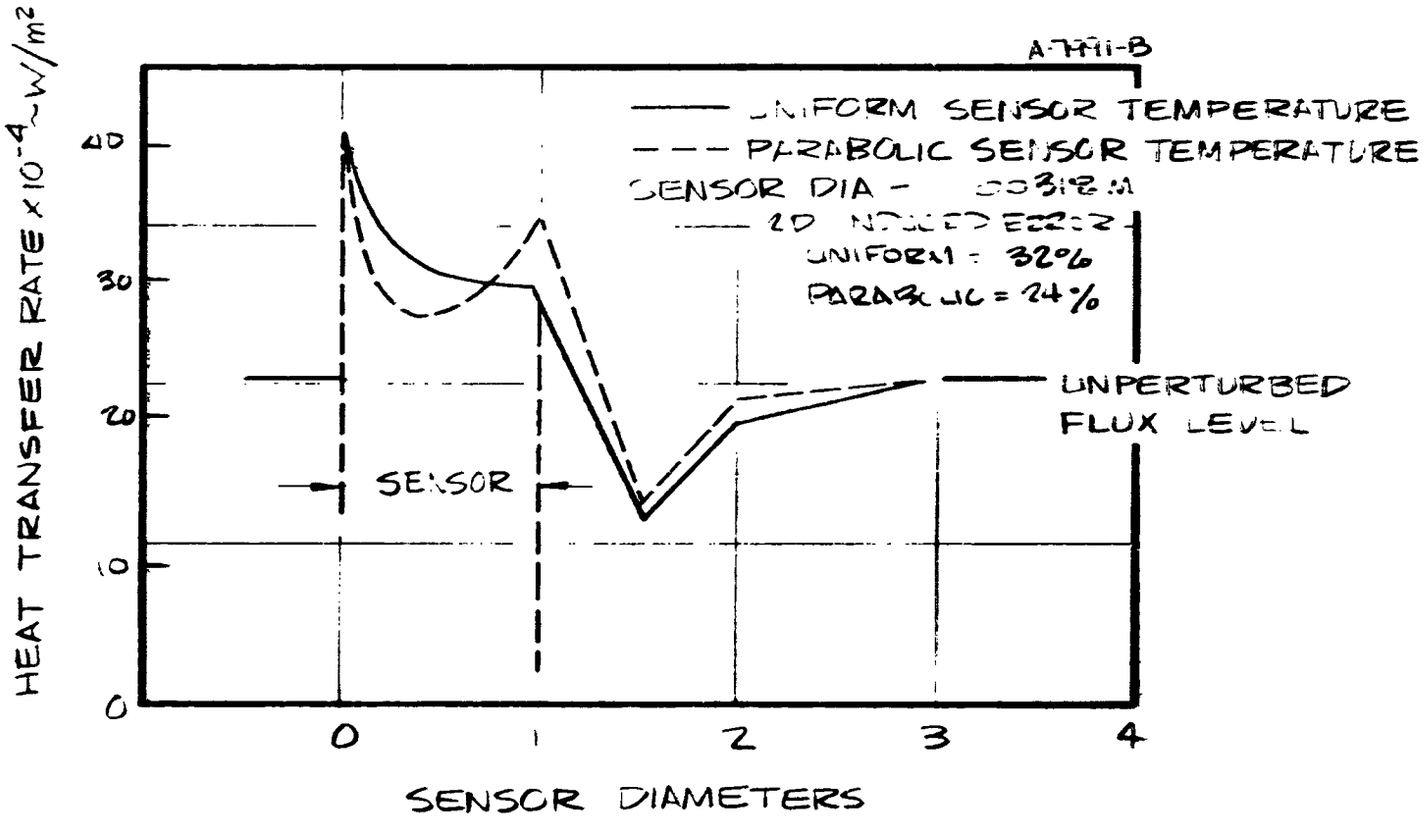

Figure 25. Calorimeter cold wall boundary layer perturbation.

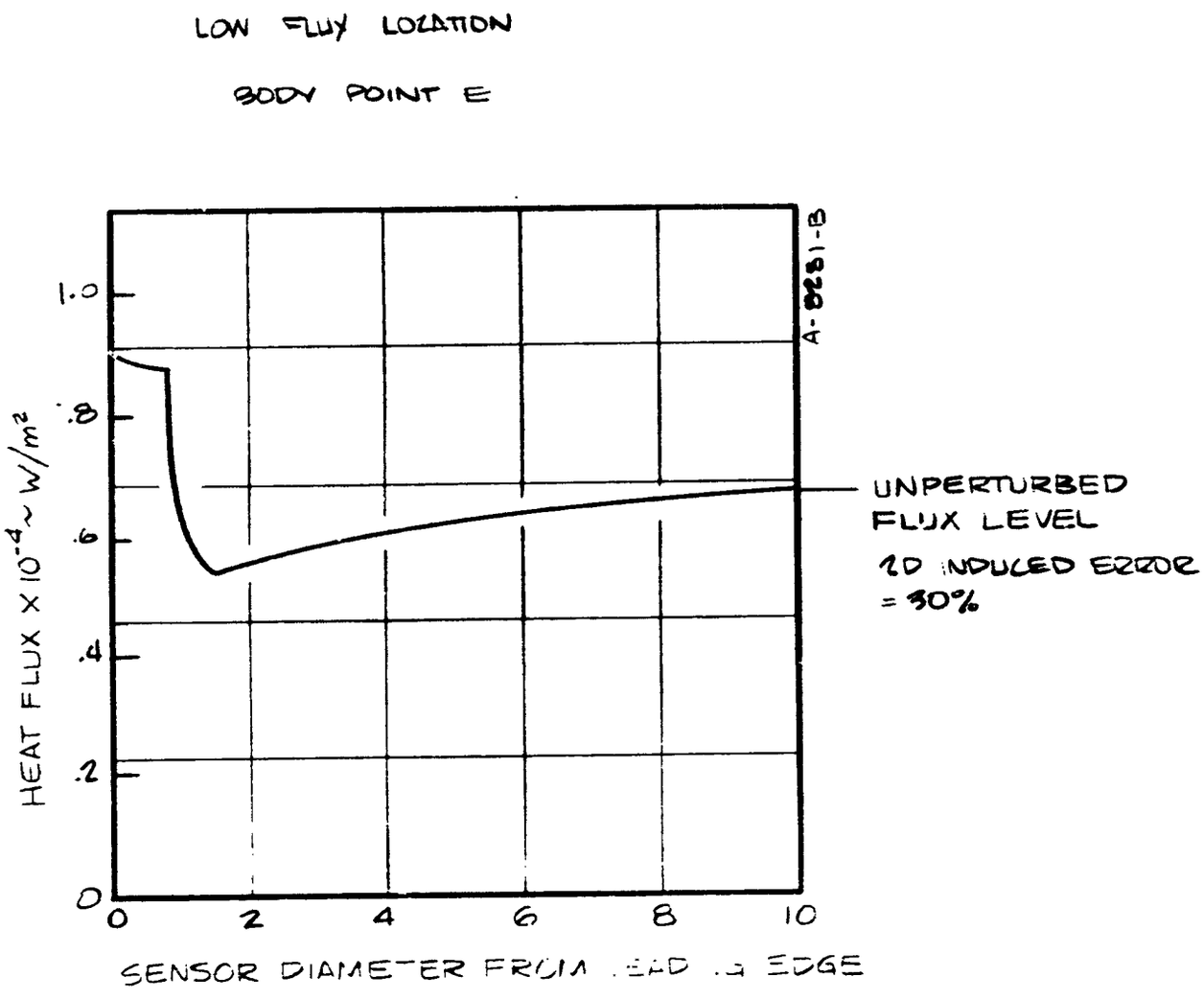

Figure 26. Sensitivity of heat flux measurements to boundary layer perturbation.

- PROVIDES MORE UNIFORM FLUX DISTRIBUTION ACROSS SENSOR
- REQUIRES ADDITIONAL HEAT SINK CAPACITY FOR PASSIVE DESIGN

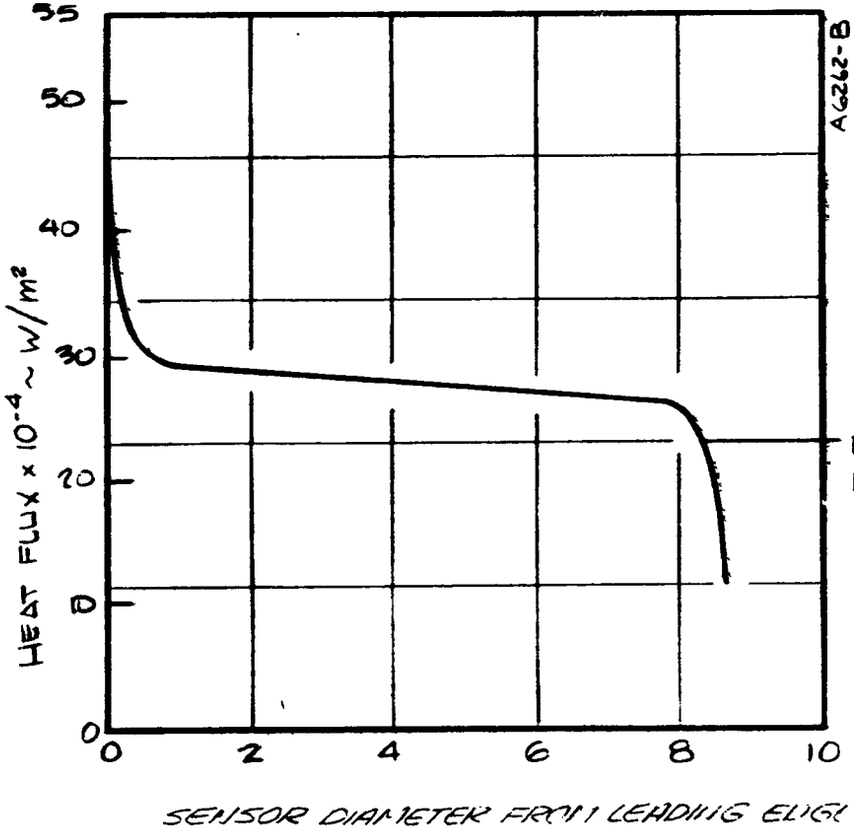

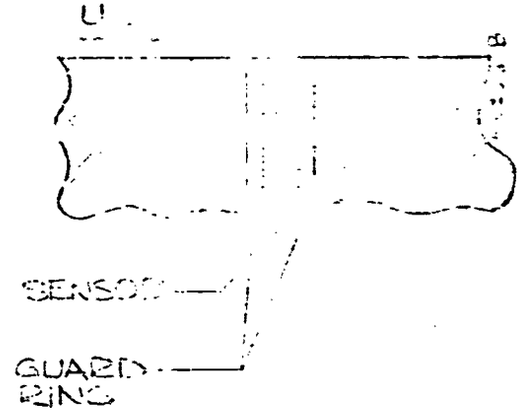

UNPERTURBED FLUX LEVEL

Figure 27. Sensitivity of heat flux measurement errors to cold guard ring.

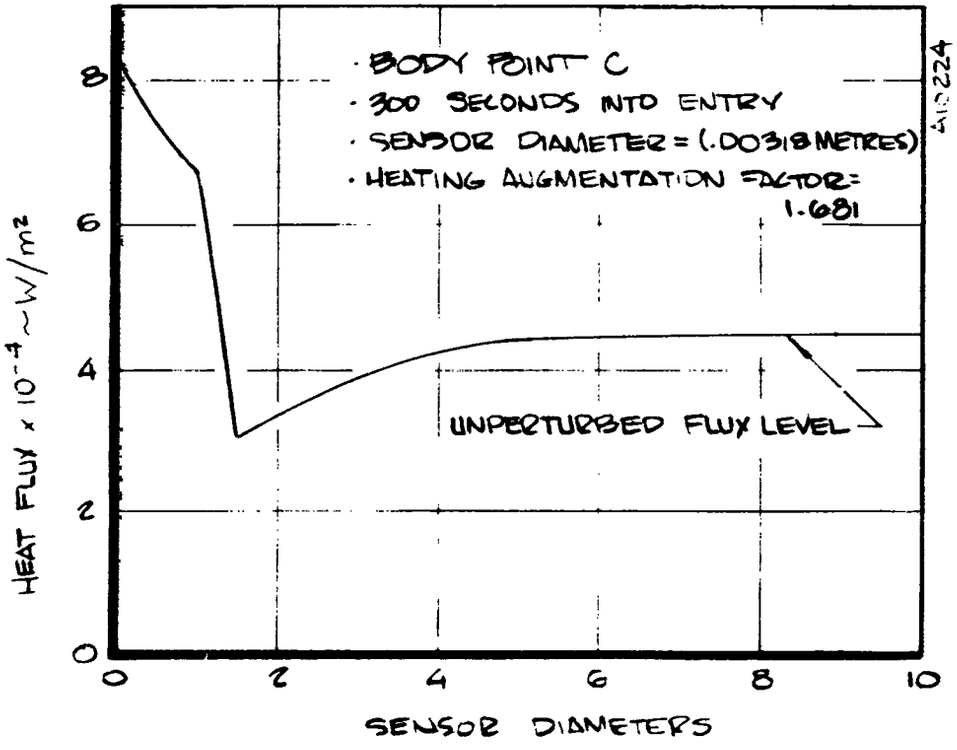

Figure 28. Cold wall boundary layer perturbation analysis.

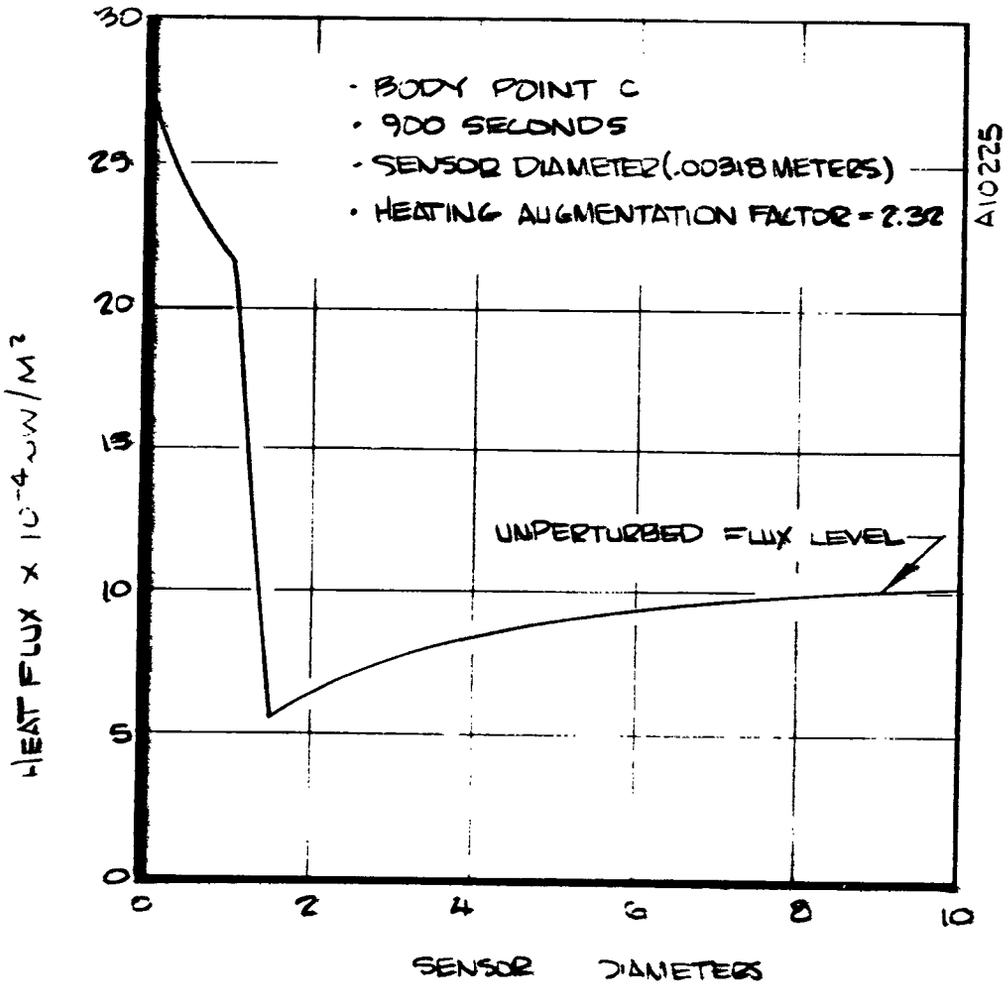

Figure 29. Cold wall boundary layer perturbation analysis.

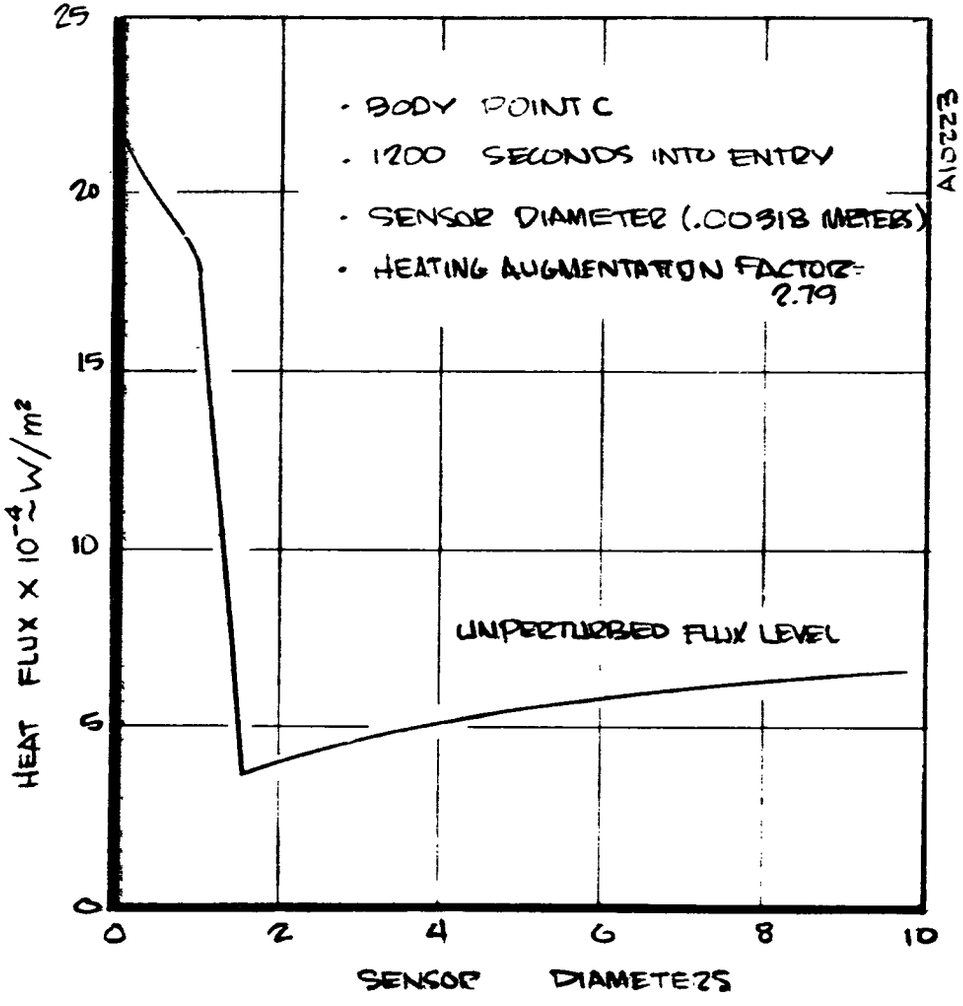

Figure 30. Cold wall boundary layer perturbation analysis.

heating. The analysis results, presented in Figure 31, indicate a 46 percent increase in the incident heat flux due to this phenomenon. This heating augmentation is slightly higher than typical entry augmentations (30 percent). However, due to the reduced peak heat flux, this condition does not generally impact the heat sink design.

In summary, installation of a cold calorimeter in a hot HRSI tile perturbs the boundary layer and associated heat transfer to the sensor. The experiments performed have verified that the analysis techniques are valid qualitatively and quantitatively. For the shuttle operational environment, it is important to locally evaluate the pressure/enthalpy state of the boundary layer. In certain instances, the cold wall may cause the reactive component of the thermal conductivity to additionally augment the incident flux.

2.2.4.2 Temperature Measurement Error Analysis

Two basic types of TPS on the shuttle vehicle require temperature measurement: RCC and HRSI. This section summarizes the error analyses performed for each TPS type within the shuttle operational enviornmental contraints as described in the design criteria section.

2.2.4.2.1 RCC Back Face Temperature Measurement Error Analysis

A one-dimensional transient heat transfer analysis was performed to determine the relative magnitude of the temperature measurement errors that can be expected with a thermocouple attached to the back surface of the RCC. Figure 32 shows the model used for this preliminary analysis. The resistance due to radiation exchange in the cavity behind the RCC was assumed negligible relative to the high thermal resistivity of the HRSI. When one considers the effects of 2-D cross-reradiation within the leading edge cavity, the error in the RCC back face temperature measurement will increase slightly. Using the heating profile for Body Point A, figure 33 shows the results of this analysis both in terms of absolute error magnitude, and percentage error. The errors produced are almost entirely due to the additional thermal capacity of the cement layer with the error magnitude being almost exactly proportional to cement thickness.

2.2.4.2.2 HRSI Temperature Measurement Error Analysis

Several techniques have been employed to evaluate the errors associated with a thermocouple installed in an HRSI panel. A simplified steady-state analysis was formulated to provide insight to expected sensitivities of the error to wire land length, diameter, and type. A more complicated three-dimensional SINDA analysis was used to define transient response errors.

The simplified steady-state fin analysis is based on the following energy balance for a fin

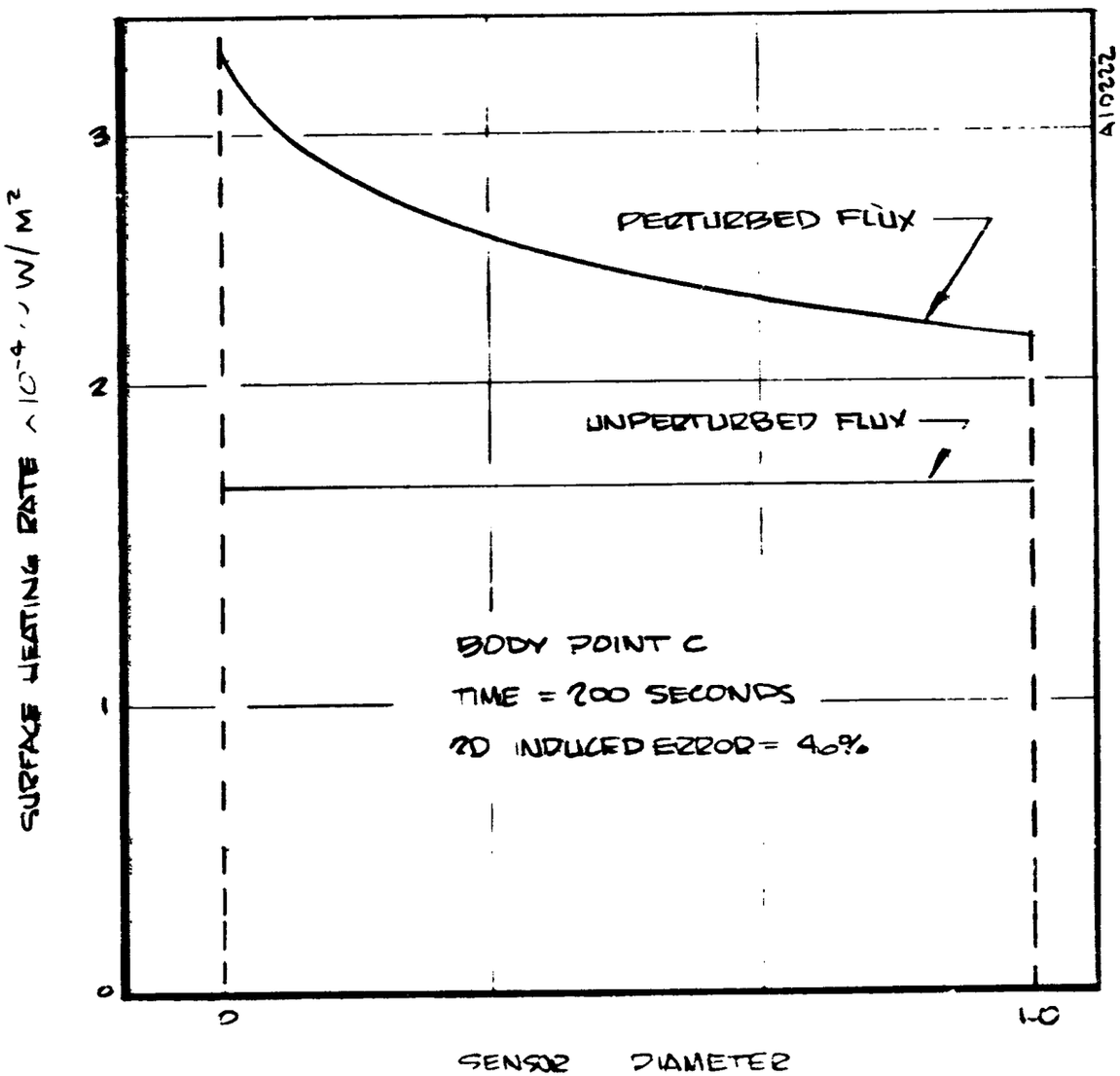

Figure 31. Cold wall boundary layer heating augmentation analysis.

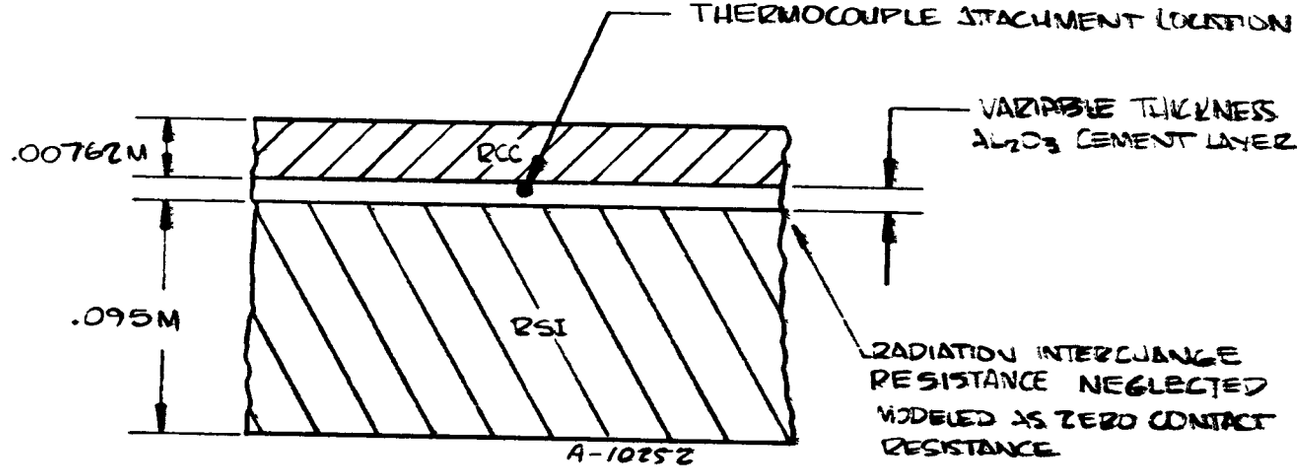

Figure 32. Simplified one-dimensional model used to obtain approximate thermocouple attachment error magnitude.

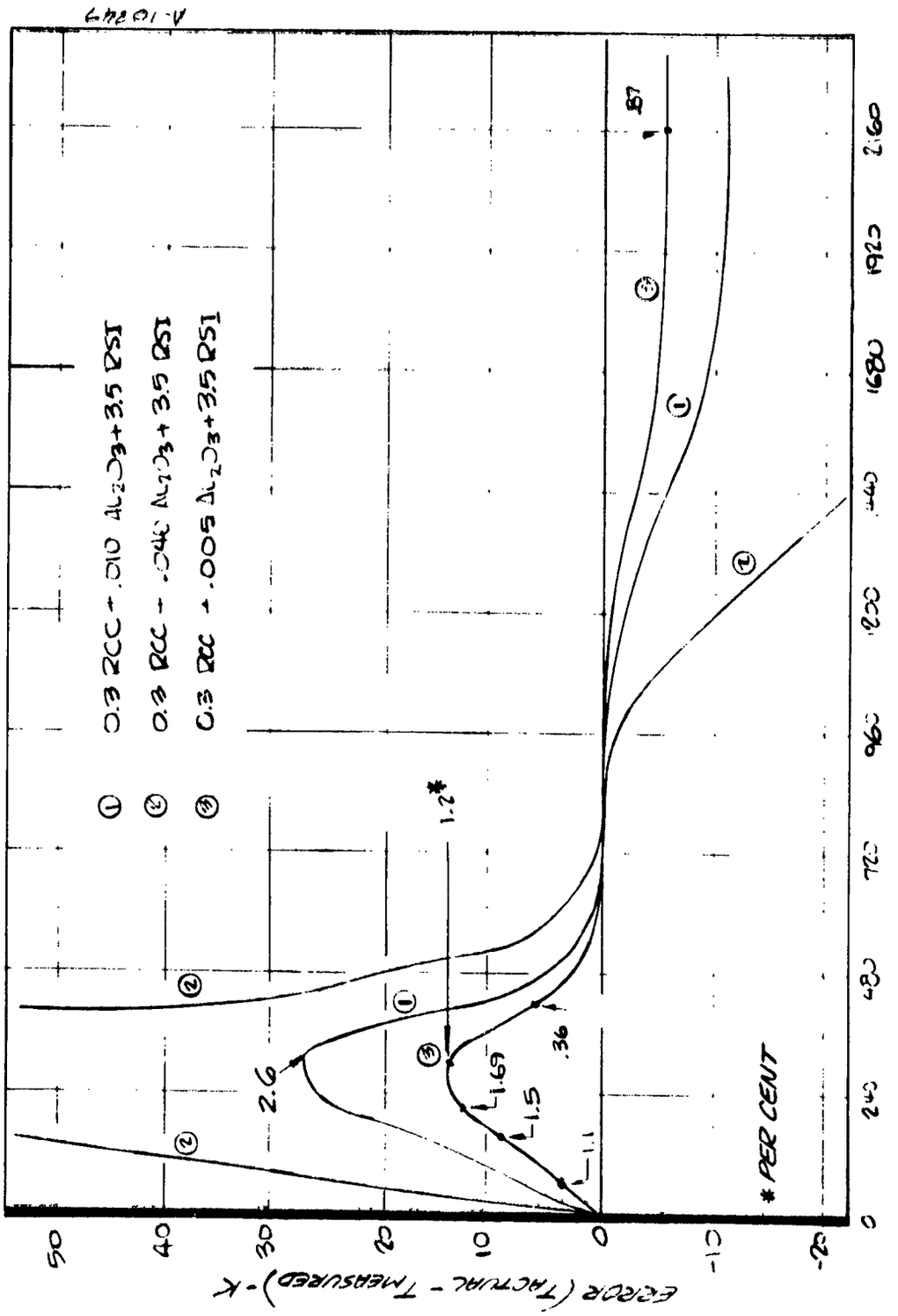

Figure 33. Thermocouple attachment error for varying cement thicknesses.

$$\frac{d^2\theta}{dX^2} - \frac{hP}{KA}\theta = 0 \qquad (1)$$

where $\theta = T - T_1$ and the fin configuration is defined in Figure 34. Solving Equation (1) for heat flow into the base of the fin and equating to the conduction loss to the structure/internal cavity through ℓ_2

$$\frac{KA(T_2 - T_3)}{\ell_2} = \sqrt{hPKA}\,(T_{UP} - T_2)\tanh(m\ell) \qquad (2)$$

where
- T_{UP} = unperturbed temperature
- m = $\sqrt{hP/KA}$
- h = effective heat transfer coefficient between fin and surrounding insulation
- P = thermocouple wire perimeter
- K = thermal conductivity of thermocouple wire
- A = cross-sectional area of thermocouple wire

Solving Equation (2) for T_2, the temperature error is then given by

$$T_{error}\ (\text{degrees K}) = \frac{T_{UP} - T_2}{\cosh(m\ell)} \qquad (3)$$

This result was then used to define the conduction induced errors for various thermocouple configurations. Figure 35 presents a typical sensitivity of this error to the relative thermocouple location. Figure 36 also presents a typical error sensitivity to wire diameter, land length and wire type.

An alternate thermocouple error analysis technique has also been evaluated. In this analysis the thermocouple is immersed in the insulation with a heat transfer coefficient, h, between the insulation and the thermocouple wire. The temperature of the surrounding insulation at large distances from the thermocouple is assumed to have an exponential variation with distance from the heated surface. From a steady state energy balance on an infinitesimally small element (see Reference 4)

$$\nabla^2 T_i = \frac{hP_i}{K_i A_i}(T_i - T_i')$$

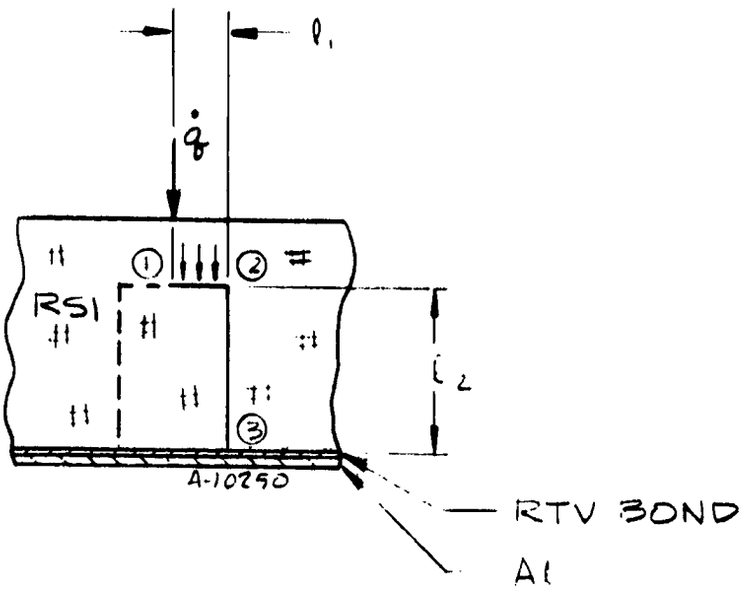

Figure 34. Configuration for fin analysis.

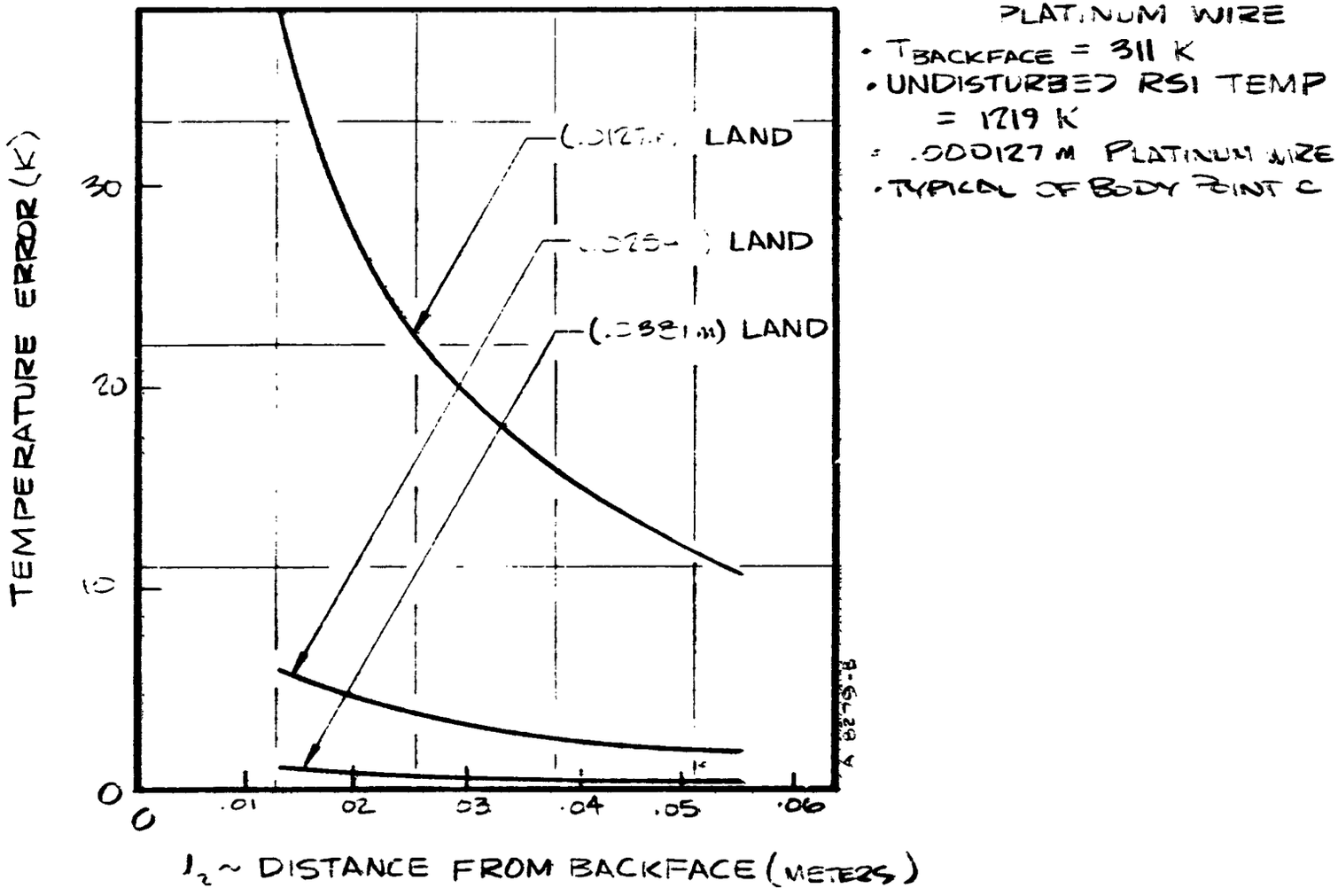

Figure 35. Sensitivity of conduction induced errors to relative thermocouple location.

- UNPERTURBED TEMPERATURE = 1219 K
- PRESSURE = 1013 Pa
- (.0549m) RSI PANEL THICKNESS
- TYPICAL OF BODY POINT C

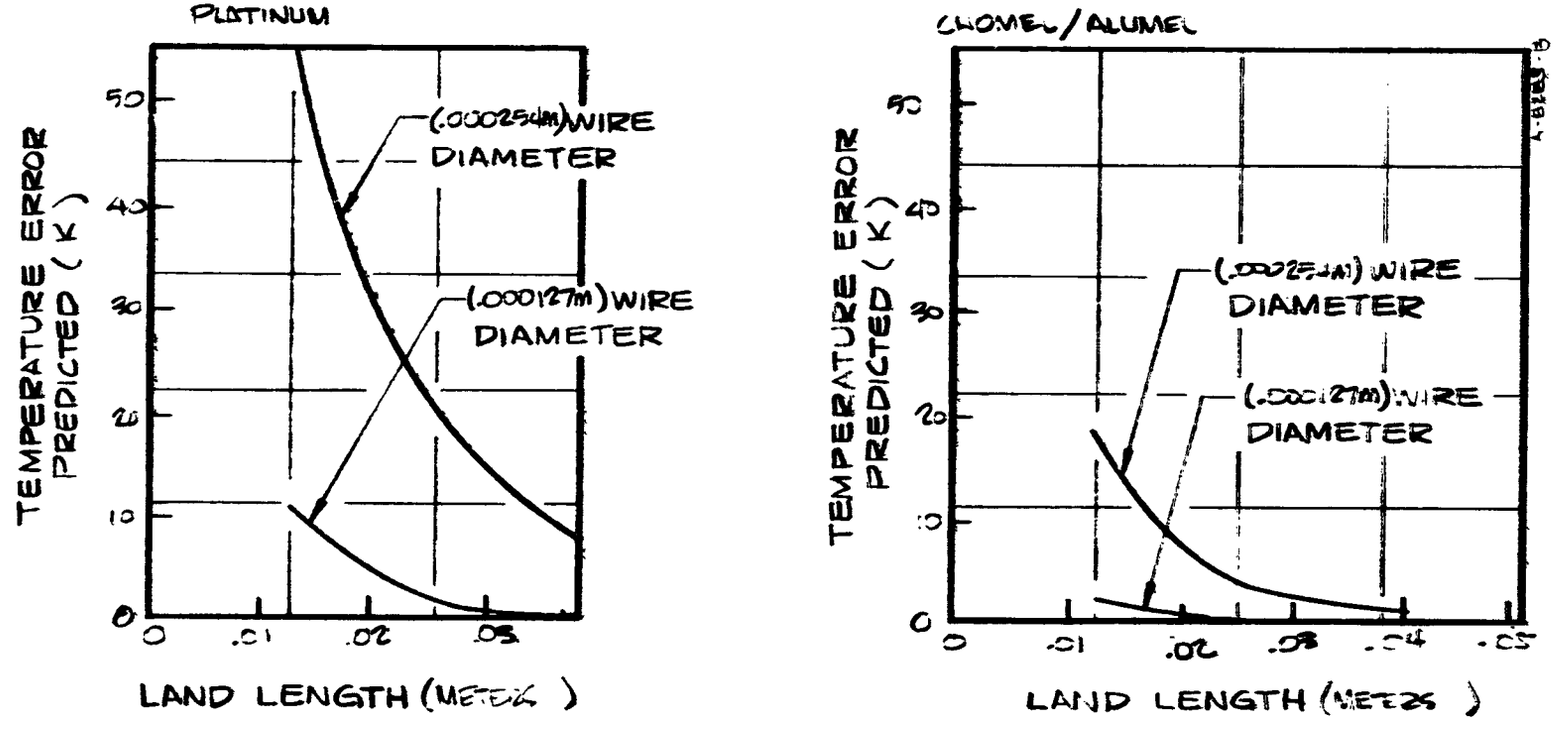

Figure 36. Measurement sensitivity to wire diameter land length [illegible] thermoelement.

where K_1 = thermal conductivity of the thermocouple leg

A_1 = cross-sectional area of the thermocouple leg

T_1 = temperature of the element at any point

h = equivalent heat transfer coefficient between the thermocouple and the insulation

P_1 = perimeter of the thermocouple

T'_∞ = temperature of the insulation at the same coordinate T_1 but without the effect of the thermocouple

but T'_∞ may be approximated by

$$T'_\infty = T_\infty e^{-\beta x}$$

where T_∞ = the temperature of the insulation in the plane of measurement

x = coordinate in the direction of the thermal gradient

β = constant depending upon the thermal gradient

Thus for the system under consideration $0 \leq x \leq L$ (refer to Figure 37)

$$\frac{d^2T_1}{dx^2} - \gamma_1^2 (T_1 - T_\infty) = 0$$

$$T_\infty = \text{constant}$$

$$\left.\frac{dT_1}{dx}\right)_{x=0} = 0$$

$L \leq x \leq \infty$

$$\frac{dT_2}{dx^2} - \gamma_2 (T_2 - T'_\infty) = 0$$

$$T_1\Big)_{x=\infty} = 0$$

$$T'_\infty = T_\infty e^{-\beta(x-L)}$$

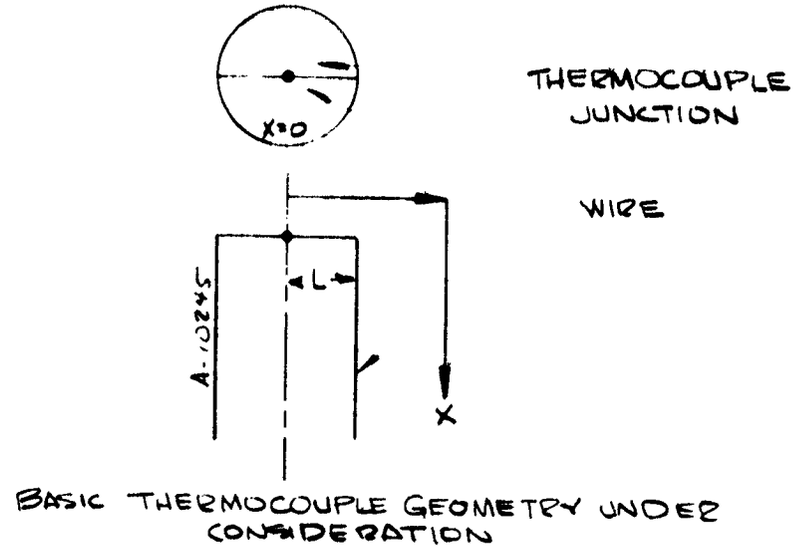

BASIC THERMOCOUPLE GEOMETRY UNDER CONSIDERATION

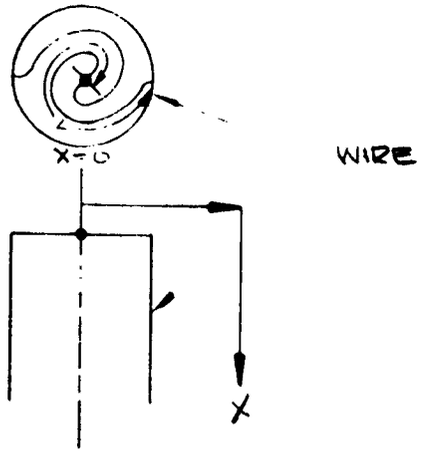

HELICOIL THERMOCOUPLE CONFIGURATION

Figure 37. Thermocouple configuration definition.

at $x = L$

$$T_2 = T_1$$

$$\frac{dT_2}{dx} = \frac{dT_1}{dx}$$

where

$$\gamma_{1,2} = \sqrt{\frac{h_{1,2} P_{1,2}}{K_{1,2} A_{1,2}}}$$

1 refers to $0 < x < L$

2 refers to $L < x < \infty$

The solution with the boundary conditions delineated above is:

$$T_1 - T_\infty = \frac{-2\gamma_2 P T_\infty}{(h + \gamma_2)\left[e^{\gamma_2 L}(\gamma_2 + \gamma_1) + e^{-\gamma_1 L}(\gamma_2 - \gamma_1)\right]}$$

Now, the equivalent heat transfer coefficients for the various legs must be evaluated:

$$h = \frac{K_{INS} \left(\frac{dT}{dr}\right)_{r=R}}{T_\infty - T)_{r=R}}$$

K_{INS} = insulation thermal conductivity

$T)_{r=R}$ = temperature at the insulation thermocouple interface

For the section $0 < x < L$, the thermocouple lies perpendicular to the temperature gradient. Therefore, at steady state the gradient at the thermocouple insulation interface is composed of the gradient in an undisturbed material plus the gradient due to a thermocouple of radius R and length ℓ.

$$h_i = \frac{2K_{INS}}{R}\left[\ln\left\{\frac{R/\ell\left[-1 + \sqrt{\left(\frac{R}{\ell}\right)^2 + 1}\right]}{\left[1 + \sqrt{\left(\frac{R}{\ell}\right)^2 + 1}\right]\left[2 + \sqrt{\left(\frac{R}{\ell}\right)^2 + 4}\right]}\right\}^{-1}\right]^{-1} + K_{INS}\ell$$

Along the leg parallel to the temperature gradient, the first term in the foregoing relationship represents the heat transfer coefficient. Thus,

$$h_2 = \frac{2K_{INS}}{R}\left[\ell n\left\{\frac{R/\ell\left[-1+\sqrt{\left(\frac{R}{\ell}\right)^2+1}\right]}{\left[1+\sqrt{\frac{R}{\ell}^2+1}\right]\left[2+\sqrt{\frac{R}{\ell}^2+4}\right]}\right\}^{-1}\right]^{-1}$$

Now, the remaining assessment necessary to complete the analysis is to evaluate ℓ. This parameter must be evaluated as a function of the insulation temperature profile (i.e., linear for steady state tests, and typically exponential for transient heating pulses).

A comparison of results from these two simplified thermocouple error analysis techniques demonstrates reasonable agreement. However, due to the added complexity associated with using the second technique, the simplified fin analysis methodology was used in the analysis of test data.

A three-dimensional SINDA model was used to define the conduction error for the transient case corresponding to the expected flight environment. Figure 38 presents the error as a function of land length and reentry time. The corresponding response for this case is shown in Figure 39 which reveals the differences between 0.0127 m and 0.0381 m (0.5 and 1.5 inch) land length produce only an amplitude perturbation with no detectable lag characteristic. The SINDA model for transient thermocouple error analysis is extremely complex, and consequently the predicted trends are reasonable; however, the magnitude of the predicted errors is questionable.

With the simplified analysis approach, a good physical understanding of the expected trends in error analysis is provided for steady state conditions. Consequently, order of magnitude assessments of the relative importance of design variables may thus be obtained. Providing reasonable solutions cheaply and easily, the simplified fin analysis procedure for evaluating thermocouple errors has been applied to produce the parametric evaluation of steady state thermocouple errors presented in Figures A-1 through A-6 in Appendix A. These analysis results provide a basis for evaluating errors of various thermocouple types and installation throughout a variety of environments typical of the expected shuttle operational envelope.

2.2.5 Installation Evaluation

The accuracy and reliability of an instrument installed in or on a tile of TPS material is a strong function of the installation technique. The effect of that technique on the overall TPS performance must also be considered. The following discussions concern those techniques identified as the most likely to provide a

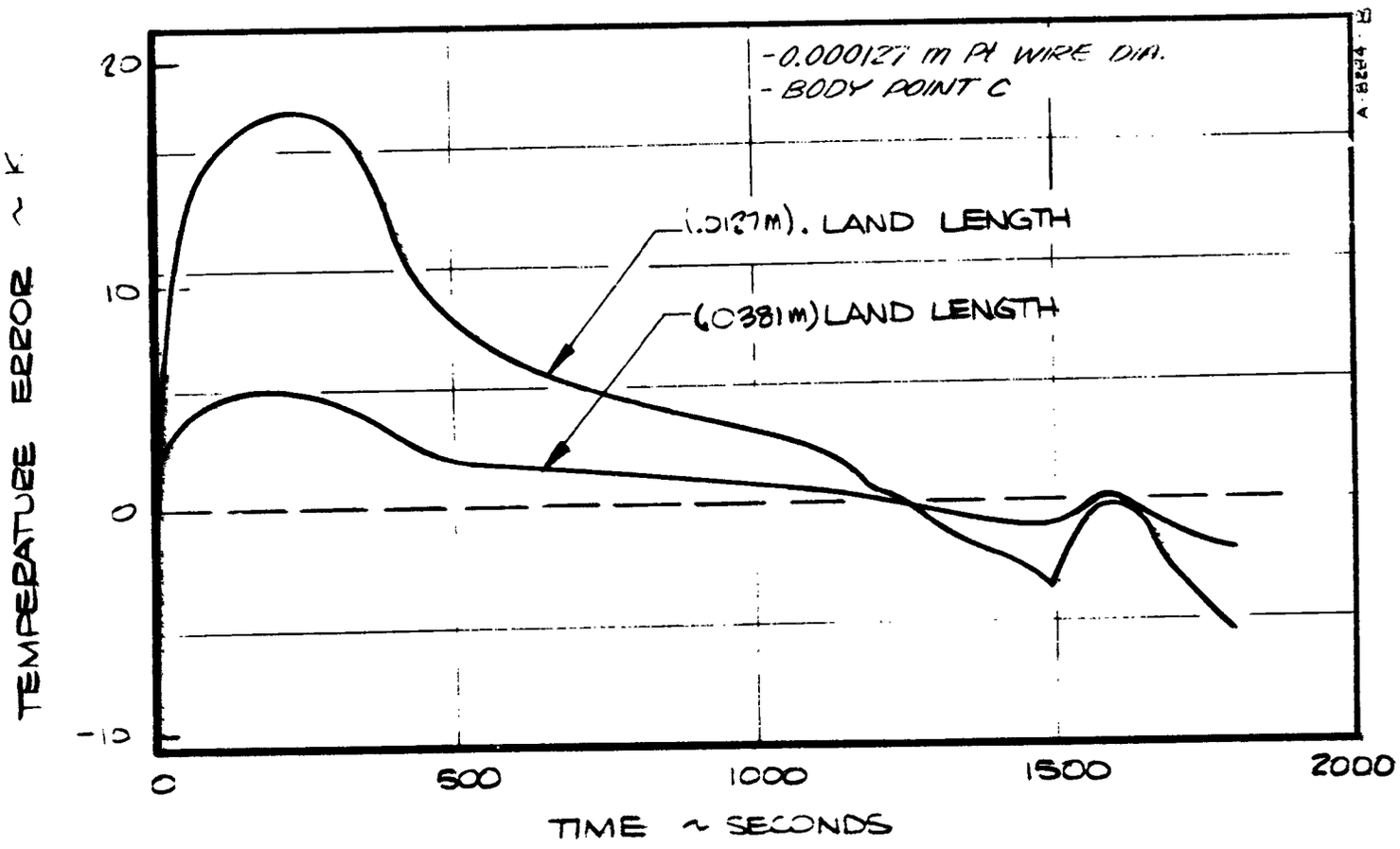

Figure 38. Measurement sensitivity to land length, transient analysis.

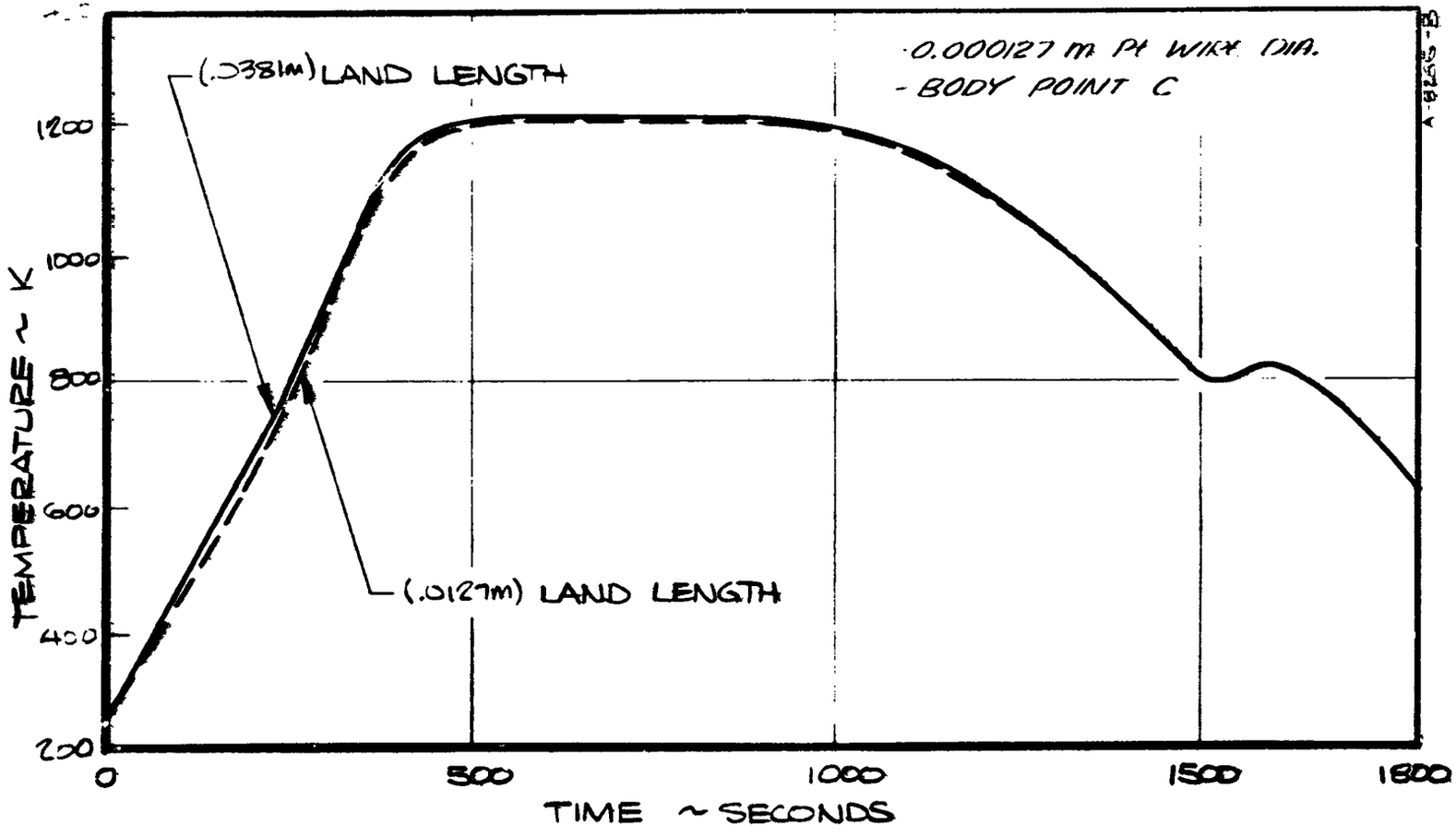

Figure 39. Sensitivity of the response characteristic to land length.

satisfactory installation with highest possible instrument accuracy. The instrument types selected during the design phase were the only ones considered in the installation evaluation.

2.2.5.1 HRSI Instrumentation

2.2.5.1.1 HRSI Thermocouple Installation

The installation of a small diameter thermocouple wire in a tile of HRSI while maintaining the structural integrity of the tile was the primary constraint in evaluating the many possible techniques. Figure 40 illustrates the basic techniques selected as feasible. The embedded thermocouple technique offers the minimum disturbance to the material since the thermocouple is installed during manufacture, typically before the coating process. The instrumented plug technique may be applied before or after the coating process. The best surface thermocouple installation is obtained with the thermocouple in place during the coating process, allowing for intimate contact of the thermocouple and coating. The plug may be instrumented with one or more thermocouples. The installation with one thermocouple on the top of the plug offers the best accuracy in the positioning of the thermocouple, i.e., the depth from the front face. This is critical if the data obtained is to be meaningful in evaluating TPS performance.

The "Helicoil" wire configuration can be employed as a means of improving the thermocouple accuracy by further reducing the conduction errors due to the lead wire. The use of the helicoil configuration instead of a larger plug is based on the fact that the thin HRSI coating is limited in strength. Since the coating over the plug must be considered self-supporting in the worst case, and considering the importance of the coating to the integrity of the HRSI, it is desirable to use as small a plug diameter as possible.

If the installations are limited to the use of precoated HRSI tiles, a situation that existed for all test samples and could very well be a requirement for the ultimate application, a slightly more involved technique is required. Coring of the tile must be carefully done to the location or depth desired or in the case of a surface thermocouple, to slightly short of the coating with hand removal of all RSI material from the coating. The plug is fabricated in the normal manner using care to provide the proper fit. Experience with this technique showed that a good surface thermocouple (one in contact with the coating) could be achieved. No cements or adhesives were used to hold the plug in place. The bonding of the panel to the vehicle substrate provides the ultimate retention of the plug.

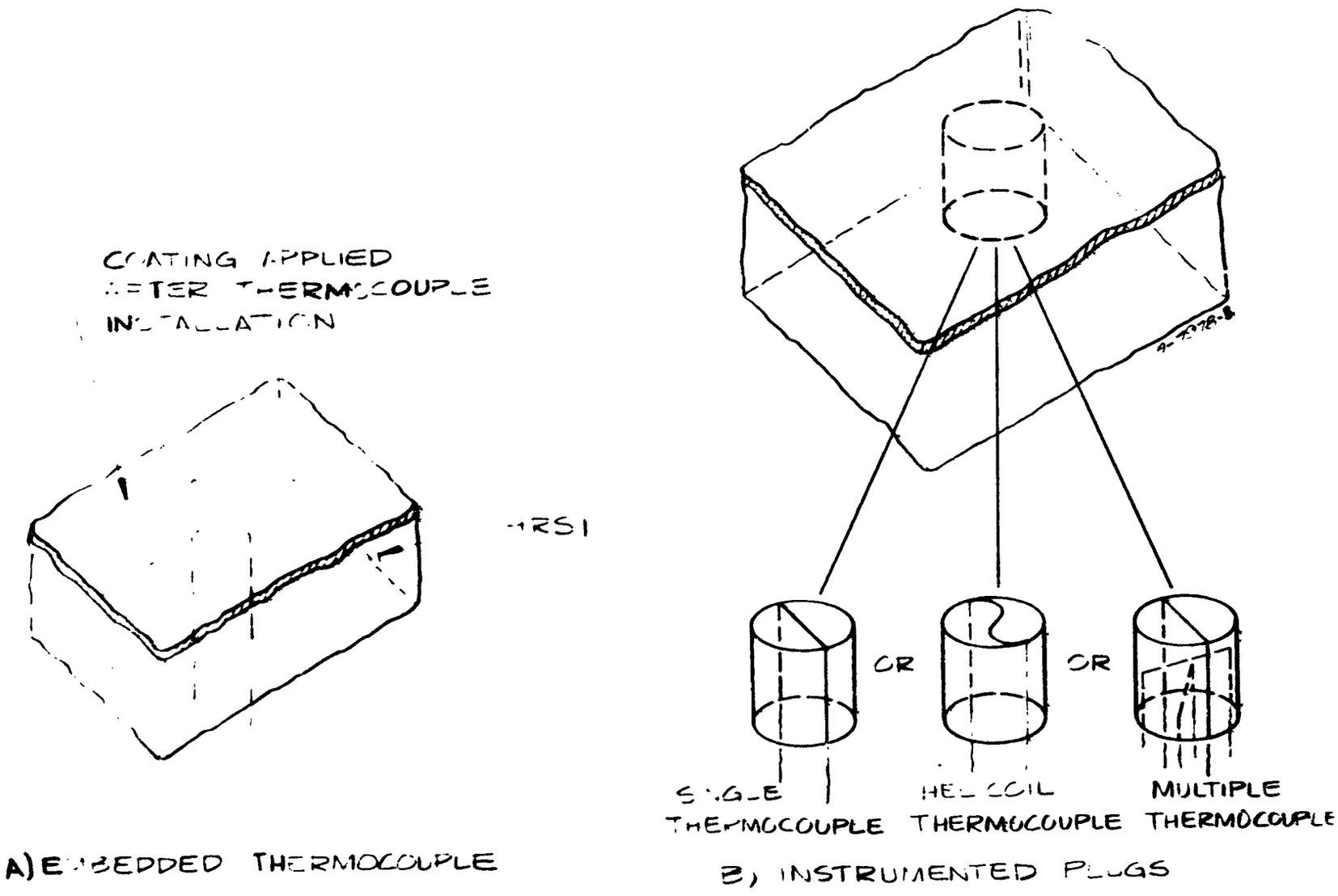

Figure 40. HRSI thermocouple installation.

2.2.5.1.2 HRSI Calorimeter Installation

With the selection of the augmented Gardon gage for the HRSI calorimeter, several contraints on the gage installation are then required. First, the gage must be maintained below about 519 K (475°F) throughout the reentry profile requiring some form of passive cooling, active cooling being unacceptable for basic system reliability reasons. Second, the gage installation must not compromise the HRSI performance either thermally or structurally. Heat sink cooling, with the sink located in the relatively cool area of the HRSI near the bondline, has been selected as the most attractive approach. A large emphasis is thus placed on the size of the calorimeter in order to minimize the imposed heat load and consequently the heat sink mass. The shape and mass of the heat sink is optimized for its vehicle location, i.e., imposed heat load.

The heat sink is connected to the Gardon gage through means of a slender stem, designed to produce the smallest temperature gradient possible between the gage and heat sink. On the other hand the stem must also provide as little cylindrical surface area as possible thus minimizing hot HRSI/stem heat transfer, which must also be accommodated by the heat sink. While these two requirements seem to dictate different stem designs, the total imposed heat load must be minimized, increasing the gage/heat sink temperature gradient as the stem diameter decreases to its absolute minimum.

The Gardon gage/heat sink installation used in the Task 2 test program is shown in Figure 41. The overall stem diameter was 0.00318 m (0.125 inch). Note that the heat sink was installed behind the thin (0.0254 m (1 inch)) test panel because of space limitations. The sink was completely insulated to duplicate thermally the actual expected vehicle installation while allowing temperature measurements to be taken on the heat sink as a check on performance.

The maximum reliability of this installation will be realized if the gage/stem/sink are fabricated as an integral unit. The unit should be bonded to the vehicle substrate, relieving some of the structural loads from the low density HRSI. Gold plating on the unit will decrease the radiative interchange with the hot HRSI. The interface between the HRSI coating and the stem face (containing the Gardon gage) must be extremely smooth if accurate heat flux data is to be recorded.

2.2.5.1.3 HRSI Pressure Port

The measurement of local surface pressure on the HRSI can most easily be accomplished by providing a pressure port through the HRSI panel, pneumatically coupling the pressure transducer with the surface. In this manner, the gage or transducer may be located in a relatively cool region of the vehicle, relaxing the requirements on the transducer.

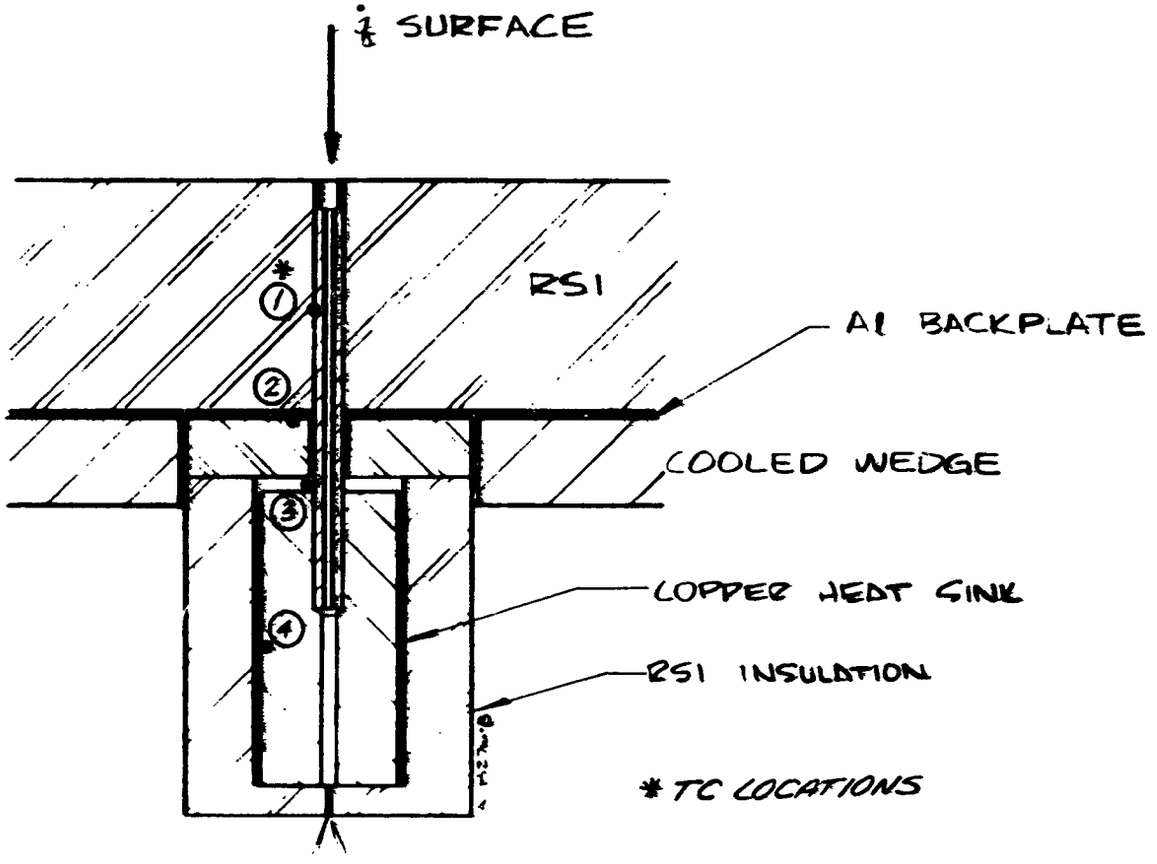

Figure 41. Gardon gage/heat sink installation for Task 2 testing.

The effect a pressure port may have on the HRSI tile integrity (the hole through the coating acts like a flaw) must be experimentally determined. Previous testing results would indicate this is no problem if hole or port sizes are kept below about 0 00318 m (0.125 inch) diameter.

2.2.5.2 RCC Temperature Measurement

The installation of any temperature measurement instrument on RCC is complicated by the radiant interchange cavity behind the RCC panels and the coating of the RCC itself. The requirement that the oxidation inhibiting coating of the RCC not be breached requires a surface type temperature measurement on the rear face of the RCC.

The primary choice is thermocouples attached to the surface by means of high temperature cements or the high purity alumina flame spray technique. The high temperature environment behind the RCC requires a sheath-type thermocouple wire be employed as lead wire. The reactive nature of the siliconized coating of the RCC requires a coated or sheathed thermocouple itself for maximum lifetime for this installation.

An alternate temperature measurement technique is available if the thermocouple attachment technique proves to be unsuitable for the 100 mission lifetime. An optical sensor would be located in a cool region of the vehicle structure with either a direct view of the RCC rear surface or coupling by means of a light pipe or fiber optics technique. Problems in applying this technique include sensor drift with time and temperature, stray radiation errors, viewing area definition, surface emittance determination and system calibration or checking.

2.3 TASK 2 - TESTING

Duplicating as closely as possible the shuttle flight conditions, local vehicle configuration, and flight installation configuration appropriate to the instrumentation application, a test program was conducted to screen and verify the instrumentation designs in terms of accuracy, installation and interaction with the TPS. Extensive analysis was accomplished to establish the simulation requirements and predict the instrumentation response as a basis for evaluating its performance.

2.3.1 Test Requirements

The five vehicle locations identified by NASA as representative of the range of conditions encountered by the TPS (see Section 2.2.2) were the basis for the test conditions used throughout the testing phases. The first point, B.P.A., with a peak heating rate of 4.65 x 10^6 W/m^2 (41.0 Btu/ft^2sec) is an RCC location and thus was used as the test condition for the RCC testing. The four remaining locations represent HRSI positions. Three of these were selected as covering the range of conditions

adequately, B.P.B., B.P.C., and B.P.E. with peak heating rates of 2.28 x 10^5, 1.06 x 10^5 and 6.8 x 10^4 W/m^2 (20.1, 9.3 and 0.6 Btu/ft^2sec), respectively. The Phase 1 or screening tests were performed using the peak heating point of these profiles while the test time was adjusted to duplicate the local heat load at that particular point. The Phase 2 or long term evaluation tests duplicated as closely as possible, within the operating limits of the arc plasma facility, the actual reentry profile. This was accomplished by duplicating as much of the heating rate profile as possible; generally the arc heater configuration necessary to achieve the peak heating point imposed a lower bound on the heating rate capability which is higher than that required by the reentry profile. In this case, a heating profile within the limits of the arc heater capability was used with an adjustment for duplication of the local heat load.

2.3.2 Test Program

The cyclic test procedure used in the test phases was developed under NASA Contract No. NAS2-6445 and, with the exceptions noted below, a detailed description can be found in Section 2 of Reference 5 which presents the

- Test facility
- Model and test sample configurations
- Instrumentation and data reduction
- Test procedure

2.3.2.1 Model and Test Sample Configurations

The model configurations employed in the test program were a flat-faced stagnation point model for the RCC tests, Figure 42, and a 30° half-angle wedge model for the HRSI tests, Figure 43. The flat-faced stagnation point model is 0.1206 m (4.75 inch) body diameter with a 0.00318 m (0.125 inch) corner radius. The RCC sample size was 0.108 m (4.25 inch) diameter. A radiation interchange cavity was formed behind the RCC sample with a lining of either Silfrax insulation or bare RSI.

The 30° half-angle wedge model with a 0.0127 m (0.5 inch) nose radius allows for an HRSI sample size of 0.1143 m by 0.1016 m by 0.0254 m thick (4.5 x 4.0 x 1.0 inch). The sample occupied the wedge surface running length interval (referenced from the stagnation line) from 0.0279 to 0.1422 m (1.1 to 5.6 inches). For this test configuration, the first 0.0229 meters (0.9 inch) of the test sample is considered to be a thermal and flow field transition region, the active sample thus running from 0.0508 to 0.1422 meters (2.0 to 5.6 inches).

The test stream was 0.203 m (8 inches) in diameter providing for uniform property distributions over the test sample surface for both test model configurations.

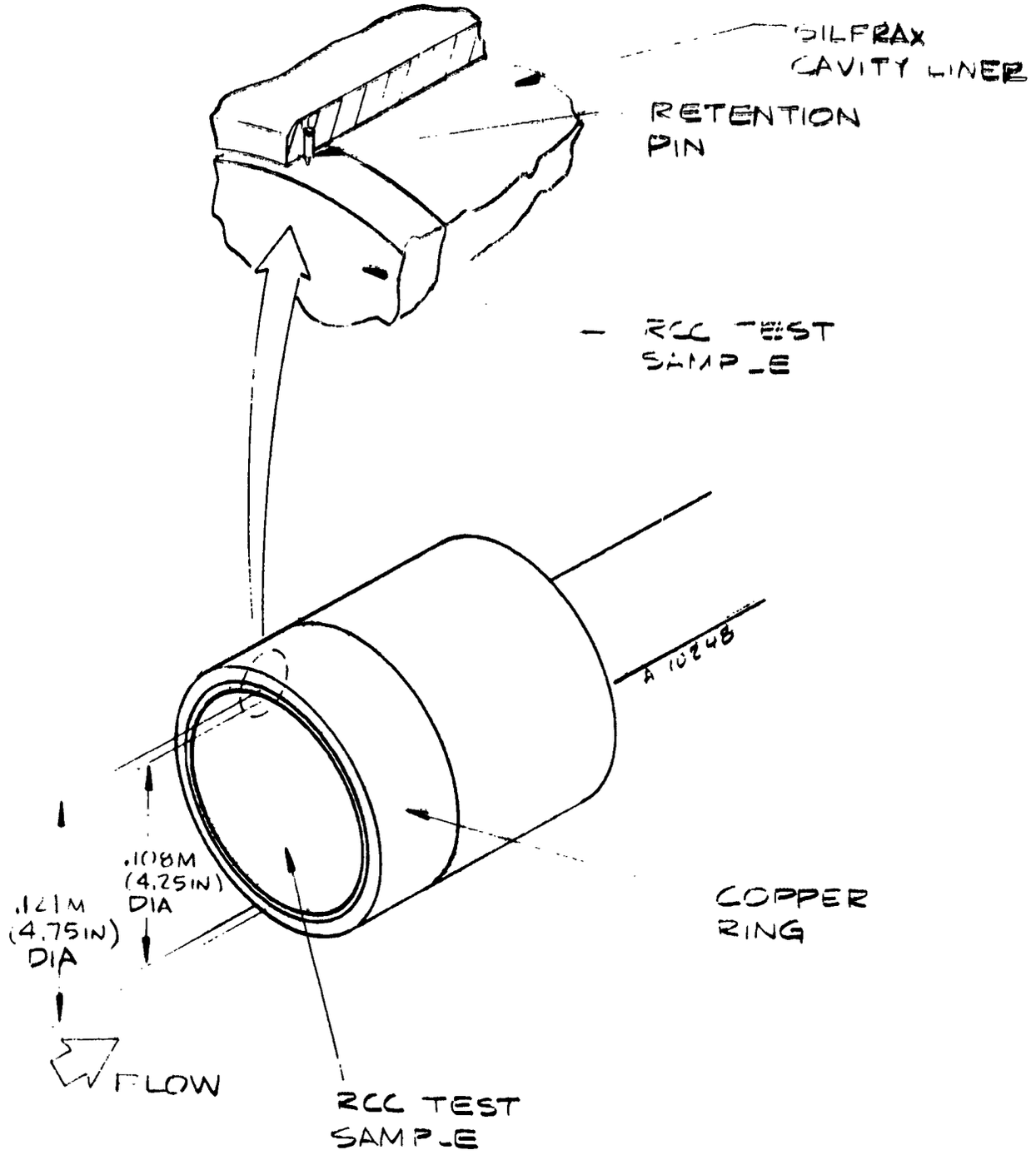

Figure 42. Flat face stagnation point model.

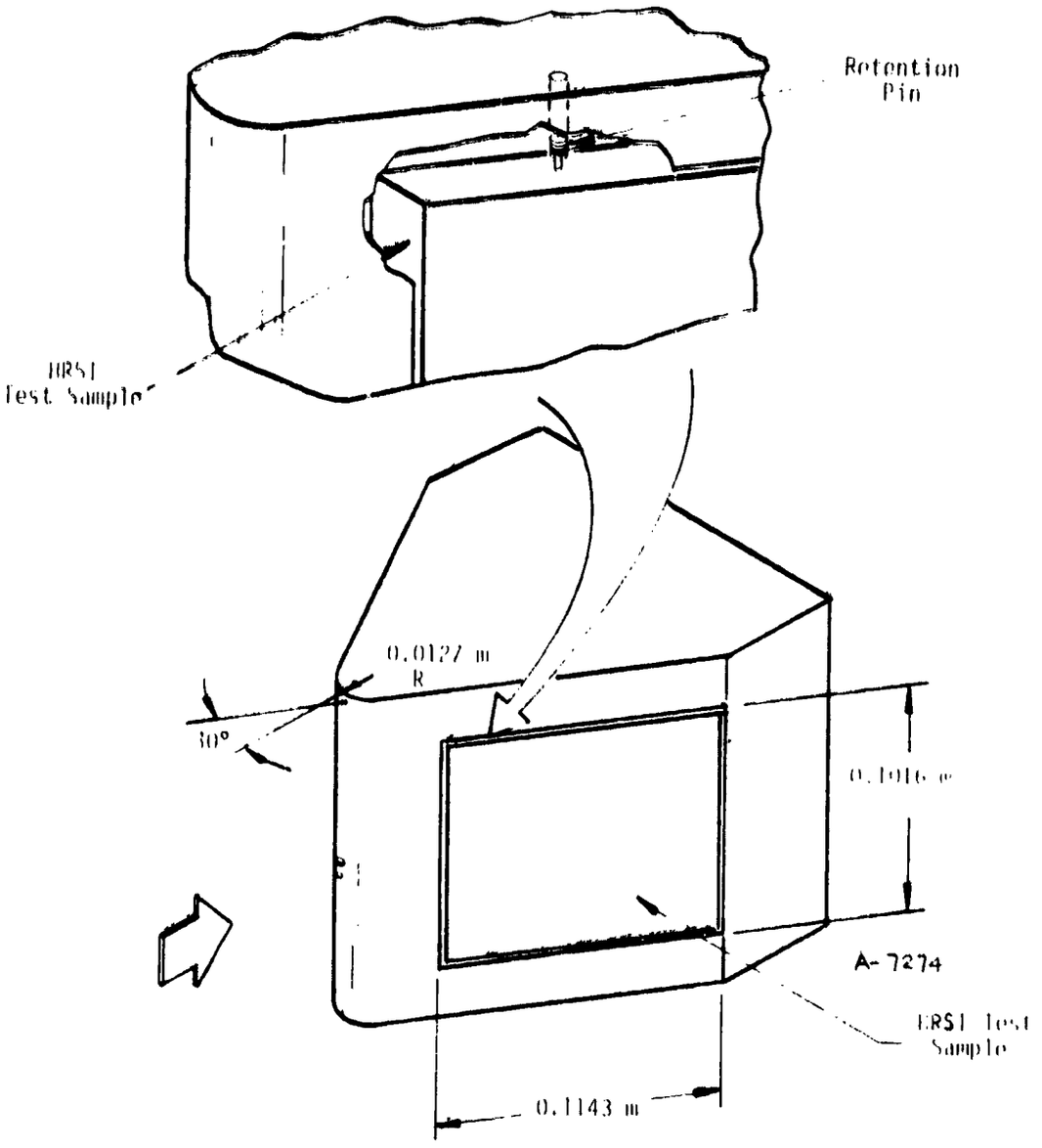

Figure 43. 30° half angle wedge model.

2.3.2.2 Analytic Predictions

Through use of the Boundary Layer Integral Matrix Procedure (BLIMP) program the boundary layer conditions at the peak heating point of the reentry profile were calculated and are presented in Table 6. These are the test conditions for the Phase 1 tests and represent the peak conditions for the Phase 2 tests.

Property distributions over the test sample surface are presented in Figure 44 for the RCC test point (stagnation point model) and Figure 45 for the HRSI wedge test model. It should be noted that the active sample surface runs from S/L = 0.358 to 1.0, providing relatively constant property distributions over the sample.

A one-dimensional thermal model was constructed for each of the four HRSI locations. Using the CMA program, computer runs were made to define the in-depth material response to the reentry profile. This data was the baseline material response for evaluation of instrumentation installations. In addition, the same model was used for calculating the response of the 1-inch thick test models to both the constant heating rate, Phase 1, tests and the heating rate profile, Phase 2, tests. This allowed for comparison and evaluation of the test sample response with the expected material response during reentry. Unperturbed material responses for the LI-900 HRSI, subjected to the reentry conditions, are presented in Figures 46, 47, 48 and 49 as typical results for the material response calculations.

2.3.2.3 Facility Instrumentation

For all tests, surface temperatures were measured pyrometrically with two Infrared Industries Thermodot pyrometers, a TD-9 and a TD-7B. The TD-9 has a sensing wavelength of 0.8 microns while the TD-7B senses over the wavelength band 1.75-2.7 micron.

In all tests, calibration data were taken with a calibration model identical to the test model which contained pressure ports and calorimeters (Gardon gages) distributed over the active test surface. The stagnation point calibration model is detailed in Reference 5, Section 2.3.2. The wedge calibration model is described in Reference 1, Section 2.0.

2.3.3 Test Results

The test results for both Phase 1 and 2 are reported together as there was a considerable overlap of the two phases. The Phase 1 tests served mainly to verify the techniques required for instrumentation installation for the long term exposure evaluation test series. Due to the shortage of available HRSI and RCC material, the initial screening tests (Phase 1) were completed with available LI-1500 HRSI, Ames RSI and scrap pieces of RCC from other programs. In some cases, test samples were sectioned from several separate pieces (in the case of the HRSI). Problems

TABLE 6. TEST CONDITIONS

	Flat Face Stagnation Point Model, Diameter = 0.1260 m (RCC)	Wedge Model (HRSI) S/L = 0.6, L = 0.142 m		
Total Enthalpy, J/kg	3.25×10^7	4.65×10^6	3.25×10^7	3.25×10^7
Catalytic Wall Heat Flux[a], W/m^2	6.24×10^5	9.08×10^3	1.41×10^5	3.04×10^5
Partially Noncatalytic Wall Heat Flux[a], W/m^2	4.65×10^5	6.81×10^3	1.06×10^5	2.28×10^5
Radiation Equilibrium Surface Temperature, K	1789	622	1233	1497
Pressure[c], Pa	417	25	49	230
Heat Transfer Coeffi				

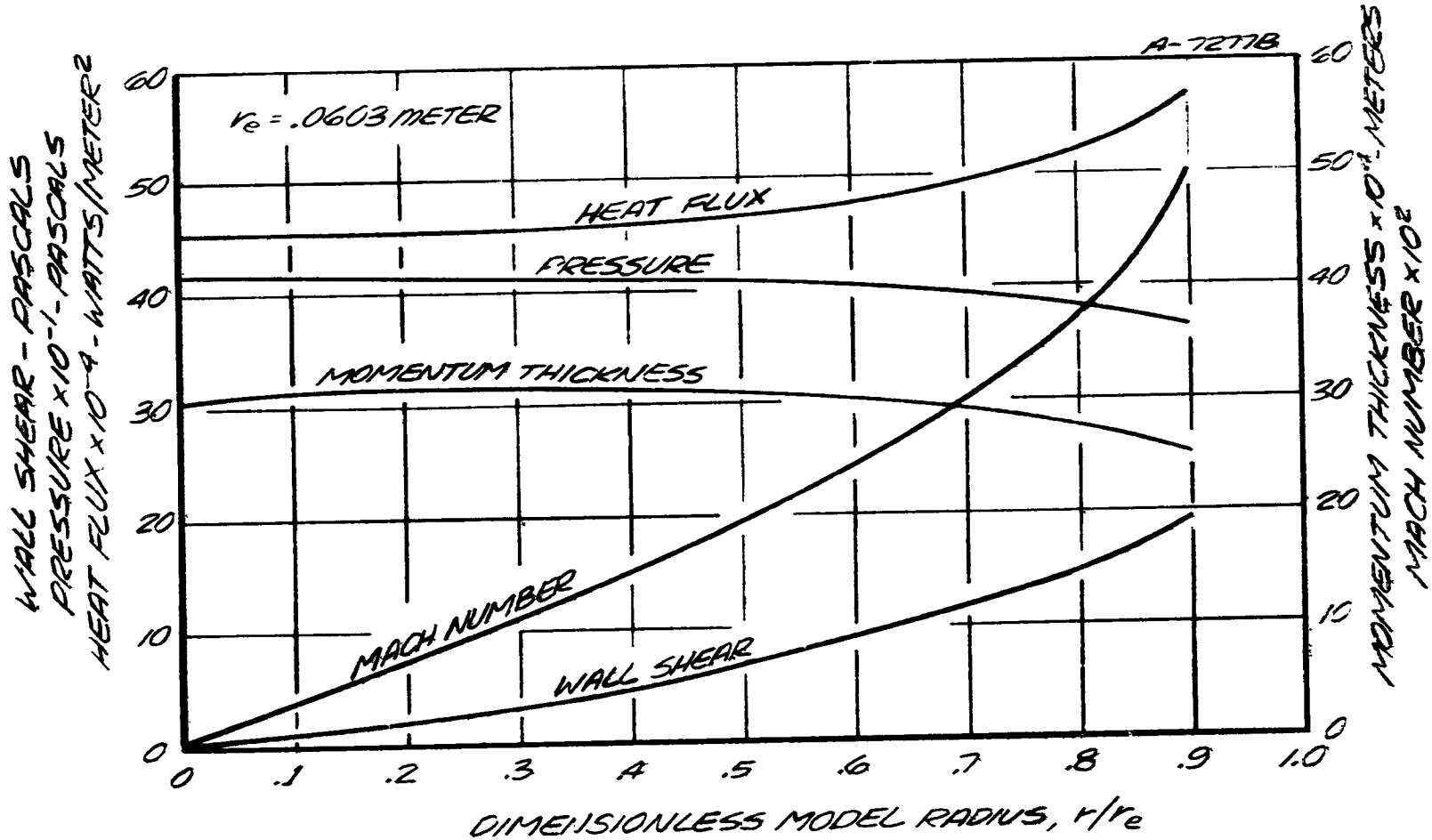

Figure 44. Calculated test sample property distribution - stagnation point model.

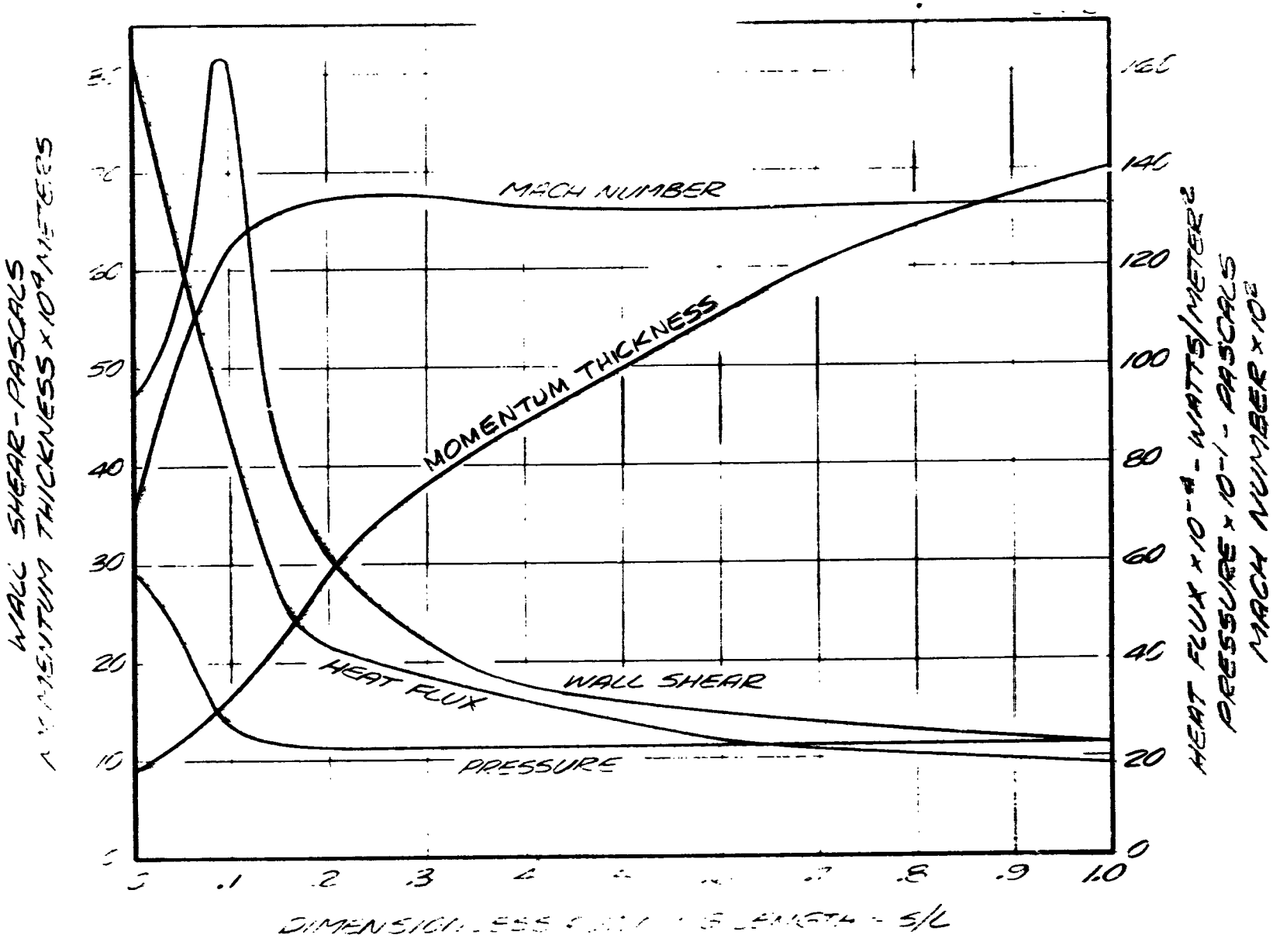

Figure 45. Wedge model surface conditions.

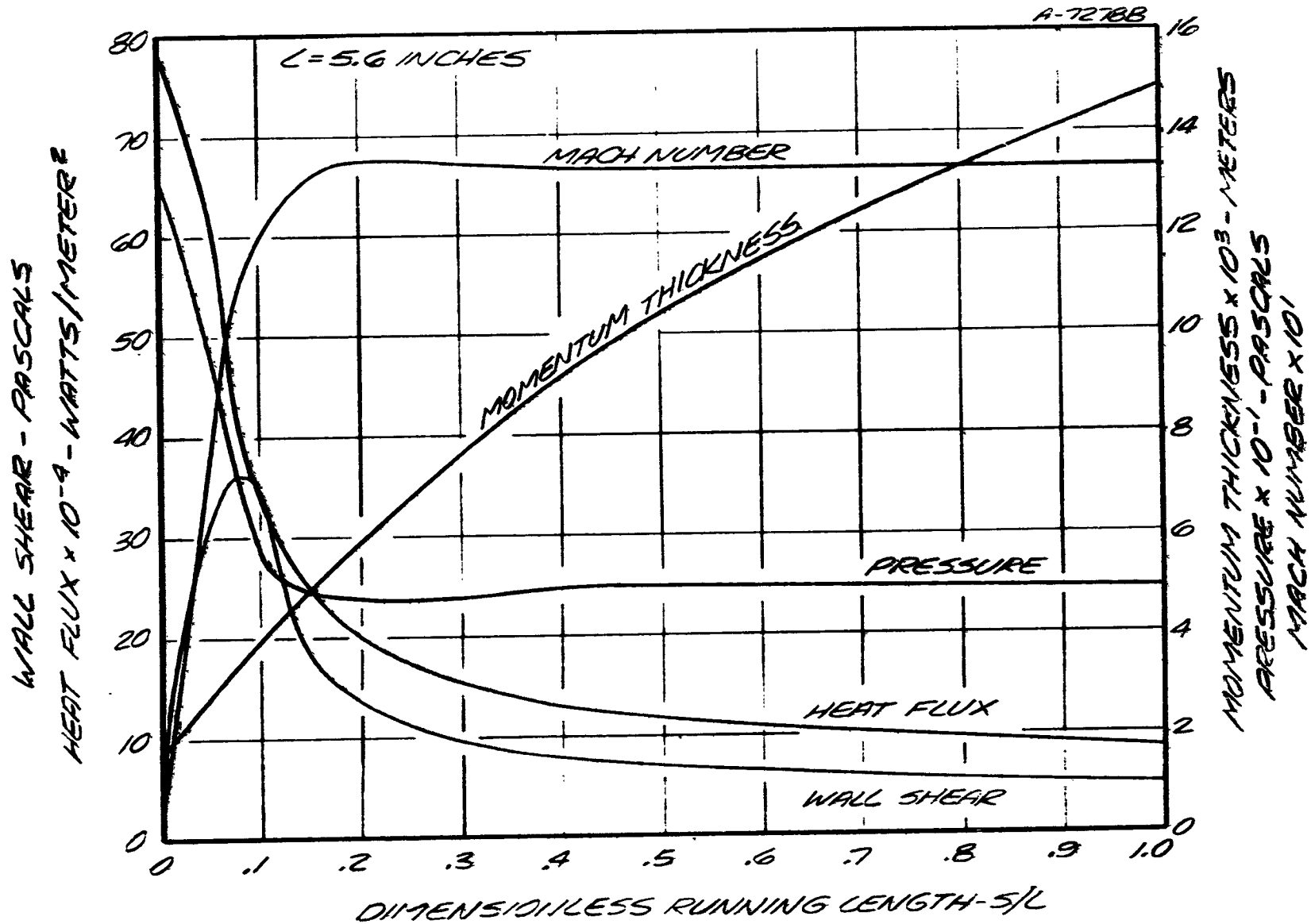

Figure 45. (Continued). Medium test condition.

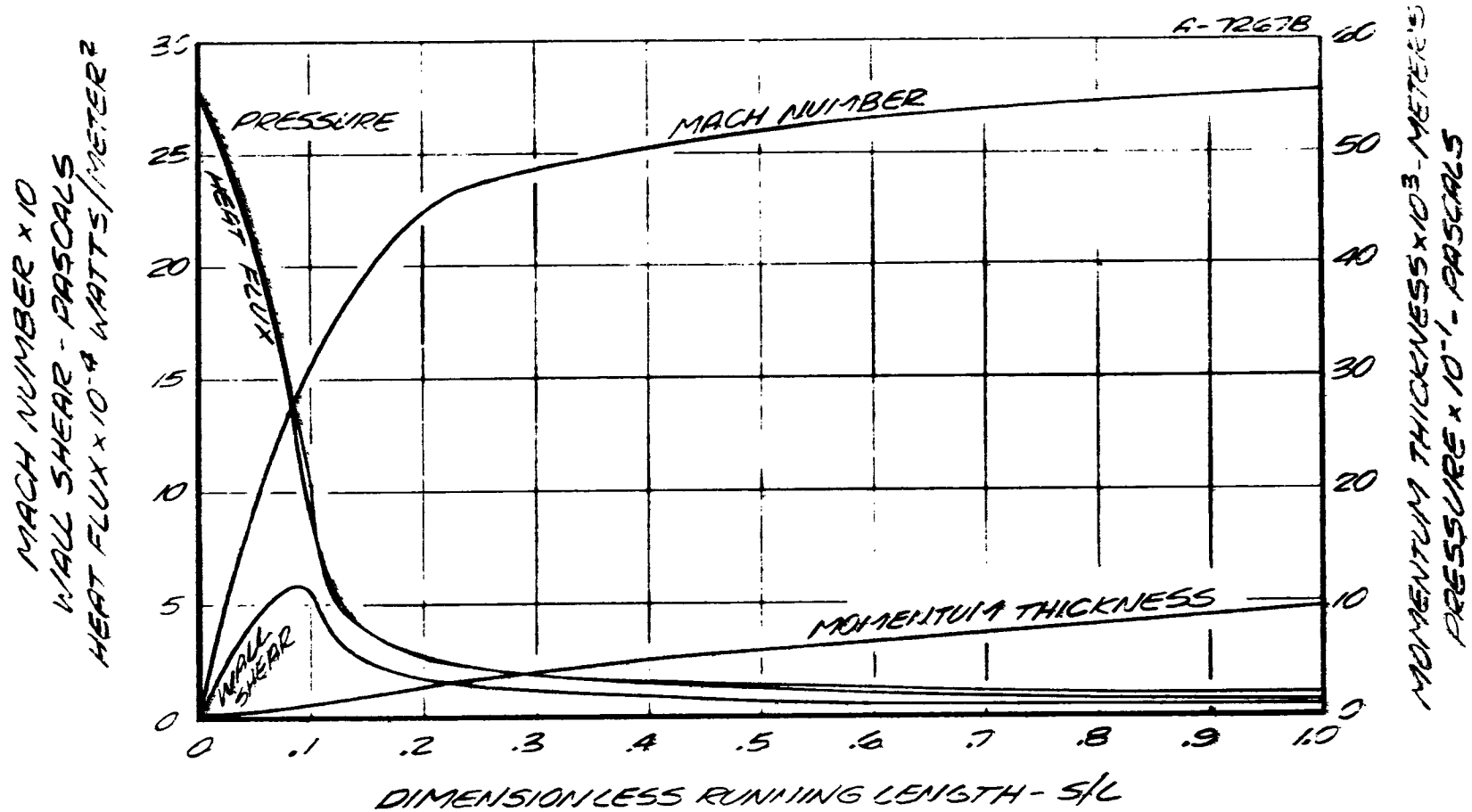

Figure 45. (Concluded). Low test condition.

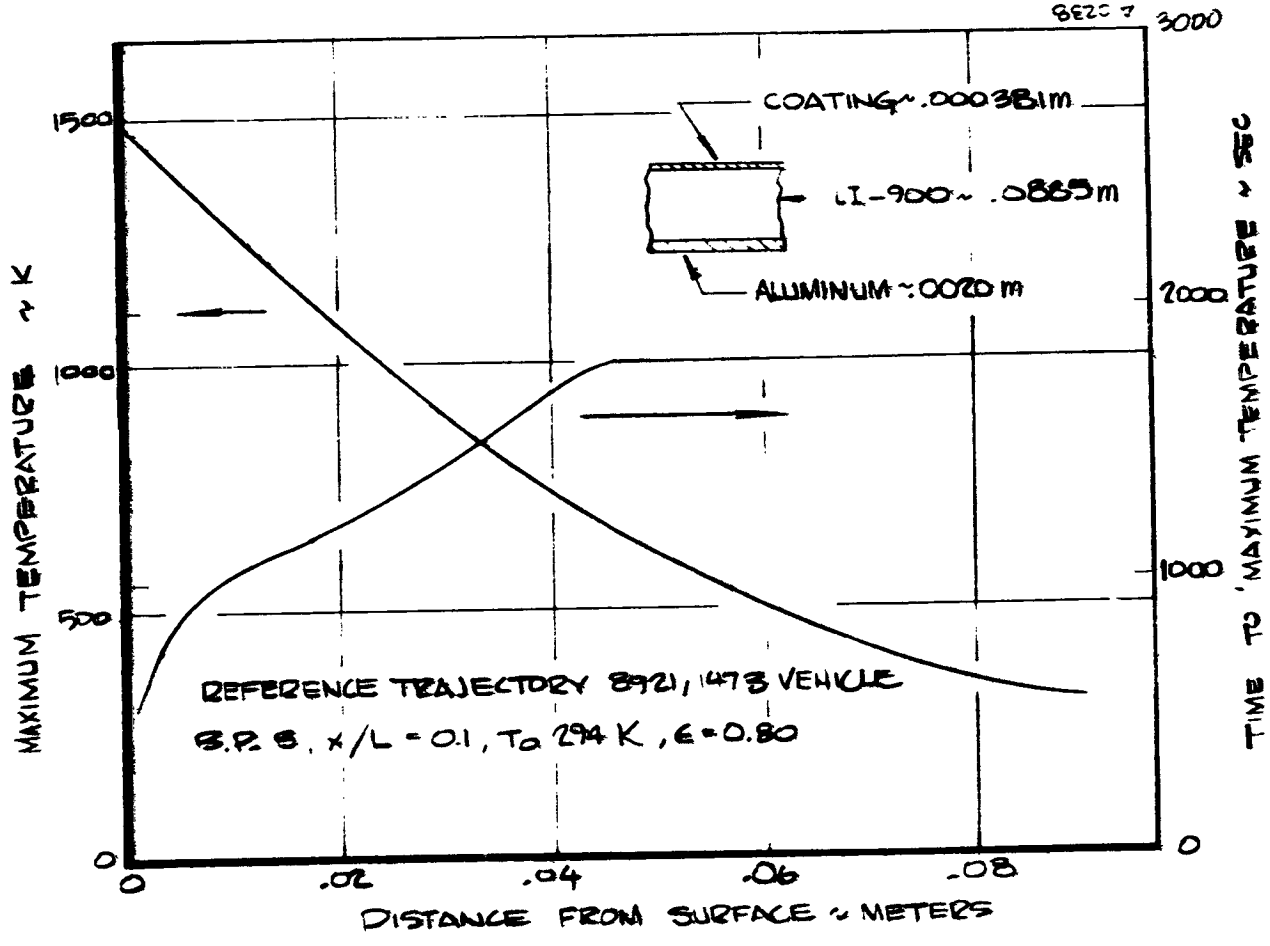

Figure 46. Unperturbed material response.

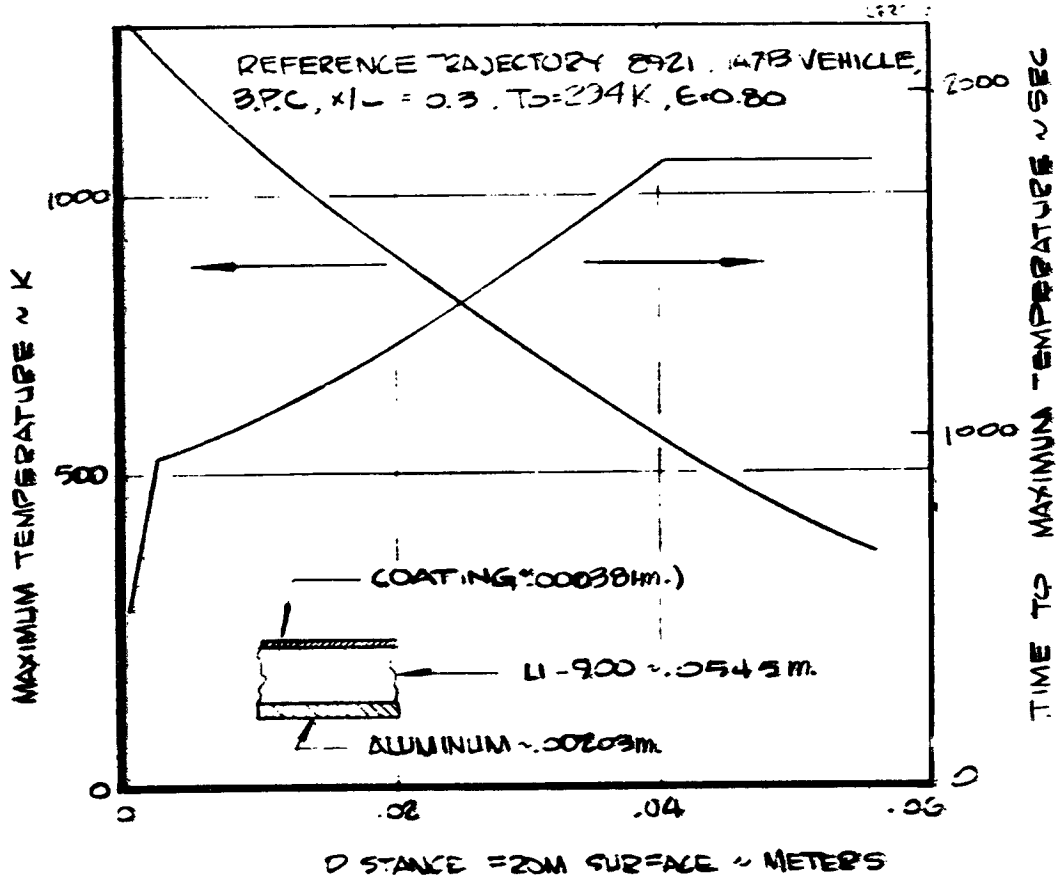

Figure 47. Unperturbed material response.

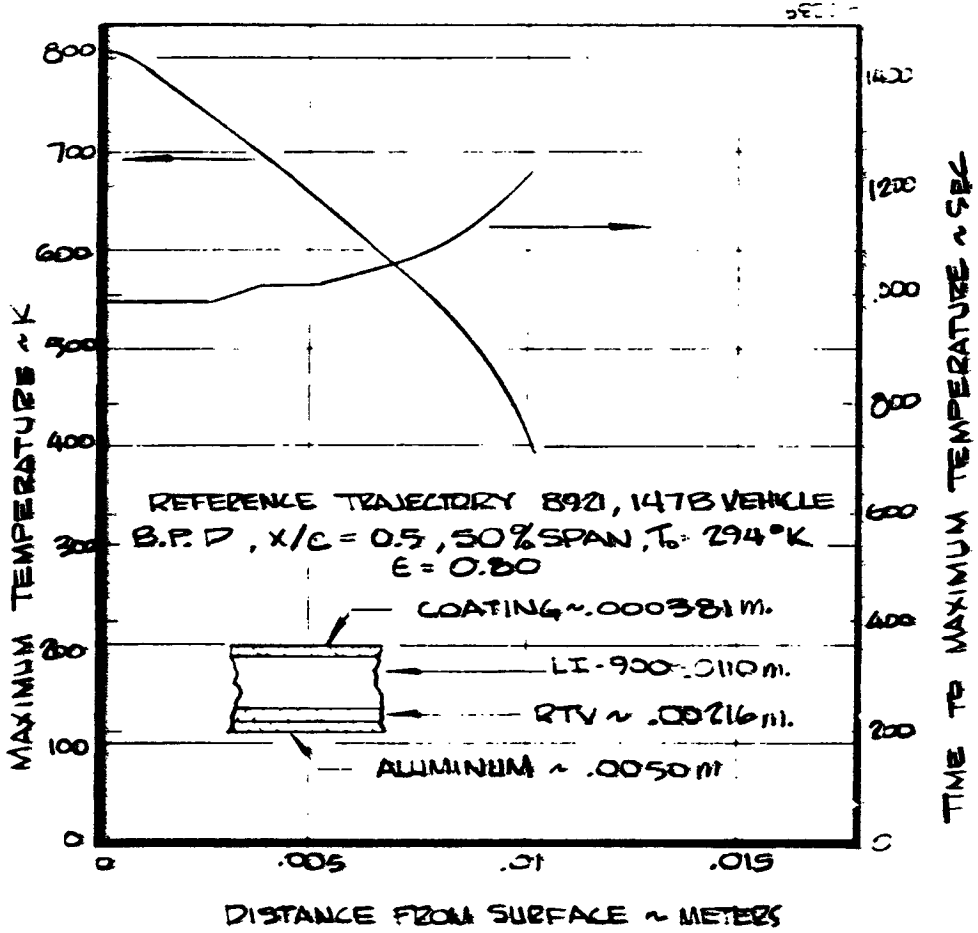

Figure 48 Unperturbed material response.

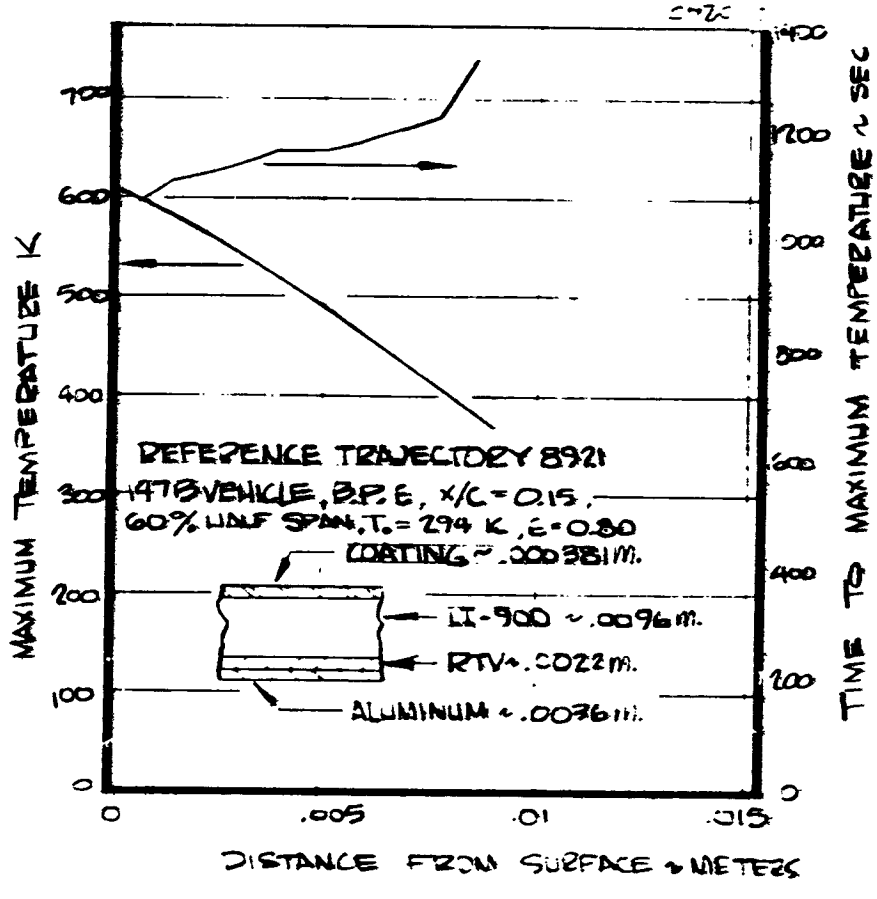

Figure 49. Unperturbed material response.

early in the testing caused a change in the test matrix. The original plans called for three levels of heating rate for the HRSI screening. However, several of the initial samples experienced coating failure either at the leading edge (melting, spalling or cracking) or in the area of the installed plug (cracking). The possibility existed that the available HRSI material had been tested in previous programs with unknown effects on the coating. The material shortage along with the coating problem forced the decision to perform all Phase 1 testing at the medium test point or that corresponding to B.P.C. The low heating test point was dropped from the test matrix because of problems in reproducing the test point and resultant nonuniformities observed in the flow field.

2.3.3.1 HRSI Test Results

The eight HRSI test samples instrumented and tested for the Phase 1 and 2 tests are described in Table 7. Sample Nos. 1, 2, 3, 4 and 11 were the early Phase 1 or screening test samples. The number of exposures and total exposure time for each of these samples is presented in Table 8. A summary of the test results is given in Table 9.

Sample No. 1 was fabricated from a piece of LI-1500 material previously used in a test program at JSC. Two instrumented, 0.0254 m (1 inch) diameter plugs were installed as a verification of the installation technique. Chromel/alumel (Type K), 36-gage thermocouple wire was used with one thermocouple at the coating and one at the test panel midplane. All thermocouple junctions were butt welded. This sample was subjected to three test cycles (see Tables 8 and 9) with a coating failure, i.e., melting along the sample leading edge, at 13 minutes of the third cycle. A probable contributing cause was a small chip in the coating at this location. Note that the sensor measurements given in Table 9 for this sample are the steady state measurements taken from the uncorrected thermocouple data.

Sample No. 2 was fabricated from the same material as Sample No. 1. One Type K, 36-gage thermocouple was installed at the coating using a 0.0381 m (1.5 inch) diameter plug. This sample was tested to study the effect of a large plug diameter on coating integrity while comparing the temperature measurements to those taken with smaller plug diameters. One test cycle was run on this sample with resulting outward buckling and cracking of the coating over the plug. The measured high surface temperature for this test, when compared to similar test conditions on Sample No. 1 (see Table 9), is most likely due to the separation of the coating from the plug creating a local higher heating rate.

Sample No. 3 used the same material as Nos. 1 and 2. This sample was instrumented with a Gardon gage/heat sink calorimeter to verify the concept and measure the imposed heat sink heating load at known test conditions. The heat sink/stem was

TABLE 7. HRSI TEST SAMPLE DESCRIPTION

Sample No.	Material	Installed Instrumentation	Purpose
1	LI-1500	Type K thermocouples, 36 gage, — one at coating, one at midplane; 0.0254-m plug diameter	Verify installation procedures
2	LI-1500	Type K thermocouple, 36 gage, — at coating; 0.0381-m plug diameter	Study feasibility of large plug diameter comparison with small plug data
3	LI-1500	Op-amp Gardon gage, simple stem design with OFHC heat sink	Verify heat sink cooling concept; quantify heat sink heat load
4	LI-1500	Type K thermocouples, 36 gage, — both at coating; one with 0.0254-m wire length and other with 0.0381-m wire length on 0.0254-m diameter plugs	Direct comparison between 1.0- and 0.0381-m "land length" verify feasibility — of Helicoil TC
11	AMES RSI	Two pressure ports thru panel, 0.00087-m and 0.00161-m diameter; no lining or edge sealer	Evaluation of "hole defect" on material performance
6	LI-900	Two thermocouples, one Type K, one Type R, at coating; 36 gage; 0.0381-m wire length on 0.0254-m plug diameter	Long term exposure evaluation/ comparison between TC types
7	LI-900	Three thermocouples, two 0.0254-m diameter plugs, one plug at midplane with one Type K thermocouple, 0.0381-m wire length; other plug at coating with Type R thermocouple at coating, 0.0381-m wire length and Type K thermocouple at midplane, 0.0254-m wire length; all thermocouples 36 gage	Evaluate effect of installing multiple TC's on same plug
8	LI-900	Op-amp Gardon gage, simple stem design with OFHC heat sink	Further evaluation of heat leaks from RSI to heat sink

TABLE 8. TEST SUMMARY

Sample	Number of Exposures	Heating Rate (Catalytic) (W/m^2)	Surface Temperature (K)	Total Exposure Time (sec)
1	3	1.28×10^5 to 1.82×10^5	1189 to 1276	2700
2	1	1.34×10^5	1223	1000
3	5	5.45×10^4 to 1.16×10^5	1189	1660
4	3	1.52×10^5 to 1.59×10^5	1256 to 1272	3060
11	5	1.36×10^5 to 1.44×10^5	1223	5100

TABLE 9. SUMMARY OF SCREENING TEST RESULTS

Sample No.	Test Cycle No.	Sample Configuration	Static Pressure P (Pa)	Steam Enthalpy, H_o (J/kg)	Cold Wall, Catalytic Heat Flux at Sensor (W/m^2)	Sensor Measurement
						S.S. Temperature (K)
						Surface / 0.0127-m In-Depth
1	2401-1	0.0254-m D. T/C Plug (Surface & In-Depth T/C)	608	2.86×10^7	1.40×10^6	1189 / 767
	2402-2		567	3.00×10^7	1.28×10^6	1184 / 787
	2402-3		547	3.04×10^7	1.32×10^6	1244 / 811
2	2403-1	0.0318-m D. T/C Plug (Surface T/C)	547	3.33×10^7	1.26×10^6	1283 / ---
3		Gardon Gage, Copper Stem & Heat Sink				Heat Flux (W/m^2)
	2406-1		---	$1.[illegible] \times 10^7$	5.45×10^5	6.24×10^5
	2407-3		---	$2.[illegible] \times 10^7$	1.09×10^6	9.53×10^5
	2408-4		659	2.67×10^7	1.13×10^6	1.03×10^6
	2408-5		648	2.56×10^7	1.10×10^6	1.11×10^6
4	2410-1	Two 0.0254-m D. T/C Plugs (Surface T/C's)	507	2.91×10^7	=1 / =2	S.S. Temperature (K) =1 / =2
					[illegible]	1261 / 1250
	2411-2	=1: 0.0318-m Land (Helix)			[illegible]	1275 / 1267
	2411-3	=2: 0.0254-m Land			[illegible]	[illegible] / 1259

fabricated from OFHC copper, and the heat sink measured 0.015 m (0.59 inch) diameter by 0.0318 m (1.249 inch) long with a total mass of 51.544 grams. The stem was 0.00318 m in diameter with a Thermogage Gardon Gage calorimeter (S/N 248) press fit into the end. This calorimeter was Op-amp augmented. Five test cycles were run on this sample with the first cycle at about half the heating rate of the remaining four. No problems were experienced with this design. The results in Table 9 allow comparison between the calibration heating rates taken with the calibration model and the uncorrected data from the Op-amp Gardon gage with heat sink temperature control.

Sample No. 4, again fabricated from LI-1500, contained two 0.0254 m (1 inch) diameter plugs. Thermocouples were installed at the coating and were 36-gage wire, Type K, butt welded. Thermocouple 1 was of the helicoil design allowing a "land length" of 0.0381 m (1.5 inches). Thermocouple 2 was configured straight across the top of the plug, providing a direct comparison between the two land lengths. This sample was subjected to three test cycles before the coating failed at the leading edge. Steady state temperature data is shown in Table 9.

Sample No. 11 was fabricated from Ames RSI (unused material) as an evaluation of the "Hole Defect" of a pressure port on tile performance. Two holes, 0.000813 m and 0.00161 m (0.032 and 0.0635 inch) diameter were drilled through the panel. No lining or edge sealer was used. After five test cycles, no change in the coating or substrate material was noted.

Sample Nos. 6, 7, and 8 were fabricated from tiles of unused LI-900 material (nonspec) received from Rockwell International. Sample No. 7 was instrumented with two 0.0254 m (1 inch) diameter plugs. The first contained on Type R, 36-gage thermocouple in the helicoil configuration at the coating, with a second Type R, 36-gage thermocouple inserted into the plug, 0.0127 m (0.5 inch) below the coating. The second plug contained one Type K, 36-gage thermocouple of the helicoil configuration 0.0127 m (0.5 inch) below the coating. Screening tests were run to evaluate the effect of multiple thermocouples on a single plug. At the start of the first cycle, the sample was damaged. Repairs were made and five more cycles run. Arc heater problems during the first three test cycles made data analysis difficult. Note also that the coating was in very bad condition even after repairs.

Sample No. 8 contained another Gardon gage/heat sink calorimeter (S/N 249) for further evaluation of the heat leaks from the RSI to the heat sink and stem. Four Type K thermocouples were installed at various locations on the stem and heat sink to aid in the evaluation. Four test cycles were run on this sample. The Gardon gage was damaged in handling of the sample and the heating rate data obtained from these tests is questionable. The thermocouple data, however, was not affected and yielded useful information.

On the basis of the above screening tests the following conclusions on instrumentation installation concepts were reached:

- Plug technique provides acceptable method of installing thermocouples at HRSI coating without penetrating the coating.
- Plug diameter should be no greater than 0.0254 m (1.0 inch) to limit stress on coating.
- Chromel/alumel thermocouples have demonstrated good stability and lifetime at temperatures up to 1278 K (1840°F).
- Gardon gage stem/heat sink cooling concept performed as expected, feasibility demonstrated.
- Pressure port hole through panel does not seem to affect material/coating performance.

A single long term evaluation test series was run with Sample No. 6. Two 0.0254 m (1 inch) diameter plugs were installed in this sample. One Type K and one Type R thermocouple was used, both 36 gage and both using the helicoil configuration (0.0381 m (1.5 inch) effective land length). The primary objective of the test series was to evaluate the relative performance of the two thermocouple materials under long term exposure conditions. A programmed heating rate profile was used for this series, Figure 50. A total of 47 cycles were run with this sample. Periodic calibrations were run throughout the series to monitor test conditions. This series lead to the following conclusions:

- Stability of chromel/alumel (Type K) and platinum-13 percent rhodium/platinum (Type R) thermocouples is comparable.
- Coating seems unaffected by presence of plug in the RSI.

2.3.3.2 RCC Test Results

Initial Phase 1 tests on RCC used the scraps obtained from previous test programs at Ames and LTV. Their size precluded the usual arc heater tests and therefore a small radiant lamp facility was used to evaluate the thermocouple bonding techniques using various ceramic cements. The objective of these tests was to screen a limited number of cement types and/or attachment techniques with a view towards identifying those with the greatest potential for the actual application to the arc heated facility tests. Two techniques were identified as feasible:

- Ceramic cement - Astroceram Type A-LP
- Alumina Flame Spray (Rokide Process)

With the availability of RCC samples in the proper configuration for arc heater tests, three RCC samples were instrumented as further screening of the thermocouple attachment technique (see Table 10).

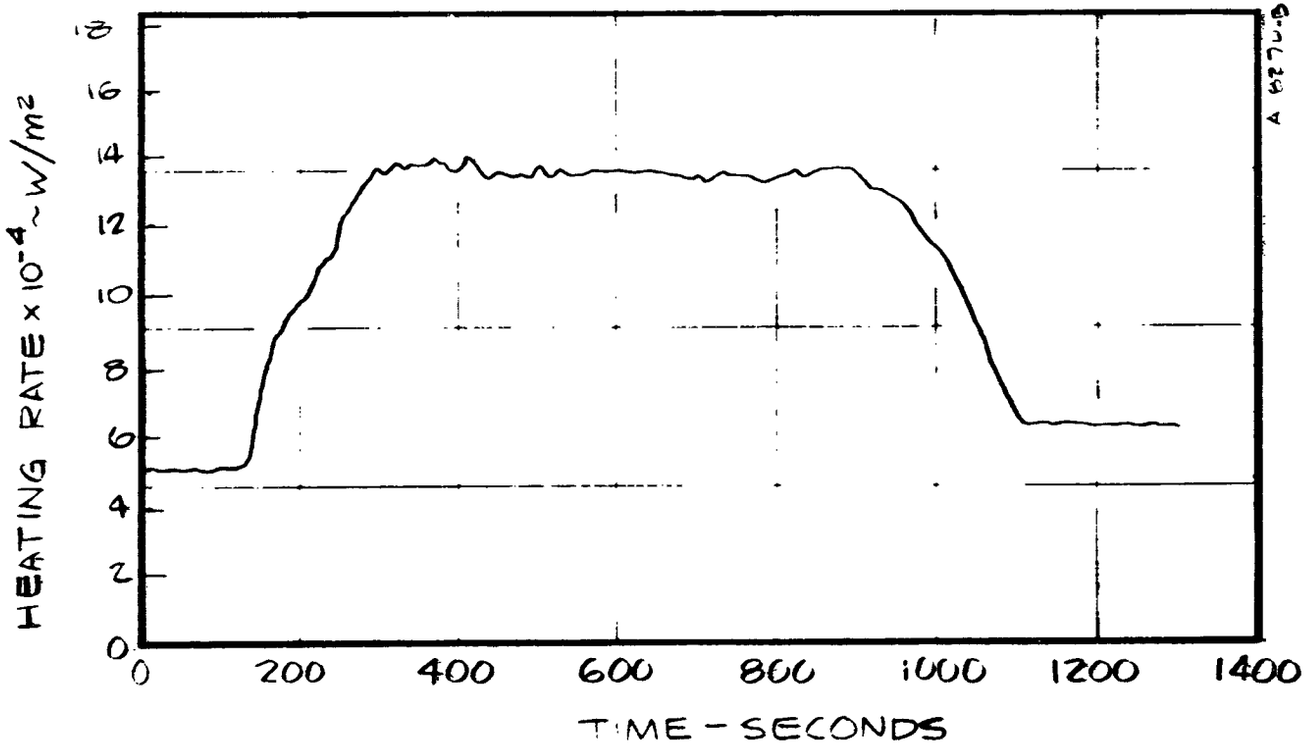

Figure 50. Nominal heating rate profile.

TABLE 10. TEST SAMPLE DESCRIPTION

Sample No.	Installed Instrumentation	Purpose
4-2	One grid type thermocouple, flame sprayed alumina over complete rear face.	Evaluate flame spray technique
4-4	One Type R thermocouple, 36 gage, flame sprayed alumina, 0.0127-m by 0.0127-m pad.	Study feasibility of small pad of flame sprayed alumina
4-3	One Type R thermocouple, 36 gage, Astroceran cement, Type A-LP, 0.019-m by 0.0254-m pad.	Evaluate ceramic cement technique

The first sample (No. 4-2) used a "grid type" thermocouple attached with the alumina flame spray technique. The "grid type" thermocouple was specifically developed for this attachment technique and resembles a wire type strain gage in configuration, using 0.0000127 m (0.0005 inch) thermocouple wire diameter. The thermocouple was damaged during the flame spray process. However, the attachment characteristics could be evaluated and a 12-minute test at a surface temperature of 1478 K (2200°F) was run. The alumina, which was sprayed over the entire rear face, was not damaged and remained attached to the RCC surface.

Sample No. 4-4 used a single Type R, 36-gage thermocouple flame sprayed on with a pad 0.0127 m (0.5 inch) square. A single test cycle was run with a failure of the attachment.

Finally, Sample No. 4-3 was instrumented with one Type R, 36-gage thermocouple cemented in place with Astroceram, Type A-LP. The thermocouple wire was precoated with PC-1 precoat. All recommended cure processes were followed. Pad size for this installation was 0.0190 m by 0.0254 m (0.75 by 1.0 inch). Two cycles were run with this sample with no apparent degradation of the bond. Cracks in the ceramic which appeared before the final cure did not get worse. Some discoloration of the RCC coating was noted around the area of the bond.

The following conclusions were drawn from these screening tests:

- Astroceram A-LP has good bond characteristics but may interact with the RCC coating.
- The alumina flame spray technique has no observed effect on the RCC coating.
- The size of the alumina pad is critical for thermal shock resistance.

The late arrival of the RCC samples, along with difficulties in obtaining out-of-house flame spray applications made further evaluation (such as a pad size study) impossible. However, preliminary testing favors the flame spray technique due to its "purity" of materials and previous experience in similar applications.

2.4 DATA REDUCTION AND ANALYSIS

A detailed evaluation of the instrumentation systems was performed throughout the program. This evaluation included comparisons of measured output with analytical predictions and the measured boundary conditions. Additionally, the relative error of each instrumentation system as an integral part of the TPS was established.

2.4.1 Definition of Boundary Conditions

Appropriate evaluation of the instrumentation system performance may only be achieved when known controlled test boundary conditions are imposed upon the test

specimen. The accuracy of monitoring the facility performance is coupled to instrumentation errors and data acquisition system induced errors. In arc plasma jet testing, the test stream stability is an uncertainty which is difficult if not impossible to quantify. In order to assess accuracy within which HRSI surface temperature may be evaluated, a summary of facility related errors is presented in Table 11. The total uncertainty is 18.3 K (33°F) for a surface temperature of approximately 1256 K (1800°F). Thus, surface temperature measurements may be resolved to within approximately 1-1/2 percent. One additional uncertainty associated with the correlation of heat flux and HRSI surface temperature is due to variations in the HRSI coating surface emittance. The accuracy within which heat flux measurement may be evaluated is approximately the error associated with the calibration of the Gardon gages. However, not included in this error (~5 percent) is the uncertainty associated with the surface catalycity of the Gardon gage which may further reduce the available accuracy.

2.4.2 Analytical Comparisons with Measured Instrumentation Response

Within this section, the test data is compared with analytical predictions. This data comprises four categories:

- HRSI Temperature Measurements
- RCC Temperature Measurements
- HRSI Calorimeter Response
- HRSI Calorimeter Heat Sink Thermal Response

A summary of each will provide an understanding of the errors associated with the respective measurements.

2.4.2.1 HRSI Temperature Measurements

Instrumented HRSI samples were tested in the Aerotherm arc plasma jet facility to evaluate thermocouple installation techniques, measurement accuracy, and instrument lifetime. Thermocouple instrumentation testing was directed towards defining and optimizing the measurement accuracy.

One source of thermocouple installation induced error is due to lead wire conduction losses from the thermocouple bead. This allows the thermcouple junction to experience a temperature lower than the unperturbed temperature level at the bead location. Testing was performed to evaluate the effect of land length (i.e., wire length in the isothermal plane) upon the observed measurement error. Figure 51 shows the results of these tests plotted against the local heating rate. The conclusion drawn from this data is that for the 0.000127 m (0.005 inch) wire diameter, the 0.0381 m (1.5 inch) land length produces negligible error while the 0.0254 m (1.0 inch) land length measurement can be 11.1 K to 22.2 K (20°F to 40°F) in error.

TABLE 11. UNCERTAINTY IN CORRELATION OF HEAT FLUX WITH SURFACE TEMPERATURE (AT 1256 K (1800°F))

Measurement	Error Band	Resulting Uncertainty in RSI Surface Temperature	
		(°F)	(K)
Gardon Gage Calorimeter	±5% on Heat Flux	±28	±16
Thermocouple emf	±3/4%	±15	±8
Thermocouple Location	±3 mils (±7.62-05m)	±3	±2
Data Handling System	±1/2% of Full Scale	±10	±6
Total (RMS)		±33°F or ±18 K	

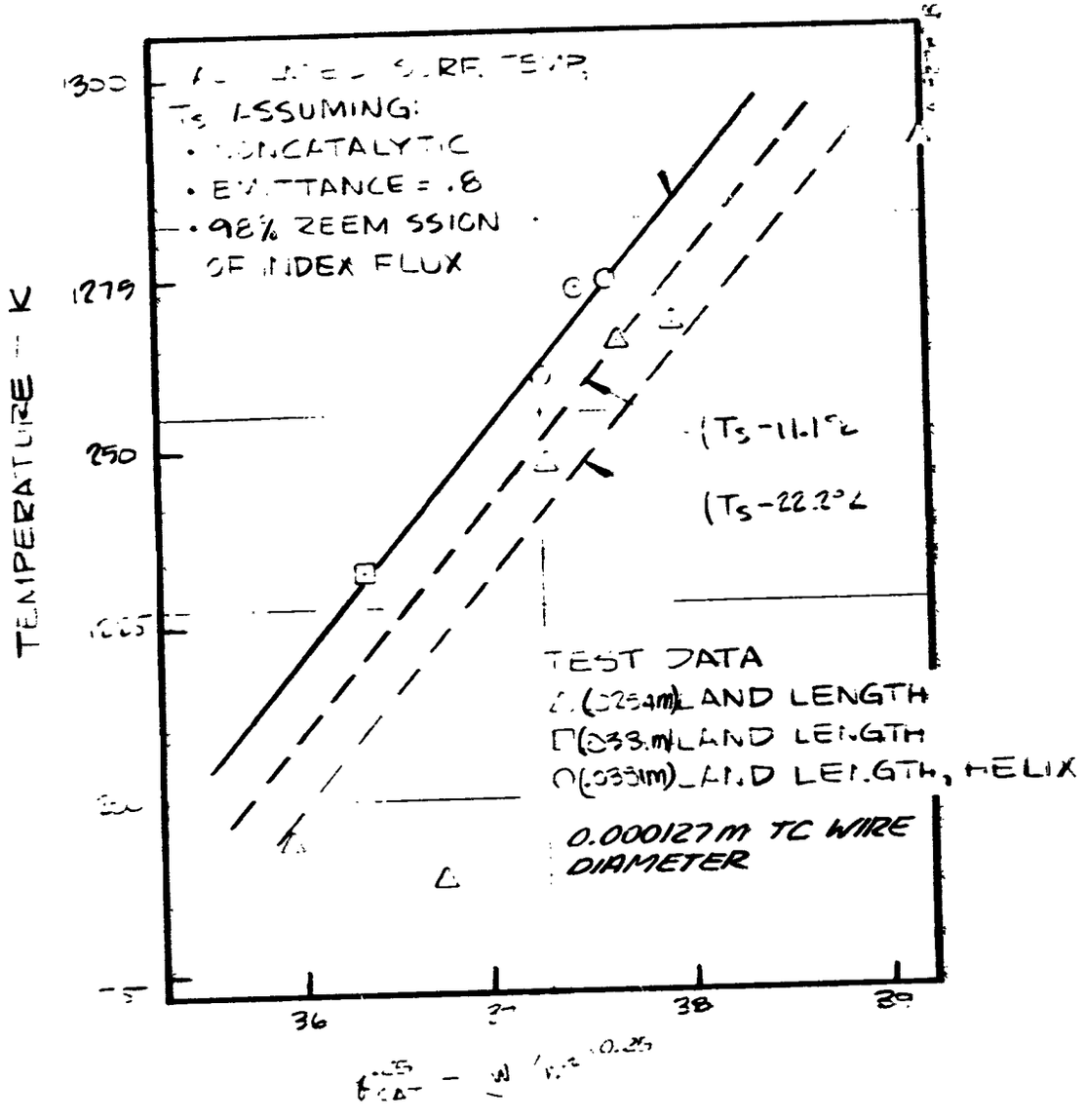

Figure 51. Land length error evaluation.

This result must be considered in light of other errors inherent in the sensors and recording equipment used for the tests (as previously summarized in Table 11). Using the simplified thermocouple error analysis procedure described in Section 2.2.4.2, the analytical results indicated that the 0.0381 m (1.5 inch) land length installation should have a negligible error; whereas, the 0.0254 m (1.0 inch) land length installation should have approximately a 0.56 K (1°F) error. These analytical comparisons are summaried in Figure 52 along with the SINDA three-dimensional thermal analysis results. The SINDA results must be considered in terms of the extreme complexity of the model. These results present reasonable trends, however, the magnitude of the predicted errors is questionable.

In-depth thermocouple installations of two varieties have been experimentally evaluated. One technique uses a plug cut to the desired location (depth) whereas the other technique uses a thermocouple pulled through a hole lanced in a plug that extends to the coating. Both techniques exhibit comparable accuracy within the data reduction capabilities of the arc plasma facility.

2.4.2.2 RCC Temperature Measurements

Arc plasma jet tests were performed to evaluate RCC temperature measurement accuracy and thermocouple attachment techniques. Throughout these tests, the specimen was subjected to a constant environment typical of the peak heating condition during reentry. A schematic of the instrumentation is presented in Figure 53, and a summary of the test data obtained are presented in Table 12. As the surface temperature has been determined by optical pyrometry, the uncertainty associated with the surface emittance of the RCC specimen affects the indicated surface temperature. Reviewing Table 12, it is apparent that this uncertainty may be translated to a surface temperature ranging from 1422 K to 1595 K (2100°F to 2411°F) with a nominal value of 1491 K (2223°F) as the accepted standard. When these temperatures and the back face temperature measurement are used to perform an energy balance upon the specimen, it is observed that the incident flux is significantly lower than the cold wall fully catalytic value measured by the calibration model. Assuming that test fixture heat leaks are negligible, the difference may be attributed to the catalycity of the test specimen (catalytic efficiency ranging from 0.46 to 0.54).

2.4.2.3 HRSI Calorimeter Response

ARC plasma testing was performed on HRSI samples with augmented Gardon gages installed to monitor the incident heat flux. These measurements, compared with calibration model, fully catalytic heat flux measurements, may be used to evaluate the magnitude of the cold wall boundary layer perturbation effects upon the local heat transfer. Three basic measurements were used to evaluate the cold wall effect for a particular test. First, a calibration wedge measurement as adjusted for catalycity yields a flux of 8.85 x 10^6 W/m^2 (7.8 Btu/ft^2sec). Assuming radiation

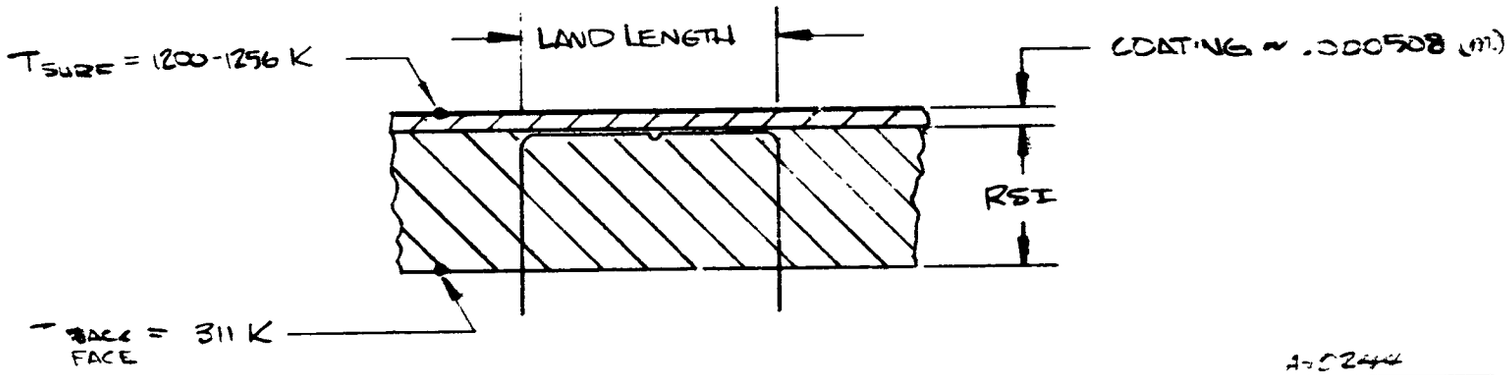

A-02442

TECHNIQUE	STEADY STATE THERMOCOUPLE MEASUREMENT ERROR (K)		
	.000127m PLAT. WIRE .0762m. RSI THICKNESS .0127m LAND	.000127m CHROMEL/ALUMEL WIRE .0254m RSI THICKNESS	
		.0254 m. LAND	.0381 m. LAND
SIMPLIFIED MODEL (FIN ANALYSIS)	8	96	NEGLIGIBLE
SINDA MODEL	2	<2	NEGLIGIBLE
SCREENING TEST RESULTS	NO DATA	11-22	NEGLIGIBLE

Figure 52. Thermocouple land length analysis summary.

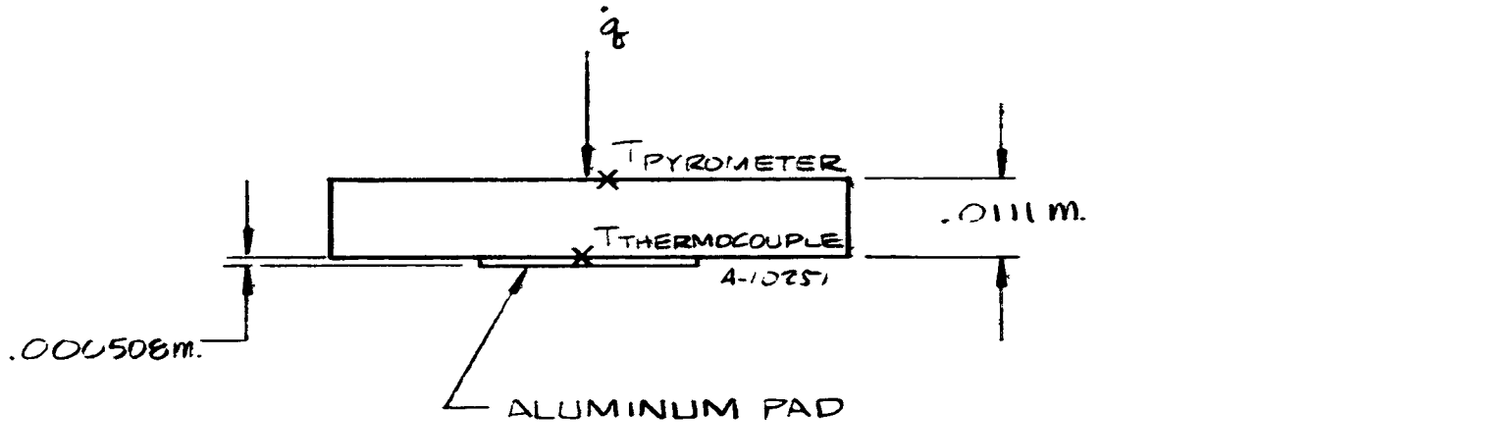

• ALUMINA FLAME SPRAY ATTACHMENT OF GRID THERMOCOUPLE

Figure 53. RCC test instrumentation.

TABLE 12. RCC DATA ANALYSIS

$T_{thermocouple}$ K (°F)	Assumed Surface Emittance λ =	$T_{pyrometer}$ K (°F)	Catalytic Efficiency
1344 (1960)	0.6	1422 (2100)	0.46
1344 (1960)	0.8	1491 (2223)	0.49
1344 (1960)	1.0	1595 (2411)	0.54

- Cold Wall Catalytic Heat Flux = 5.20×10^5 W/m^2 (45.8 Btu/ft^{2}sec)

equilibrium with a nominal surface emittance of 0.8, a surface thermocouple temperature measurement has been converted to an incident flux of 9.08 x 10^4 W/m^2 (8.0 Btu/ft^{2}sec). For this particular test, the flux registered by the installed augmented Gardon gage was 1.11 x 10^5 W/m^2 (9.8 Btu/ft^{2}sec). When the analytically derived adjustment for the cold wall boundary layer effects are factored into the measured flux, the deduced measurement was 8.85 x 10^4 W/m^2 (7.8 Btu/ft^{2}sec). This consistency of test data and analysis verifies that cold wall calorimeter measurements must be corrected for boundary layer perturbation effects in order to accurately ascertain the heat flux boundary conditions to which the HRSI is subjected. Additional tests have been conducted, and agreement with analytical predictions reinforces the need for correcting the data.

2.4.2.4 HRSI Calorimeter Heat Sink Thermal Response

Throughout the calorimeter testing, the temperature of the heat sink was monitored in an effort directed toward assessing the passive heat sink requirements for typical shuttle calorimeter installations. Monitoring the heat sink temperature rise rate, the heat flux into the sink may be computed when the mass and specific heat of the sink material are known. A typical heat sink installation for testing is depicted in Figure 41, while a corresponding thermal response observed during typical test cycle is presented in Figure 54. The heat flux into the sink comes from (a) the incident flux upon the sensor surface, and (b) the flux from the HRSI surrounding the cold stem connecting the sensor to the heat sink. The total flux as determined by simplified analysis techniques should be approximately 2.78 watts (9.5 Btu/hr). The essence of the simplified calorimeter heat sink analysis is depicted in Figure 55.

However, the steady state heat flux to the sink as derived from the test data was 6.12 watts (20.9 Btu/hr). It is to be expected that as the temperature of the heat sink increases, the heat leaks to the cold cavity surrounding the heat sink would reduce the temperature rise rate of the heat sink. This was observed (even with insulation surrounding the sink) and the heat flux to the sink at the end of the test period was 3.19 watts (10.9 Btu/hr). It had become obvious that additional analysis of the test setup was warranted to evaluate this inconsistency between the predicted and observed heat sink responses. Consequently, during the second phase of the test program, additional instrumentation was incorporated to monitor the temperature gradient down the stem of the heat sink and to monitor the aluminum plate temperature. The stem thermal gradient provides one method for evaluating the heating rate to the sink. Additionally, monitoring the aluminum plate temperature provides the required information for evaluating the heat leaks through the HRSI specimen to the heat sink. A typical measured incident flux profile is displayed in Figure 56 along with the observed thermal response of the heat sink assembly.

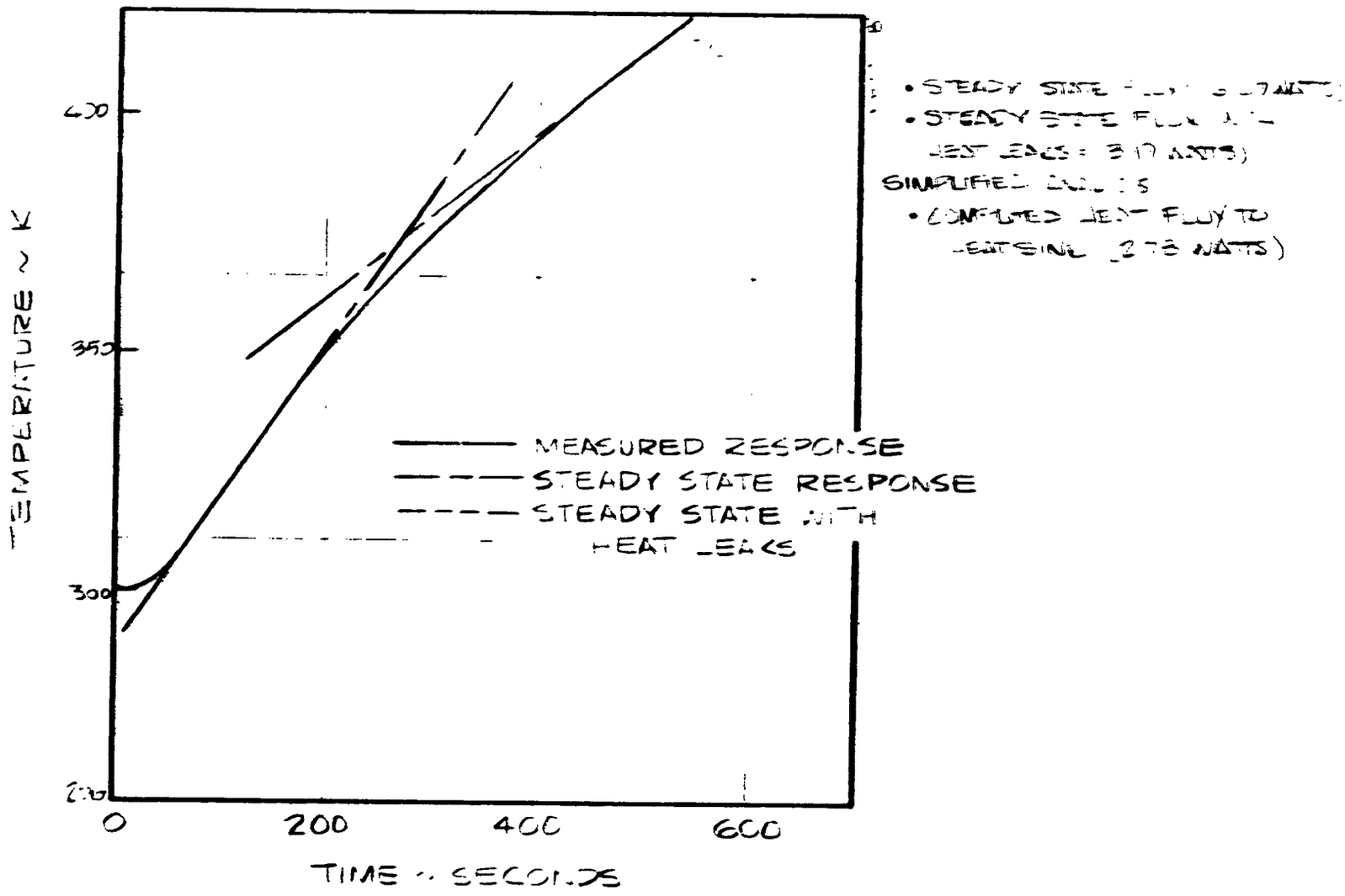

Figure 54. Test read

$\dot{q}_{SURFACE} = \dot{q}_{GENERATED} \times AREA$

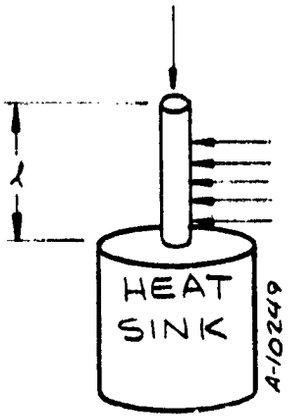

$$\dot{q}_{HEAT\ SINK} = \dot{q}_{SURFACE} + \dot{q}_{STEM}$$

IF THE STEM IS TREATED AS A FINITE FIN:

$$\dot{q}_{STEM} = \sqrt{hPKA}\,(\overline{T}_{UP} - T_{STEM})\,\tanh m\ell$$

$$M = \sqrt{\frac{hP}{KA}}$$

P = PERIMETER ~ FT
K = STEM THERMOCONDUCTIVITY ~ BTU/FT HR °F
A = STEM CROSS SECTIONAL AREA ~ FT^2
h = EFFECTIVE HEAT TRANSFER COEFFICIENT BETWEEN STEM AND INSULATION

Figure 55. Simplified calorimeter heat sink analysis.

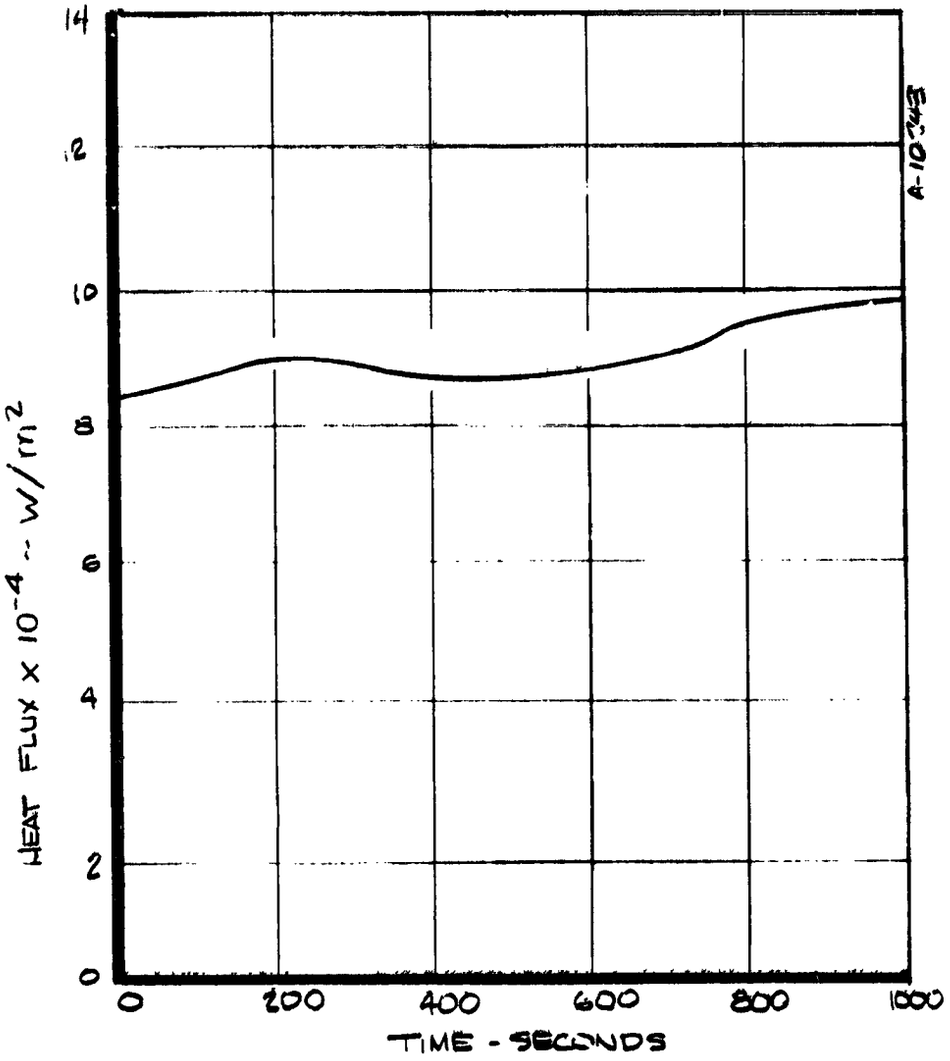

Figure 56a. Typical incident flux measurement for installed Gardon gage (test 2430, sample no. 8, cycle 3).

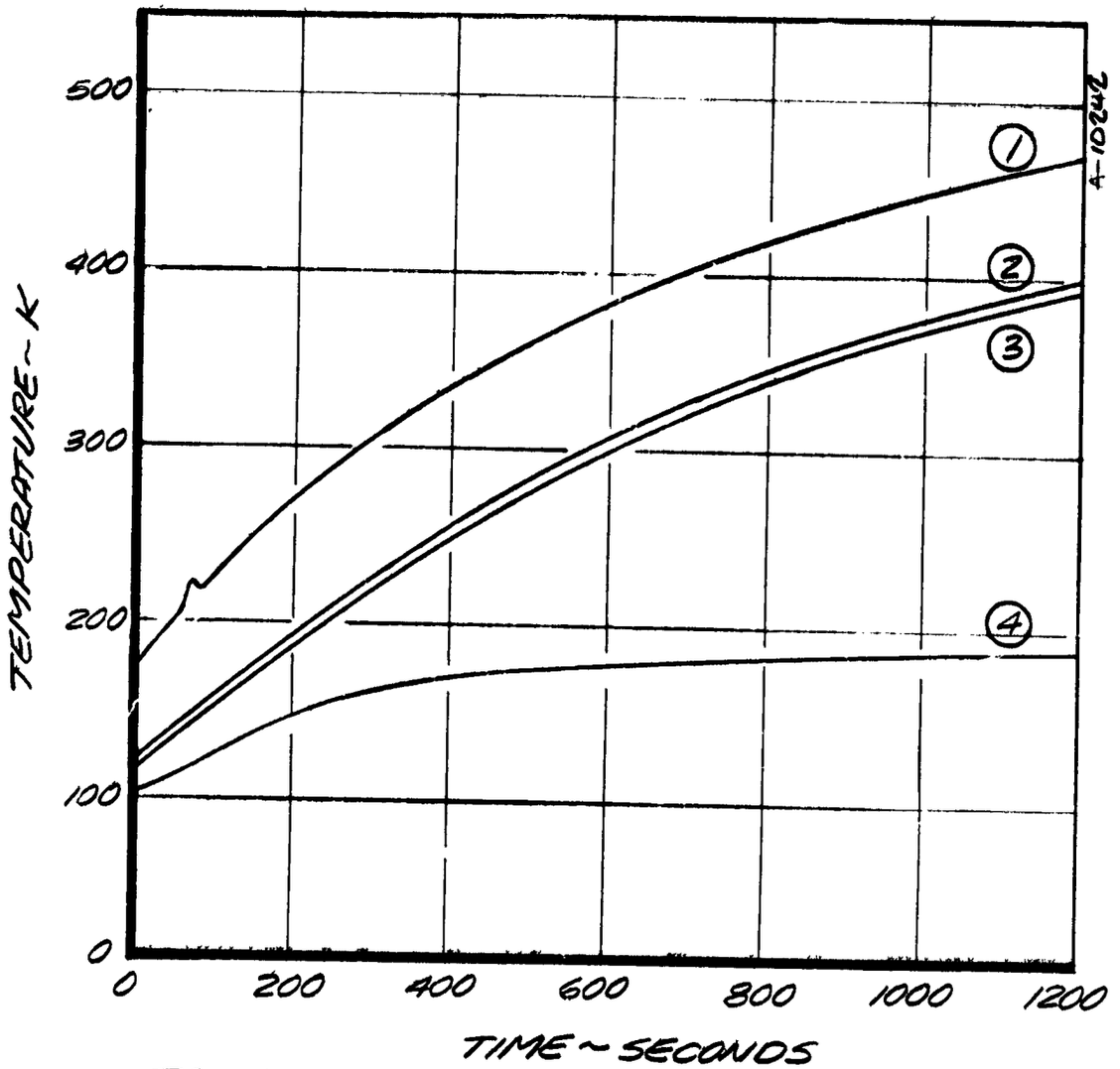

TC LOCATIONS:

1. STEM SURFACE, 0.0127m BELOW HEATED HRSI SURFACE
2. ON ALUMINUM BACKING PLATE OF HRSI TEST PANEL, IN VICINITY OF STEM.
3. AT STEM/HEAT SINK INTERFACE.
4. HEAT SINK CYLINDRICAL SURFACE MIDPOINT.

Figure 56b. Heat sink thermal response (test 2431, sample no. 8, cycle 3).

Computing the heat flux to the sink from temperature gradient information, a heat flux of 5.54 watts (18.9 Btu/hr) is deduced. From the heat sink temperature rise rate, mass, and material specific heat, the absorbed flux was found to be 3.16 watts (10.8 Btu/hr). Simplified analysis approaches indicate that an expected flux into the heac sink would be 1.35 watts (4.6 Btu/hr). If, in the simplified analysis procedure, the heat transfer coefficient were low by a factor of from 3.8 to 7.4, the computed heat flux would match the observed heat sink response. The previous test series (which was at the same nominal incident heat flux level) experienced a heat sink behavior similar to that predicted when the gradient information is used to deduce the heat sink absorbed loading. Consequently, this information is deemed to be the most appropriate. Therefore, a conservative passive heat sink design for shuttle environmental exposures may be estimated from simplified approaches and test data extrapolation, however further analysis of the heat transfer from the surrounding insulation to the heat sink stem is warranted to improve the accuracy and usability of the simplified analysis technique.

SECTION 3

CONCLUSIONS AND RECOMMENDATIONS

Reviewing existing instrumentation systems and their installations, it is apparent that previous experience is not adequate for the TPS instrumentation requirements of the Shuttle vehicle. The error margin analysis associated with thermocouple and calorimeter installation in a low conductivity material (HRSI) has been nonexistent. The additional questions of instrument lifetime repeatability, and compatibility with HRSI have not previously been addressed. This study has defined a simplified analysis technique to evaluate thermocouple errors as a function of thermoelement and installation and an evaluation of calorimeter heat sink requirements has similarly been performed. These analyses indicate that for HRSI performance evaluation and certification through testing, where specimen sizes are typically smaller (i.e., thinner) than flight articles, instrumentation errors may be magnified significantly. Consequently, test sample instrumentation should be scrutinized prior to data evaluation to determine the magnitude of the potential error. In addition, correlation between ground test data and flight data presupposes commonality of instrumentation installation and design techniques.

Testing and analysis have demonstrated that, for the conditions evaluated, a thermocouple land length of 0.0318 m (1.5 inches) provides an undetectable error. However, a 0.0318 m (1.5 inch) plug is unacceptable as coating failures have been experienced during testing, but a 0.0254 m (1.0 inch) plug with a helical wound (helicoil) 0.0318 m (1.5 inch) thermocouple land length has performed well in cyclic testing done to date. In-depth thermocouple installation should be made with a plug cut to the desired depth with the thermocouple on the top of the plug. The two primary advantages of this installation technique are; (1) the thermocouple land length may be easily varied, and (2) the HRSI above the measurement remains unperturbed. Analytical predictions and observed in-depth thermocouple response have agreed well indicating the validity of this installaton procedure.

Thermocouple selection based upon repeatability, material compatibility, temperature range capability, and handling characteristics results in the selection of chromel-alumel (Type K) and platinum-platinum/13 percent rhodium (Type R) for HRSI temperature measurements. Testing has indicated that after 47 entry cycles the

response has remained unchanged (i.e., no calibration shift) for both of these thermocouple types. Also, material compatibility constraints are satisfied by both of these thermocouples.

Analysis of HRSI heat flux measurement techniques and their applicability to Shuttle TPS environmental boundary condition measurement has indicated that for cold wall measurements, the augmented Gardon gage represents the best method. Ruggedness, sensitivity, repeatability, calibration, time constant, handling, and installation constraints have been satisfied with the selection of this type of gage. However, as is characteristic of all cold wall heat flux measurement techniques, the perturbation to the boundary layer from a discontinuity in the wall temperature complicates the data reduction. For the most part, heating augmentation factors to the sensor have been on the order of 30 percent for entry conditions, but under certain local pressure/enthalpy conditions the predicted augmentation may be as much as 179 percent of the unperturbed value. This increased augmentation factor is attributable to a significant increase in the chemically reactive component of the gas thermal conductivity (effective catalycity). Testing has verified, both qualitatively and quantitatively, the prediction techniques employed to define the boundary layer perturbation. The basic conclusion is that any data retrieved by cold wall measurement techniques must be evaluated in light of this potential anomaly.

Preliminary testing has indicated that passive heat sink designs are feasible for shuttle heat flux measurements with augmented Gardon gages. Simplified analysis procedures require some modification to accurately predict the observed response, however a combination of test data and simplified analysis may be used to define passive heat sink requirements for flight application.

Measuring surface and internal HRSI tile pressures requires a coupling between the measurement transducer and the location of the measurement. In the case of a surface pressure measurement, will a pressure port through the HRSI coating affect the tile integrity? Arc jet plasma testing of a typical coated tile with a hole through the coating indicates that this type of tile defect will not compromise the tile. However, it is suggested that further testing be performed to investigate the actual coupling of the surface location with the pressure transducer.

Due to the unavailability of test specimens, RCC testing was restricted to the evaluation of thermocouple attachment concepts, and errors. Two techniques of attachment studied were: 1) Astroceram Cement, and 2) flame spray alumina attachment. Both concepts provide comparable data accuracy for steady state measurements, and both attachment techniques appear to survive cyclic exposures to the extreme shuttle environment.

Preliminary testing and analysis indicate that for monitoring transient temperature histories, the flame spray alumina attachment technique is preferred as reduced errors should occur.

RCC testing has demonstrated a surface catalytic efficiency of approximately 50 percent. In addition, temperature gradients through the RCC must be considered if a backface temperature measurement is to be converted to a surface thermal response. Due to the extreme thermal operating environment behind RCC panels, a high temperature thermocouple material must be used. In addition, the oxidizing environment requires that most thermocouples be sheathed so that their performance will not degrade. The recommended thermocouple for RCC measurements is a platinum-platinum/13 percent rhodium (Type R) thermocouple insulated with aluminum oxide (Al_2O_3) in an Inconel sheath. Experience has indicated that this is an appropriate choice for the Shuttle RCC temperature measurement requirement.

APPENDIX A

PARAMETRIC STEADY STATE THERMOCOUPLE ERROR ANALYSIS RESULTS (SIMPLIFIED FIN APPROACH)

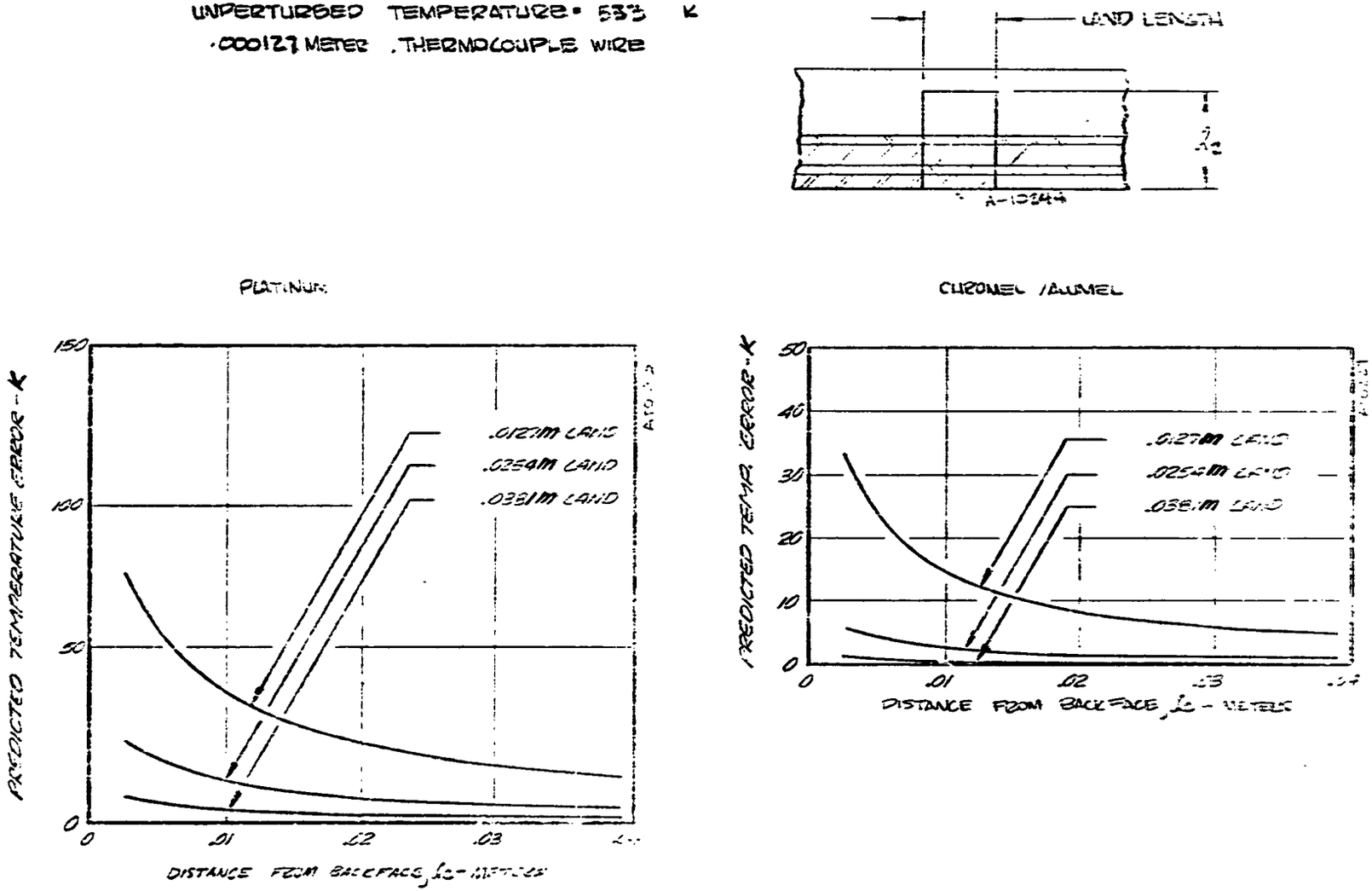

Figure A-1. Steady state analysis of conduction induced thermocouple errors.

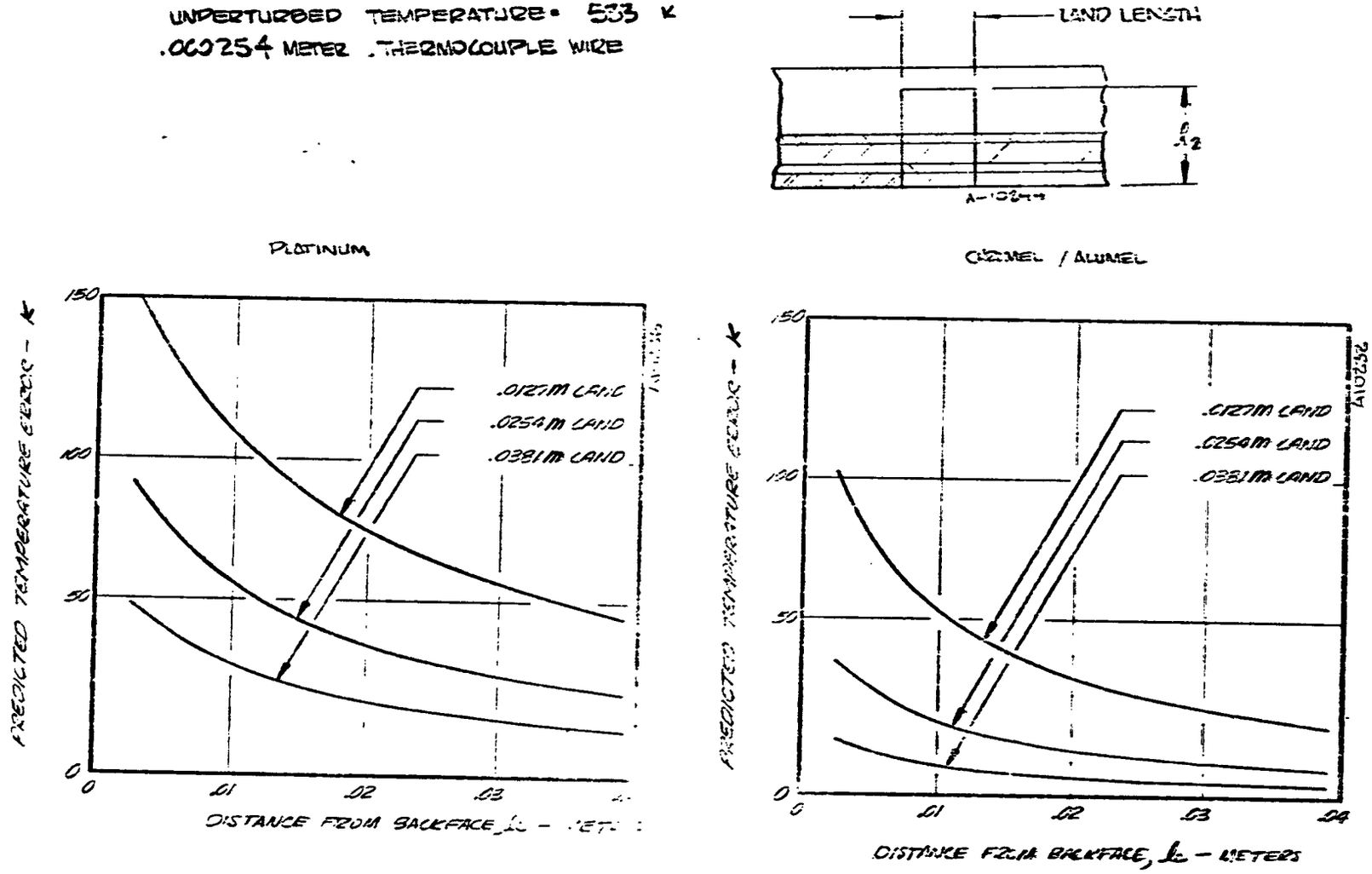

Figure A-2. Steady state analysis of conduction induced thermocouple errors.

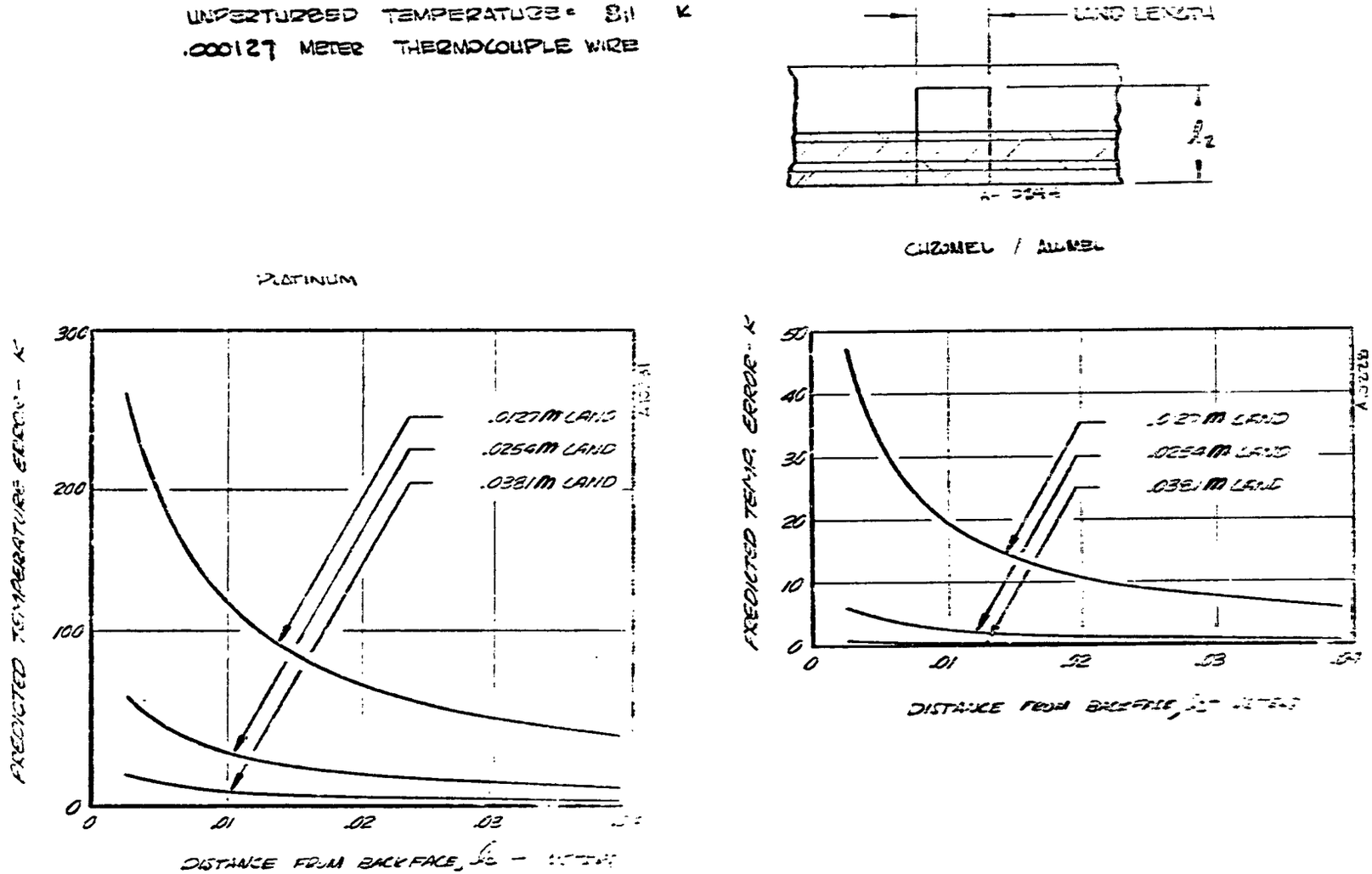

Figure A-3. Steady state analysis of conduction induced thermocouple errors.

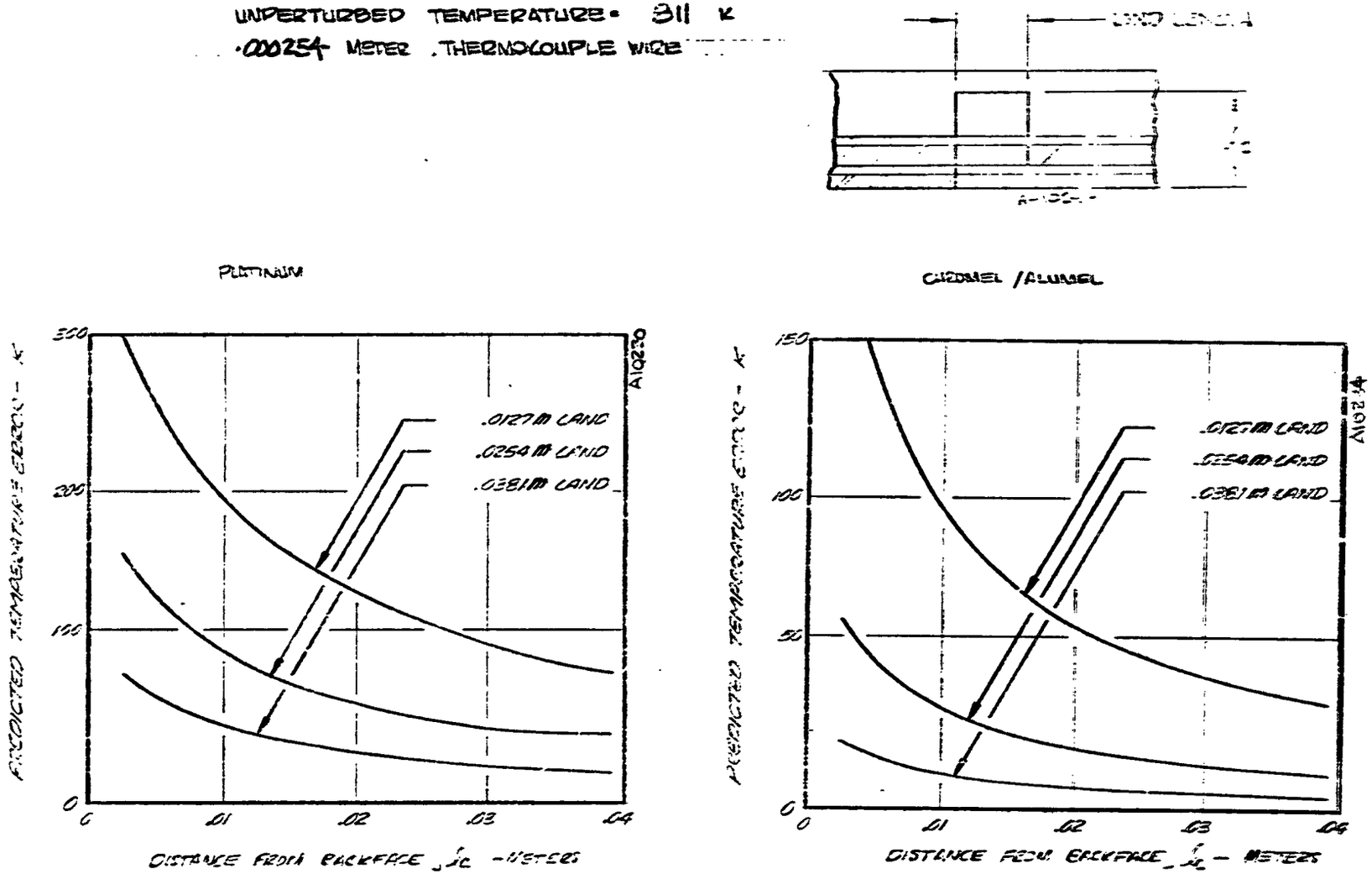

Figure A-4. Steady state analysis of conduction induced thermocouple errors.

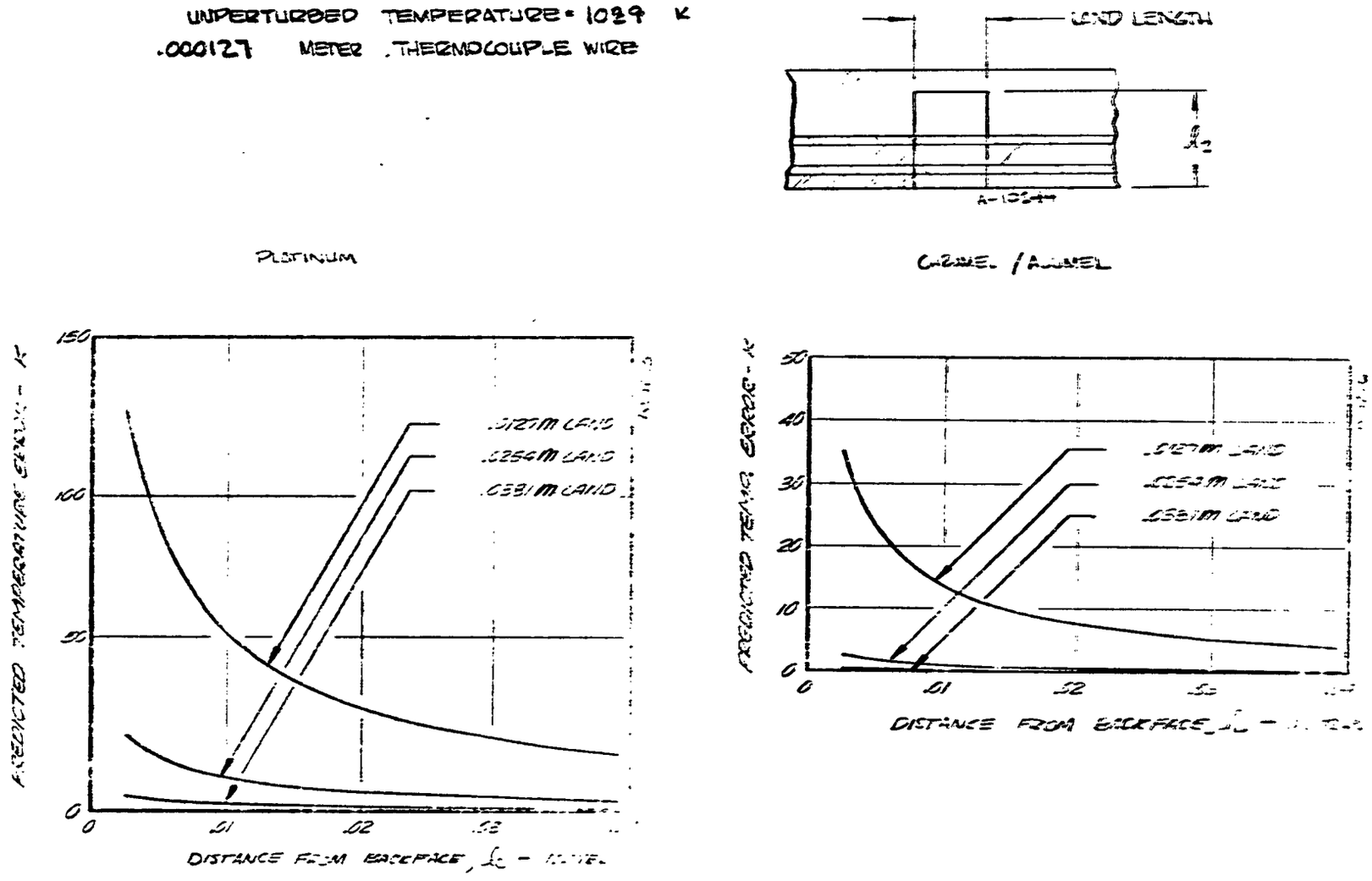

Figure A-5. Steady state analysis of conduction induced thermocouple errors.

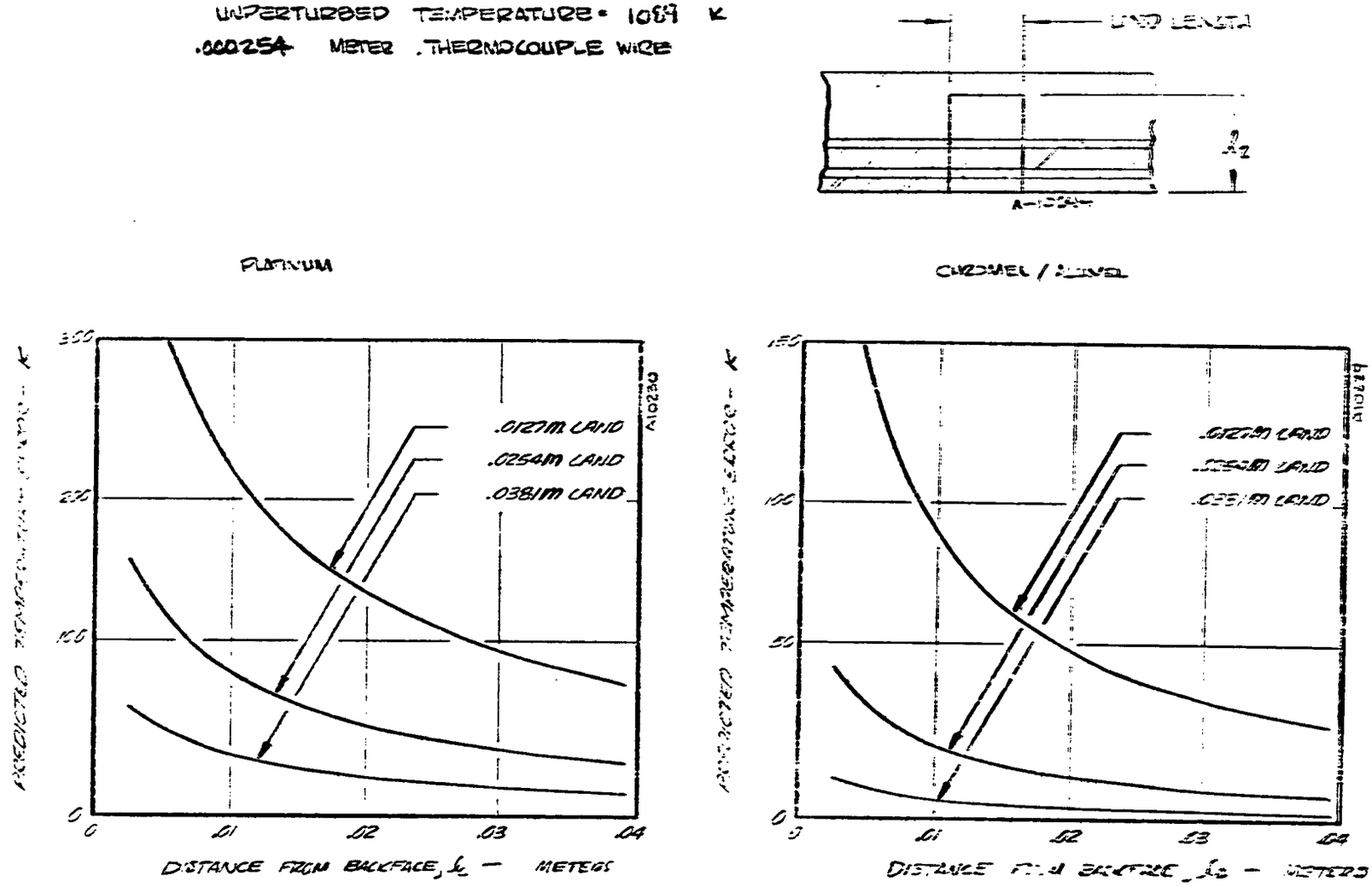

Figure A-6. Steady state analysis of conduction induced thermocouple errors.

REFERENCES

1. Reese, John J., Jr., "Wedge Model Tests to Evaluate Ablative, Metallic and Carbon/Carbon Composite Reentry Heat Shield Materials, Joints and Interfaces," Aerotherm Division, Acurex Corporation, Final Report No. 72-53, June 2, 1972.

2. "Development of a Fail Safe Design Oxidation Resistant Reinforced Carbon System for the Wing Leading Edge of a Space Shuttle Vehicle, Vought Missiles and Space Co., LTV Aerospace Corp., Monthly Progress Report No. 4, T143-5R-20200, Contract No. NAS9-12763, 29 July 1972 through 1 September 1972, pp. 28-31.

3. "User's Manual, Boundary Layer Integral Matrix Procedure," Aerotherm Report UM 70-20, June 1970.

4. Nydich, S. E., "Thermocouple Errors in Ablation Materials," ISA Preprint 16.12-3-66.

5. Schaefer, J. W., "Thermal Screening of Shuttle Orbitor Vehicle TPS Materials Under Convective Heating Conditions," Aerotherm Division, Acurex Corporation, Final Report No. 72-56, Volume I Final Report, NASA CR 114521, Volume II Tabulation of Test Results, NASA CR 114522, August 1973.